# Analysis of Acid Gas Absorption in a Mixed Amine System

A thesis submitted by

## Nyasha Madziva

in partial fulfillment of the requirements for the degree of

Master of Science

in

Chemical Engineering

## Tufts University

May 2017

Adviser: Jerry H. Meldon, Ph.D.

# Abstract

Chemical absorption and stripping of the acid gases, carbon dioxide and hydrogen sulfide, is an important unit operation in industrial gas processing. The goal of this thesis was to develop computationally efficient, accurate and robust algorithms for calculating local interphase transfer rates in absorption and stripping columns. Within the context of steady-state Film Theory, mass transfer is governed by a set of nonlinear differential equations. An approximate solution was developed by applying a variant of the linearization technique of Van Krevelen and Hoftijzer (1948). The algorithm was applied to simulate absorption of $CO_2$ and $H_2S$ in aqueous blends of diethanolamine (a secondary amine) and methyldiethanolamine (a tertiary amine). Calculated enhancement factors, by which reactions multiply absorption rates, differed by less than 5% from exact values. The results also conformed with the well-established behavior of tertiary amine solutions: $H_2S$ absorption is gas-phase mass transfer-limited and $CO_2$ absorption is liquid-phase kinetics-limited.

# Contents

# Figures

# Tables

# Nomenclature

$OH^-$        $OH^-$ concentration $\left(\frac{mol}{cm^3}\right)$

$A$        $CO_2$ concentration $\left(\frac{mol}{cm^3}\right)$

$a$        dimensionless $CO_2$ concentration, $\frac{A}{P_{A,bulk}H_A}$

$B$        $HCO_3^-$ concentration $\left(\frac{mol}{cm^3}\right)$

$b$        dimensionless $HCO_3^-$ concentration, $\frac{B}{C_T}$

$C$        $CO_3^{2-}$ concentration $\left(\frac{mol}{cm^3}\right)$

$c$        dimensionless $CO_3^{2-}$ concentration, $\frac{C}{C_T}$

$C_T$        defined in Equation (3.60) $\left(\frac{mol}{cm^3}\right)$

$C_{\varphi,bulk}$        liquid-phase concentration of species $\varphi$ in bulk liquid $\left(\frac{mol}{cm^3}\right)$

$C_{\varphi,int}$        concentration of species $\varphi$ at gas-liquid interface $\left(\frac{mol}{dcmm^3}\right)$

$D_\varphi$        diffusivity of dissolved species $\varphi$ $\left(\frac{cm^2}{s}\right)$

$D_{GA}, D_{GS}$        gas-phase diffusivities of $CO_2$ and $H_2S$, respectively $\left(\frac{cm^2}{s}\right)$

$E$        enhancement factor defined in Equation (4.47)

$E_A, E_S$        enhancement factors of $CO_2$ and $H_2S$, respectively

$G$        thickness of gas film (cm)

$H$        $H^+$ concentration $\left(\frac{mol}{cm^3}\right)$

$h$        dimensionless $H^+$ concentration, $\frac{H}{C_T}$

$H_A, H_S$      Henry law's constants of $CO_2$ and $H_2S$, respectively $\left(\frac{mol}{cm^3\ atm}\right)$

$Ha_1$      Hatta number defined in Equation (7.2)

$J$      flux $\left(\frac{mol}{cm^2 s}\right)$

$k_b$      forward rate constant of zwitterion deprotonation

$k_G$      gas-phase mass transfer coefficient

$k_L$      liquid-phase mass transfer coefficient

$K_n$      equilibrium constant of reaction n

$k_n$      forward rate constant of reaction n

$k_{-b}$      reverse rate constant of zwitterion deprotonation

$k_{-n}$      reverse rate constant of reaction n

$K_{\tilde{B}^+}$      defined in Equation (3.64)

$K_{\tilde{B}}$      defined in Equation (3.63)

$K_{H,A}, K_{H,S}$      inverses of solubility constants of $CO_2$ and $H_2S$, respectively $\left(\frac{atm\ cm^3}{mol}\right)$

$L$      thickness of liquid film (cm)

$M$      strong acid (or base) concentration added to maintain pH in bulk liquid $\left(\frac{mol}{cm^3}\right)$

$m$      dimensionless M concentration, $\frac{M}{C_T}$

$oh$      dimensionless $OH^-$ concentration, $\frac{OH^-}{C_T}$

$P$      pressure (atm)

$P_{\varphi,bulk}$      partial pressure of species $\varphi$ in bulk (atm)

$P_{\varphi,int}$      partial pressure of species $\varphi$ at gas-liquid interface (atm)

$R$      DEA concentration $\left(\frac{mol}{cm^3}\right)$

$r$      dimensionless DEA concentration, $\frac{R}{R_{LT}}$

| | |
|---|---|
| $R^+$ | DEAH$^+$ concentration $\left(\frac{mol}{cm^3}\right)$ |
| $r^+$ | dimensionless DEAH$^+$ concentration, $\frac{\text{R}^+}{\text{R}_{LT}}$ |
| $R^-$ | DEACOO$^-$ concentration $\left(\frac{mol}{cm^3}\right)$ |
| $r^-$ | dimensionless DEACOO$^-$ concentration, $\frac{\text{R}^-}{\text{R}_{LT}}$ |
| $R_3$ | MDEA concentration $\left(\frac{mol}{cm^3}\right)$ |
| $r_3$ | dimensionless MDEA concentration, $\frac{\text{R}_3}{\text{R}_{3,LT}}$ |
| $R_3^+$ | MDEA$^+$ concentration $\left(\frac{mol}{cm^3}\right)$ |
| $r_3^+$ | dimensionless MDEA$^+$ concentration, $\frac{\text{R}_3{}^+}{\text{R}_{3,LT}}$ |
| $R_\varphi$ | rate of production of species $\varphi$ $\left(\frac{mol}{cm^3\,s}\right)$ |
| $S$ | H$_2$S concentration $\left(\frac{mol}{cm^3}\right)$ |
| $s$ | dimensionless H$_2$S concentration, $\frac{S}{P_{S,bulk}H_S}$ |
| $S^-$ | HS$^-$ concentration $\left(\frac{mol}{cm^3}\right)$ |
| $s^-$ | dimensionless HS$^-$ concentration, $\frac{\text{S}^-}{C_T}$ |
| $x$ | distance from to gas-liquid interface (cm) |
| $y$ | dimensionless distance, $\frac{x}{L}$ |

**Greek Symbols**

| | |
|---|---|
| $\alpha$ | defined in Equation (4.13) |
| $\beta$ | defined in Equation (4.13) |
| $\chi_1$ | defined in Equation (5.30) |
| $\chi_2$ | defined in Equation (5.30) |
| $\eta_i$ | dimensionless constants defined in Equation (4.12) |
| $\kappa_{\tilde{B}^+}$ | defined in Equation (3.66) |
| $\kappa_{\tilde{B}}$ | defined in Equation (3.65) |

| | |
|---|---|
| $\lambda_i$ | $i = 1 - 13$ dimensionless constants defined in Section 3.6.6 |
| $\Lambda_j$ | defined in Equation (4.26) |
| $\mu$ | defined in Equation (4.19) |
| $\mu_1, \mu_2$ | defined in Equations (4.23) and (4.24) |
| $\omega_a, \omega_{r^-}$ | defined in Equation (4.16) |
| $\phi_i$ | $i = 2 - 8$ dimensionless constants defined in Equation (4.4) |
| $\Phi_\varphi$ | absorption flux of species $\varphi$ ($\frac{mol}{cm^2\ s}$) |
| $\psi_{\varphi j}$ | defined in Equations (4.19) and (4.25) |
| $\theta_i$ | defined in Equations (3.54), (3.56) and (3.57) |
| $\Upsilon$ | dimensionless constant defined in Section 3.1 |
| $\varphi^*$ | normalizing concentration of species $\varphi$ ($\frac{mol}{cm^3}$) in Chapter 3 |
| $\varrho_i$ | overall reaction rate of reaction i, ($\frac{mol}{cm^3 s}$) |
| $\vartheta$ | cross-sectional area of control volume defined in Section 3.1 |

*Subscripts*

| | |
|---|---|
| $(g)$ | gaseous state |
| $(l)$ | liquid state |
| 0 | conditions at the gas-liquid interface |
| 1 | conditions at y=1 |
| $\varphi$ | species index |
| $G, g$ | conditions in the bulk gas, i.e., at x=G |
| $int$ | conditions at the gas-liquid interface |
| $L$ | conditions in the bulk liquid, i.e. at x=L |

$LT$          total element concentration in the bulk liquid (e.g. of all species containing R (C, S or $R_3$)

*no rxn*        condition in the absense of reactions

# Chapter 1

# Introduction

Despite the rapid growth in renewable energy sources, it is estimated that in 2040 fossil fuels will still account for 80% of global energy consumption (ExxonMobil, 2012). Currently, this implies a constant increase in the market of +3%/year for natural gas and +7%/year for the liquefied form, which is more adaptable for easier transportation to the customer (Magné-Drisch, Julia *et al.*, 2016). As use of this fossil fuel increases, limits to its allowable composition, specifically the content of the potentially harmful acid gases, $CO_2$ and $H_2S$, have become more stringent. This has spurred intense research aimed at developing more cost-effective "gas sweetening" (i.e., acid gas separation) technologies (Torres-Ortega *et al.*, 2014).

Gas sweetening technologies include absorption (chemical and physical), adsorption, cryogenic distillation and membrane processes. Reactive absorption of $CO_2$ and $H_2S$ in aqueous alkanoamine solutions, typically in packed columns, is particularly well-suited for treating the relatively low acid gas concentration in fossil fuels (Barchas and Davis, 1992; Torres-Ortega *et al.*, 2014). The principal goal in absorption/reaction research and development is to reduce operating and capital costs through judicious screening of candidate absorbents (i.e., scrubbing solutions) (MacDowell *et al.*, 2010). This is

because the absorbent's properties (such as its reactivity, enthalpy and availability) have a direct effect on the rate of gas sweetening, and consequently, the size of the absorbing unit. An inexpensive yet potentially important component of the screening program is introduced by the modeling and simulation of column performance which may reduce the time an efforts spent in collecting experimental data.

Equilibrium-stage modeling assumes the equilibrium of streams leaving each stage or height-of-packing equivalent to a theoretical stage (Stewart, 1995). This somewhat outdated and approximate method accounts for mass and heat transfer limitations with empirical stage efficiency correlations (Falahat *et al.*, 2011).

Currently, the much-preferred approach is a "rate-based" model which accounts for the finite rates of heat and mass transfer, chemical reaction kinetics, as well as thermodynamics to predict local absorption rates, which are inserted in differential mass and energy balances (Glasscock and Rochelle, 1989). The latter, when integrated, yield the height of packing required to ensure the transfer of a specified fraction of a targeted component's inlet flowrate from the feed gas to the scrubbing solution.

The simplest absorption model is based on the Film Theory originally proposed by Lewis and Whitman 1924. It assumes that there are stagnant films on either side of the gas-liquid interface. Figure 1-1 illustrates this for the simple case of a single gas component (A) undergoing a single reaction in the liquid. When gas-side mass transfer effects are not important, the gas film may be disregarded in the analysis. More generally, gas species are assumed to transfer via molecular diffusion in both fluid films, and attain instantaneous phase equilibrium at the interface. Outside of the films, turbulence is assumed to ensure well-mixed bulk fluid phases.
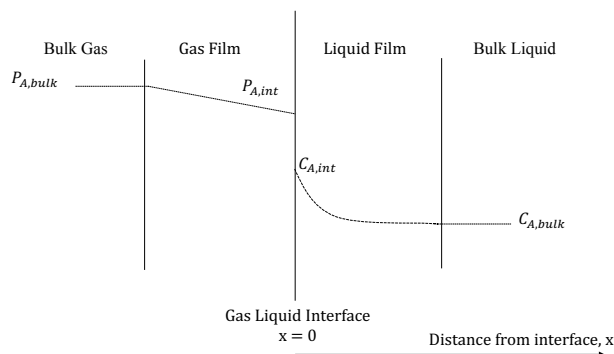
Figure 1-1: Two-Film Model schematic for the reactive absorption of species A. Bulk and interfacial gas pressures and liquid concentrations are shown as $P_{A,bulk}$, $C_{A,int}$, $C_{A,bulk}$, $C_{A,int}$ respectively.

Non-equilibrium reactions in the liquid film and are typically assumed to equilibrate in bulk liquid. Chemical reaction enhances absorption rates by steepening liquid phase concentration gradients as shown in fig. 1-1. A reasonable question is whether it is necessary to adopt a hydrodynamically more complex model than Film Theory?

Higbie introduced an alternative known as Penetration Theory, which relaxes the assumption of stagnant films. Instead, Higbie postulated that clusters of bulk liquid periodically exchange with fluid at the gas-liquid interface where they undergo reaction and diffusion before being swept back into the bulk solution (Higbie, 1935). Danckwerts later took Higbie's theory one step further when he proposed Surface Renewal Theory, which allows for a distribution of periods between exchanges of liquid between interface and bulk (Danckwerts, 1951). Surface Renewal Theory is more consistent with experimentally measured mass transfer rates; however, Film Theory predictions can be manipulated to bring them closer into alignment with Surface Renewal Theory. Chang and Rochelle showed that the Film Theory could be corrected to yield

3

mass transfer rate predictions more in line with the Surface Renewal Theory by applying a square root correction to diffusivity ratios 1982.

For absorption modeling purposes, the interfacial dynamics, reaction kinetics and equilibria are expressed as arrays of algebraic and either ordinary or partial differential equations (ODEs or PDEs) in the respective cases of steady-state Film Theory and non-steady state Penetration or Surface Renewal Theory. The equations are typically non-linear and therefore not subject to exact analytical solution. They can be solved using numerical methods. However, they tend to consume considerably more computation time, complexity and numerical difficulties (Glasscock and Rochelle, 1993). This has motivated the development of much less computation-intensive approximate solutions with minimal sacrifice of accuracy.

There is particular need for approximate solutions to the complex system of differential equations that govern reactive absorption of the acid gases, $CO_2$ and $H_2S$. Reliable algorithms could facilitate advances in gas processing technology. Following Worley, Zhu and Fiordalis, in this thesis, the approximate method of van Krevelen and Hoftijzer (VKH) is applied 1948. In their original paper, VKH applied their linearization technique to analyze absorption with a single irreversible reaction between dissolved gas A and non-volatile solute, B. The governing ODEs (i.e., differential mass balances) were linearized by treating the concentration of B as it appeared in reaction rate terms as a constant equal to its unknown value at the interface. Calculated absorption rates agreed closely with values based on essentially exact numerical solutions of the same non-linear ODEs.

The VKH linearization method will be applied to simulate the complex reactive absorption of $CO_2$ and $H_2S$ in solutions of amine blends, e.g., diethanolamine (DEA) plus methyldiethanolamine (MDEA). Calculated absorp-

tion rates will again be compared with exact results based on a numerical solution.

DEA and MDEA were chosen in light of their widespread deployment for acid gas absorption (Kohl and Nielsen, 1997). They offer complementary purposes. The secondary amine, DEA (so named because of the single labile hydrogen bound to its nitrogen atom), undergoes rapid and reversible carbamate formation with $CO_2$. The tertiary amine, MDEA, like all amines, is a weak base, and therefore, boosts the capacity of aqueous solutions to absorb acid gases; in the absence of DEA, it promotes the selective absorption of $H_2S$.

The amines also have in common other attractive properties such as low vapor pressure (which minimize fugitive emissions or contamination of the "sweetened" feed gas). They also exhibit lower heats of reaction with the dissolved gases than primary amines, e.g., monoethanolamine (MEA). Blends of DEA and MDEA enhance the rates of absorption of both acid gases and, therefore require lower circulation rates (Kumar *et al.*, 2014). For this reason, as well as the wealth of available physical and chemical property data for their solutions, they were chosen for modeling purposes.

# Chapter 2

# Background

Brian *et al.* (1961) were among the first groups to validate the van Krevelen and Hoftijzer (VKH) ODE linearization method. Adopting the Film Theory approximate solution for an irreversible second-order reaction with a non-volatile solute, they modified the VKH solution to include Penetration Theory parameters. They compared the results with absorption rates calculated from a numerical solution to the corresponding partial differential equations (PDEs) also based on Penetration Theory. When the group compared the flux profiles of the adopted approximate solution to the numerical solution over a range of liquid mass transfer coefficients, the maximum deviation of the two results was a 13% difference.

Other authors have since provided additional validation of the VKH method, and not only in the context of Film Theory (Hikita and Asai, 1964; Santiago and Farina, 1970; DeCoursey, 1974). They have made a point of both its simplicity, and especially the surprisingly close agreement with the results of exact numerical solutions. Hogendoorn, for example, applied the VKH method and Surface Renewal Theory to the analysis of absorption with a second order reversible reaction(Hogendoorn *et al.*, 1997). The approximate and exact

numerical results were within 7% of each other.

Recently, the VKH method has been successfully applied to model the reactive absorption of $CO_2$ in a magnesium hydroxide slurry (Zhao *et al.*, 2016). The VKH reactive absorption model was applied in conjunction with a model for the dissolution of magnesium hydroxide, and another model for the precipitation of solid magnesium carbonate. The models were used to derive kinetic parameters from experimental data for the rate of formation of the magnesium carbonate

VKH linearization was also used recently to obtain kinetic parameters for the production of difluoromethoxymethane from chlorodifluoromethane (Prithipal *et al.*, 2016). The former chemical is an alternative refrigerant developed with the aim of conserving the ozone layer; simulation of its production is a significant aid to manufacturing. The use of the VKH method to generate data that will be used to estimate key kinetic parameters shows the continued relevance and significance of its deployment in reactive absorption models.

Glasscock and Rochelle (1993) applied approximate methods to model $CO_2$ and $H_2S$ absorption in a range of DEA and MDEA solutions. The results were compared to those generated by a numerical solution based on Eddy Diffusivity Theory, a lesser known hydrodynamic theory than Film, Penetration and Surface Renewal Theory (King, 1966; Prasher and Fricke, 1974). Glasscock and Rochelle made additional simplifying assumptions, unrelated to the VKH, which leads to significant underestimated $CO_2$ concentrations and calculated fluxes. Consequently, the errors were as much as 20%.

The prior literature motivates the application of VKH linearization and Film Theory to the analysis of simultaneous absorption of $CO_2$ and $H_2S$ in mixed amine solutions. This project builds on the results of three recent Tufts

7

University theses. The first was an M.S. thesis by Zhu who modeled the absorption of $CO_2$ in an aqueous solution of a single tertiary amine, MDEA (Zhu, 2016). The second was the M.S. thesis of Worley, who modeled the absorption of both $CO_2$ and $H_2S$ in MDEA solutions (Worley, 2016). The third is the Ph.D. thesis of Fiordalis, who modeled the absorption of $CO_2$ in aqueous blends of DEA and MDEA (Fiordalis, 2017). All three applied the VKH method and calculated absorption rates in close agreement with those based on numerical solutions. The combination of multiple gases and multiple amine solutions added a further layer of complexity. Successful implementation of VKH linearization can significantly reduce column design and optimization computation time and resource expenditures for absorption (and desorption) column design and optimization.

Confidence in Film Theory has received additional boosts from many studies in which absorption rates based on numerical solutions using Chang and Rochelle's diffusivity ratio correction have been compared to experimental results. In one study, Bolhàr-Nordenkampf *et al.* (2004) used numerical methods to calculate rates of $CO_2$ and $H_2S$ absorption in MDEA solutions based on Film Theory and compared the results with absorption rates generated by the commercial software package, TSWEET, which applies an equilibrium stage model approach to its simulations, as well as to absorptions rates measured at different points along the height of a packed column. The Film Theory-based model had an average of 13% deviation from the experimental data compared to the 53% deviation by the TSWEET. solution

Godini and Mowla (2008) presented results generated by a numerical solution of the ODEs governing a Film Theory model of reactive absorption of $CO_2$ and $H_2S$ in an MEA solution. The results were integrated over the height of the column to calculate the overall removal efficiency. It reportedly agreed

within 14% of pilot plant experimental data. More recently, Borhani *et al.* presented the results of a numerical solution of the ODEs in a Film Theory model of the same absorption system 2016. Outlet gas concentrations were similarly compared to experimental data from a pilot plant; the numerically calculated results were within 10% of the experimental data.

Earlier publications had already reported the results of numerical solutions of the differential equations, based on various mass transfer theories, with which the authors had simulated absorption of the acid gases in solutions of single or mixed alkanoamines. In one such paper, Rinker and co-workers presented a Penetration Theory model of the absorption of $CO_2$ in a solution of a DEA/ MDEA blend and the results of a numerical solution of the governing PDEs (Rinker *et al.*, 2000). Calculated absorption rates differed by an average of 17.6% from experimental data. Similarly, Hageweische and co-workers reported less than 14 $ difference between $CO_2$ absorption rates in MEA/MDEA blends, similarly measured in a bench-scale laminar jet absorber, and predictions based on a numerical solution of the Penetration Theory PDEs (Hagewiesche *et al.*, 1995).

Recent attempts to more accurately model chemical absorption have encompassed more complexity. An example is Computation Fluid Dynamics (CFD) software, which solves the Navier-Stokes equations to simulate convection-diffusion and conduction given user-defined geometries and boundary conditions. In one study, fluid mechanics and thermodynamics were rigorously applied to numerically model acid gas absorption in an amine blend solution, in a novel packed column. Unfortunately, the authors did not compare the CFD model's prediction with representative experimental data.

Aspen and other process simulators which rigorously incorporate non-ideal thermodynamic behavior are commonly deployed in industrial practice to sim-

ulate complex gas/liquid systems - e.g., vapor/liquid/reaction equilibrium involving acid gases and aqueous amine solutions. One such simulation calculated rates of acid gas absorption in a solution of MDEA. The authors reported an average 30 % deviation from experimental data measured (along the height of a column) (Falahat *et al.*, 2011).

# Chapter 3

# Mathematical Analysis

The remaining chapters focus on the reactive absorption of the "acid gases", $CO_2$ and $H_2S$, in aqueous amine blends with a primary focus on diethanolamine (DEA) and methyldiethanolamine (MDEA). MATLAB numerical analysis and VKH linearization will be applied to the system of non-linear differential equations, which will be derived in dimensional terms, then de-dimensionalized to reduce the number of parameters.

## 3.1  Differential Mass Balance Equations

This section derives the working mass balance for the absorption reaction system according to the Film Theory model. Figure 3-1 illustrates the Film Model. It includes the control volume (of thickness $\Delta x$ and cross-sectional area $\vartheta$) for the differential mass balance; $x$ denotes distance from the gas-liquid interface; G and L are the gas and liquid film thicknesses, respectively. The control volume is used to derive a mass balance for species $\varphi$ where the rates of mass in and out of the control volume are represented by the diffusive flux in and out terms (multiplied by the cross-sectional area); the generation term of the mass balance equation is dictated by the reaction rates within the

11
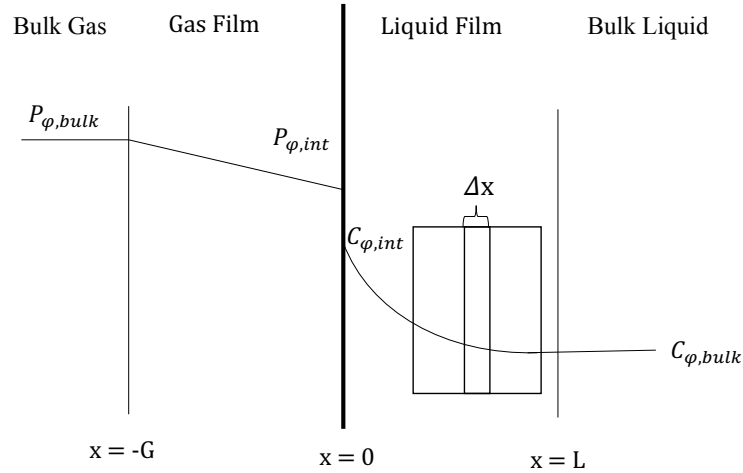
(a) Film Theory representation of the interfacial region with a control volume in the liquid film
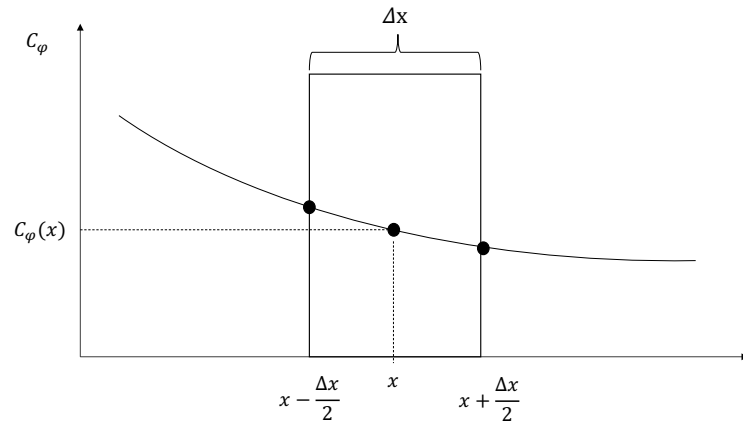


(b) Close-up of the control volume

Figure 3-1: The two-film model for species, $\varphi$, is shown in (a) with pressure profile due to diffusion in the gas phase and the concentration profile due to reactive absorption in the liquid phase. The gas and liquid films are assumed to behave like laminar boundary layers in which mass transport is via molecular diffusion. The bulk regions are assumed to be effectively well-mixed due to turbulence and instantaneous reaction equilibrium. A close up of a control volume unit in the liquid film with width $\Delta x$ that is used for mass balance analysis is shown in (b)

control volume. Diffusion is assumed to be governed by Fick's law. Referring to fig. 3-1b:

$$J_\varphi(x - \frac{\Delta x}{2}) = -D_\varphi \frac{dC_\varphi}{dx}\Big|_{(x-\frac{\Delta x}{2})} \qquad J_\varphi(x + \frac{\Delta x}{2}) = -D_\varphi \frac{dC_\varphi}{dx}\Big|_{(x+\frac{\Delta x}{2})} \qquad (3.1)$$

where $D$ is diffusivity in $\frac{cm^2}{s}$ and flux, J, is in $\frac{mol}{cm^2 s}$. Assuming a case in which dissolved gas A undergoes the following reversible reaction:

$$A_{(g)} + B_{(l)} \xrightleftharpoons[\mathrm{k_{-1}}]{\mathrm{k_1}} E_{(l)} + F_{(l)} \qquad (3.2)$$
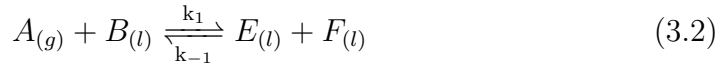
With simple kinetics, the rate of generation of species A is as follows:

$$R_A = \sum \varrho_{i,A} = \varrho_{1,A} = -k_1 C_A C_B + k_{-1} C_E C_F \qquad (3.3)$$

where $R_A$ has the units $\frac{mol}{cm^3 s}$.

A general mass balance for species $\varphi$ (including an accumulation term) is as follows (with each term in units of $\frac{mol}{s}$):

$$\frac{\Delta C_\varphi}{\Delta t}\vartheta \Delta x = J_\varphi(x - \frac{\Delta x}{2})\vartheta - J_\varphi(x + \frac{\Delta x}{2})\vartheta + R_\varphi \vartheta \Delta x \qquad (3.4)$$

$$\frac{\Delta C_\varphi}{\Delta t} = \frac{J_\varphi(x - \frac{\Delta x}{2}) - J_\varphi(x + \frac{\Delta x}{2})}{\Delta x} + R_\varphi \qquad (3.5)$$

Letting $\Delta x$ and $\Delta t$ approach zero, the following differential equation is derived.

$$\frac{dC_\varphi}{dt} = -\frac{dJ_\varphi}{dx} + R_\varphi \qquad (3.6)$$

$$\frac{dC_\varphi}{dt} = D_\varphi \frac{d^2\varphi}{dx^2} + R_\varphi \qquad (3.7)$$
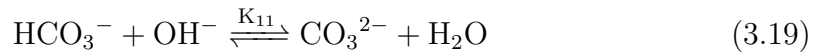
13

Assuming a steady state eq. (3.7) reduces to:

$$D_\varphi \frac{d^2 C_\varphi}{dx^2} = -R_\varphi \qquad (3.8)$$

where $\varphi = A,\ B,\ E,\ F$.

## 3.2 Reactions

In an aqueous blend of DEA and MDEA undergo an array of reactions as detailed below. DEA and MDEA are represented by R and $R_3$, respectively.

$$CO_2 + 2\,H_2O \underset{k_{-1}}{\overset{k_1}{\rightleftharpoons}} HCO_3{}^- + H_3O^+ \qquad (3.9)$$

$$CO_2 + OH^- \underset{k_{-2}}{\overset{k_2}{\rightleftharpoons}} HCO_3{}^- \qquad (3.10)$$

$$CO_2 + R_3 + H_2O \underset{k_{-3}}{\overset{k_3}{\rightleftharpoons}} R_3{}^+ + HCO_3{}^- \qquad (3.11)$$

$$CO_2 + R \underset{k_{-4}}{\overset{k_4}{\rightleftharpoons}} R^+COO^- \qquad (3.12)$$

$$R^+COO^- + R \underset{k_{-5}}{\overset{k_5}{\rightleftharpoons}} R^+ + RCOO^- \qquad (3.13)$$

$$R^+COO^- + R_3 \underset{k_{-6}}{\overset{k_6}{\rightleftharpoons}} R_3{}^+ + RCOO^- \qquad (3.14)$$

$$R^+COO^- + H_2O \underset{k_{-7}}{\overset{k_7}{\rightleftharpoons}} H_3O^+ + RCOO^- \qquad (3.15)$$

$$R^+COO^- + OH^- \underset{k_{-8}}{\overset{k_8}{\rightleftharpoons}} H_2O + RCOO^- \qquad (3.16)$$

$$R_3{}^+ + OH^- \overset{K_9}{\rightleftharpoons} R_3 + H_2O \qquad (3.17)$$

$$R^+ + OH^- \overset{K_{10}}{\rightleftharpoons} R + H_2O \qquad (3.18)$$

$$HCO_3{}^- + OH^- \overset{K_{11}}{\rightleftharpoons} CO_3{}^{2-} + H_2O \qquad (3.19)$$

$$2\,H_2O \overset{K_{12}}{\rightleftharpoons} OH^- + H_3O^+ \qquad (3.20)$$

$$H_2S + H_2O \overset{K_{13}}{\rightleftharpoons} HS^- + H_3O^+ \qquad (3.21)$$
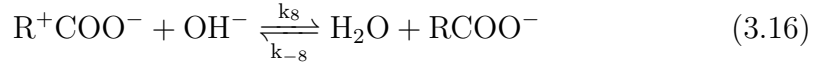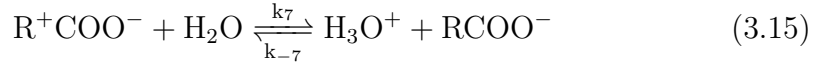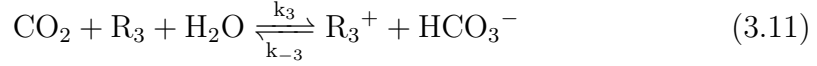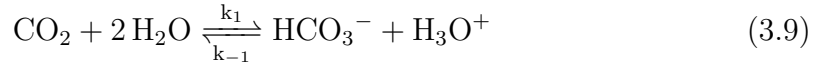
Equations (3.9) to (3.16) are finite-rate reactions and the rest (eqs. (3.17) to (3.21)) are effectively instantaneous reactions. Equations (3.9) and (3.10) show $CO_2$ hydration and reaction with hydroxyl ions. The first is intrinsically slow; and the rate at which the second proceeds is high only in very alkaline solutions (Pinsent *et al.*, 1956; Danckwerts and Sharma, 1966). $CO_2$ does not react directly with MDEA. Rather, it acts as a base catalyst of $CO_2$ hydration, and the kinetic constant has been measured by various authors (Donaldson and Nguyen, 1980a; Versteeg and van Swaaij, 1988; Littel *et al.*, 1990; Rinker *et al.*, 1995).

The mechanism of $CO_2$ reaction with DEA remains a matter of debate. In the more prevalent school of thought, $CO_2$ and a primary or secondary alkanolamine react to form a zwitterion, $R^+COO^-$, followed by deprotonation of the zwitterion by any available base to produce carbamate, $RCOO^-$, and the protonated base (Caplow, 1968; Danckwerts, 1970; Blauwhoff *et al.*, 1984; Versteeg *et al.*, 1990; Glasscock *et al.*, 1991). With DEA, the rate-determining step is the deprotonation of the zwitterion (Littel *et al.*, 1990). Any base in the system can deprotonate the zwitterion, however, each base's contribution to carbamate formation depends on its rate constant as well as its concentration. Equations (3.13) to (3.16) show deprotonation by some of the bases that are generally agreed to have experimentally observable impact on carbamate formation rates (Rinker *et al.*, 2000).

$H_2S$ apparently does not react directly with amines. As is implied by reaction 3.21, the basicity of amines fosters dissociation of the dissolved gas (which is effectively instantaneous). The writer has not come across any indication in the open literature that bisulfide ion, $HS^-$, significantly deprotonates the zwitterion.

## 3.3  Mathematical Model Development

### 3.3.1  Notation

The following notation is used to simplify the mathematical derivations:

$$A = [\mathrm{CO_2}] \qquad\qquad \mathrm{B} = [\mathrm{HCO_3}^-] \qquad\qquad \mathrm{C} = [\mathrm{CO_3}^{2-}]$$

$$H = [\mathrm{H_3O^+}] \qquad\qquad \mathrm{R} = [\mathrm{DEA}] \qquad\qquad \mathrm{R^-} = [\mathrm{DEACOO^-}]$$

$$\mathrm{R^+} = [\mathrm{DEAH^+}] \qquad\qquad \tilde{B} = R, R_3, \mathrm{H_2O}\ \text{or}\ \mathrm{OH^-} \quad R_3 = [\mathrm{MDEA}]$$

$$\mathrm{R_3}^+ = [\mathrm{MDEA^+}] \qquad\qquad S = [\mathrm{H_2S}] \qquad\qquad \mathrm{S^-} = [\mathrm{HS^-}]$$

The concentration of $\mathrm{H_2O}$ is treated as a constant . See the Appendix for detail on its estimation.

### 3.3.2  Expressions for local rates of consumption

The reactions listed in Section 3.2 imply the following consumption rates:

$$
\begin{aligned}
R_A &= -\varrho_1 - \varrho_2 - \varrho_3 - \varrho_4 \\
&= -k_1 A + \frac{k_1 B H}{K_1} - \frac{k_2 K_{12} A}{H} + \frac{k_2 B}{K_2} \\
&\quad - k_3 A \mathrm{R}_3 + \frac{k_3 B \mathrm{R}_3^+}{K3} \\
&\quad - k_4 \frac{A R - \dfrac{\mathrm{R^-}\left(\frac{k_{-5}\mathrm{R^+}}{k_4} + \frac{k_{-6}\mathrm{R}3^+}{k_4} + \frac{k_{-7}\mathrm{H}3\mathrm{O^+}}{k_4} + \frac{k_{-8}\mathrm{H}2\mathrm{O}}{k_4}\right)}{\frac{k_5 R}{k_{-4}} + \frac{k_6 \mathrm{R}3}{k_{-4}} + \frac{k_7 \mathrm{H}2\mathrm{O}}{k_{-4}} + \frac{k_8 \mathrm{OH^-}}{k_{-4}}}}{\dfrac{1}{\frac{k_5 R}{k_{-4}} + \frac{k_6 \mathrm{R}3}{k_{-4}} + \frac{k_7 \mathrm{H}2\mathrm{O}}{k_{-4}} + \frac{k_8 \mathrm{OH^-}}{k_{-4}}} + 1}
\end{aligned}
\tag{3.22a}
$$

This may be further rearranged to

$$R_A = (-k_1 - \frac{k_2 K_{12}}{H} - k_3 \mathrm{R}_3 - \frac{k_4 R}{\frac{1}{\frac{k_5 R}{k_{-4}} + \frac{k_6 \mathrm{R}_3}{k_{-4}} + \frac{k_7 \mathrm{H2O}}{k_{-4}} + \frac{k_8 \mathrm{OH}^-}{k_{-4}}} + 1})A$$

$$+ \frac{k_2 B}{K_2} + \frac{k_3 B \mathrm{R}_3^+}{K3} + \frac{k_1 B H}{K_1}$$

$$+ \frac{k_4 \mathrm{R}^- (\frac{k_{-5} \mathrm{R}^+}{k_4} + \frac{k_{-6} \mathrm{R}_3^+}{k_4} + \frac{k_{-7} \mathrm{H3O}^+}{k_4} + \frac{k_{-8} \mathrm{H2O}}{k_4})}{\frac{k_5 R}{k_{-4}} + \frac{k_6 \mathrm{R}_3}{k_{-4}} + \frac{k_7 \mathrm{H2O}}{k_{-4}} + \frac{k_8 \mathrm{OH}^-}{k_{-4}} + 1} \qquad (3.22b)$$

Similarly, a balance on carbamate, $\mathrm{R}^-$ gives the following:

$$R_{\mathrm{R}^-} = \varrho_5 + \varrho_6 + \varrho_7 + \varrho_8 \qquad (3.23)$$

$$= k_4 \frac{AR - \frac{\mathrm{R}^-(\frac{k_{-5} \mathrm{R}^+}{k_4} + \frac{k_{-6} \mathrm{R}_3^+}{k_4} + \frac{k_{-7} \mathrm{H3O}^+}{k_4} + \frac{k_{-8} \mathrm{H2O}}{k_4})}{\frac{k_5 R}{k_{-4}} + \frac{k_6 \mathrm{R}_3}{k_{-4}} + \frac{k_7 \mathrm{H2O}}{k_{-4}} + \frac{k_8 \mathrm{OH}^-}{k_{-4}}}}{\frac{1}{\frac{k_5 R}{k_{-4}} + \frac{k_6 \mathrm{R}_3}{k_{-4}} + \frac{k_7 \mathrm{H2O}}{k_{-4}} + \frac{k_8 \mathrm{OH}^-}{k_{-4}}} + 1} \qquad (3.24)$$

### 3.3.3 Reaction-Diffusion Differential Mass Balances

The generalized mass balance equation derived in section 3.1 is:

$$D_\varphi \frac{d^2 C_\varphi}{dx^2} = -R_\varphi \qquad (3.8)$$

Inserting the species consumption expressions in section 3.3.2 gives:

$$D_A \frac{d^2 A}{dx^2} = (k_1 + \frac{k_2 K_{12}}{H} + k_3 \mathrm{R}_3 + \frac{k_4 R}{\frac{k_{-4}}{\sum k_b \tilde{B}} + 1})A$$

$$- \frac{k_2 B}{K_2} - \frac{k_3 B \mathrm{R}_3^+}{K3} - \frac{k_1 B H}{K_1}$$

$$- \frac{\mathrm{R}^- \sum k_{-b} \tilde{B}^+}{\frac{\sum k_b \tilde{B}}{k_{-4}} + 1} \qquad (3.25a)$$

17

where $k_b$ and $k_{-b}$ are the forward and reverse base deprotonation rates in reactions 3.12 to 3.15, giving:

$$\frac{\sum k_b B}{k_{-4}} = \frac{k_5 R}{k_{-4}} + \frac{k_6 R_3}{k_{-4}} + \frac{k_7 H_2 O}{k_{-4}} + \frac{k_8 OH^-}{k_{-4}} \tag{3.25b}$$

$$\frac{\sum k_{-b} B^+}{k_4} = \frac{k_{-5} R^+}{k_4} + \frac{k_{-6} R_3{}^+}{k_4} + \frac{k_{-7} H_3 O^+}{k_4} + \frac{k_{-8} H_2 O}{k_4} \tag{3.25c}$$

Similarly, a balance on carbamate, $R^-$, gives:

$$D_{R^-} \frac{d^2 R^-}{dx^2} = -k_4 \frac{AR - \frac{R^- \sum k_{-b} \tilde{B}^+}{K_4 \sum k_b \tilde{B}}}{\frac{k_{-4}}{\sum k_b \tilde{B}} + 1} \tag{3.25d}$$

### 3.3.4   Linkage Equations

Total carbon, sulfur, tertiary amine and primary/secondary amine balances are implied in the following sums, sometimes referred to as linkage equations:

$$D_A \frac{d^2 A}{dx^2} + D_B \frac{d^2 B}{dx^2} + D_C \frac{d^2 C}{dx^2} + D_{R^-} \frac{d^2 R^-}{dx^2} = 0 \tag{3.26}$$

$$D_S \frac{d^2 S}{dx^2} + D_{S^-} \frac{d^2 S^-}{dx^2} = 0 \tag{3.27}$$

$$D_{R_3} \frac{d^2 R_3}{dx^2} + D_{R_3{}^+} \frac{d^2 R_3{}^+}{dx^2} = 0 \tag{3.28}$$

$$D_R \frac{d^2 R}{dx^2} + D_{R^+} \frac{d^2 R^+}{dx^2} = 0 \tag{3.29}$$

### 3.3.5 Instantaneous Reaction Equilibria

Local liquid-phase concentrations of the reactants in the instantaneous reactions, 3.17 to 3.21, satisfy the following five equilibrium relationships:

$$
\begin{aligned}
\mathrm{R_3}^+ &= \frac{R_3 H}{K_9 K_{12}} & \mathrm{R}^+ &= \frac{RH}{K_{10} K_{12}} \\
C &= \frac{K_{11} K_{12} B}{H} & \mathrm{S}^- &= \frac{K_{13} S}{H} \\
\mathrm{OH}^- &= \frac{K_{12}}{H}
\end{aligned}
\tag{3.30}
$$

## 3.4   Boundary Conditions

The two reaction-diffusion and four (linkage) sum of second-order differential equations require specification of twelve boundary conditions. The first set of boundary conditions refers to the gas-liquid interface, i.e., $x = 0$. The acid gases are the only species assumed to cross the gas-liquid interface, and thus have a flux at the interface. The volatilities of all other species (including water) and, therefore, their interfacial fluxes are assumed to be insignificant. The fluxes of the dissolved acid gases at the interface are equated with their values in the gas film, i.e.:

$$
D_A \frac{dA}{dx}\bigg|_{x=0} = -k_{G,A} \frac{(P_{A,bulk} - P_{A,0})}{RT} = -\frac{D_{G,A}}{G} \frac{K_{H,A}}{RT}(A_G - A_0)
\tag{3.31}
$$

where $K_{H,A} = \frac{1}{H_A}$, $A_G = H_A P_{A,bulk}$ and $H$ denotes a Henry's law constant. The enforcement of the local equilibrium of an instantaneous reaction, which may used to form a coupled (or linkage) equation precludes enforcement of a

boundary condition.

$$D_B \frac{dB}{dx}\bigg|_{x=0} + D_C \frac{dC}{dx}\bigg|_{x=0} = 0 \tag{3.32}$$

$$D_R \frac{dR}{dx}\bigg|_{x=0} + D_{\mathrm{R}^+} \frac{d\mathrm{R}^+}{dx}\bigg|_{x=0} = 0 \tag{3.33}$$

$$D_S \frac{dS}{dx}\bigg|_{x=0} + D_{\mathrm{S}^-} \frac{d\mathrm{S}^-}{dx}\bigg|_{x=0} = -k_{G,S} \frac{(P_{S,bulk} - P_{S,0})}{RT} = -\frac{D_{G,S}}{G} \frac{K_{H,S}}{RT}(S_G - S_0) \tag{3.34}$$

$$D_{\mathrm{R}3} \frac{d\mathrm{R}3}{dx}\bigg|_{x=0} + D_{\mathrm{R}3^+} \frac{d\mathrm{R}3^+}{dx}\bigg|_{x=0} = 0 \tag{3.35}$$

$$D_{\mathrm{R}^-} \frac{d\mathrm{R}^-}{dx}\bigg|_{x=0} = 0 \tag{3.36}$$

The second set of boundary conditions equate species concentrations at $x = L$ with those in bulk liquid (which are calculated as described in the following section):

$$A(x_L) = A_L \tag{3.37}$$

$$\mathrm{R}^-(x_L) = \mathrm{R}_L^- \tag{3.38}$$

$$B(x_L) = B_L \tag{3.39}$$

$$C(x_L) = C_L \tag{3.40}$$

$$R(x_L) = R_L \tag{3.41}$$

$$\mathrm{R}^+(x_L) = \mathrm{R}_L^+ \tag{3.42}$$

$$S(x_L) = S_L \tag{3.43}$$

$$\mathrm{S}^-(x_L) = \mathrm{S}_L^- \tag{3.44}$$

$$\mathrm{R}3(x_L) = R_{3,L} \tag{3.45}$$

$$\mathrm{R}3(x_L) + \mathrm{R}3^+(x_L) = R_{3,L} + \mathrm{R}_{3,L}^+ \tag{3.46}$$

### 3.4.1 Bulk Liquid Equilibrium

Residence times in bulk liquid are assumed to be sufficiently large that all reactions are effectively at equilibrium.

#### 3.4.1.1 Equilibrium Relationships

The following seven equilibrium relationships are assumed applicable:

$$
\begin{aligned}
\mathrm{R}_{3,L}^{+} &= \frac{R_{3,L} H_L}{K_9 K_{12}} & \mathrm{R}_L^{+} &= \frac{R_L H_L}{K_{10} K_{12}} \\
C_L &= \frac{K_{11} K_{12} B_L}{H_L} & \mathrm{S}_L^{-} &= \frac{K_{13} S_L}{H_L} \\
B_L &= \frac{K_1 A_L}{H_L} & R_L^{-} &= \frac{K_4 K_5 A_L R_L^2}{R_L^{+}} \\
\mathrm{OH}_L^{-} &= \frac{K_{12}}{H_L}
\end{aligned}
\tag{3.47}
$$

#### 3.4.1.2 Mole Balance Equations

Molar balances on carbon, sulphur and the two amines give the following equations, which are simplified using the equilibrium relationships above:

$$
A_{LT} = A_L + B_L + C_L + \mathrm{R}_L^{-} = A_L + \frac{K_1 A_L}{H_L} + \frac{K_1 K_{11} K_{12} A_L}{H_L{}^2} + \frac{K_4 K_5 K_{10} K_{12} A_L R_L}{H}
\tag{3.48}
$$

$$
S_{LT} = S_L + \mathrm{S}_L^{-} = S_L + \frac{K_{13} S_L}{H_L}
\tag{3.49}
$$

$$
R_{LT} = R_L + \mathrm{R}_L^{-} + \mathrm{R}_L^{+} = R_L + \frac{K_4 K_5 K_{10} K_{12} A_L R_L}{H} + \frac{R_L H_L}{K_{10} K_{12}}
\tag{3.50}
$$

$$
R_{3,LT} = R_{3,L} + \mathrm{R}_{3,L}^{+} = \frac{R_{3,L} H_L}{K_9 K_{12}} + R_{3,L}
\tag{3.51}
$$

where apart from the equilibrium constants, the only known values are $A_{LT}$, $S_{LT}$, $R_{LT}$ and $R_{3,LT}$, the total bulk liquid concentrations for carbon, sulphur, DEA and MDEA. Thus, there are 4 equations, and 5 unknowns to solve for.

### 3.4.1.3  Electroneutrality

Diffusion coefficients for all the ionic species are set at the same effective value so that diffusion potentials may be neglected. The following equation is proposed as the electroneutrality balance for the system in the bulk liquid:

$$R_L^- + B_L + 2C_L + S_L^- + OH^- = R_{3,L}^+ + R_L^+ + M + H_L$$

$$\text{or:} \quad \frac{K_1 A_L}{H_L} + 2\frac{K_1 K_{11} K_{12} A_L}{H_L{}^2} + \frac{K_{13} S_L}{H_L} + \frac{K_{12}}{H_L} = \frac{R_{3,L} H_L}{K_9 K_{12}} + \frac{R_L H_L}{K_{10} K_{12}} + M + H_L$$

$$(3.52)$$

M represents the concentration of a fixed-charge cation (e.g., an alkali metal ion) presumed to have been added MOH, to ensure a specified value of the bulk liquid's pH (and, therefore, $H_L$).

### 3.4.1.4  Method of solution

Including eq. (3.52), eqs. (3.48) to (3.52) now form five equations with five unknowns that can be solved. Due to the non-linear relationships, a simple form of equation substitution to solve is not possible, rather the equations must be solved by guessing a solution and iteratively solving for the optimal solution. In particular, two equations, eqs. (3.48) and (3.50), are non-linear. The equations may be combined to give the following quadratic equation 3.53 where:

$$\theta_1 A_L^2 + \theta_2 A_L + \theta_3 = 0 \quad\quad\quad (3.53)$$

where:

$$\theta_1 = (\frac{K_1 K_4 K_5 K_{10} K_{12}}{H_L^2} + \frac{K_4 K_5 K_{10} K_{12}}{H_L} + \frac{K_1 K_4 K_5 K_{10} K_{11} K_{12}^2}{H_L^3}) \tag{3.54}$$

$$\theta_2 = (1 + \frac{H_L}{K_{10} K_{12}} + \frac{K_1}{H_L} + \frac{K_1}{K_{10} K_{12}} + \frac{K_1 K_{11} K_{12}}{H_L{}^2} \tag{3.55}$$

$$+ \frac{K_1 K_{11}}{K_{10} H_L} + \frac{K_4 K_5 K_{10} K_{12} R_{LT}}{H_L} - \frac{K_4 K_5 K_{10} K_{12} A_{LT}}{H_L}) \tag{3.56}$$

$$\theta_3 = -A_{LT}(1 + \frac{H_L}{K_{10} K_{12}}) \tag{3.57}$$

$$A_L = -\frac{\theta_2 \pm \sqrt{\theta_2^2 - 4\theta_1 \theta_3}}{2\theta_1} \tag{3.58}$$

Choosing the physically realistic root, i.e., the positive one, all other bulk conditions follow.

## 3.5   Conversion to Dimensionless Variables

Nondimensionalization aids simulations in reaching faster convergence when all variables are at the same order of magnitude. It is also advantageous to nondimensionalize a system to reduce the number of parameters. The following nondimensional variables are defined as follows:

$$
\begin{aligned}
a &= \frac{A}{A^*} & b &= \frac{B}{B^*} \\
c &= \frac{C}{C^*} & r &= \frac{R}{R^*} \\
r^+ &= \frac{R^+}{R^*} & r^- &= \frac{R^-}{R^*} \\
r_3 &= \frac{R_3}{R_3^*} & r_3{}^+ &= \frac{R_3{}^+}{R_3^*} \\
h &= \frac{H}{H^*} & oh^- &= \frac{OH^-}{OH^{-*}} \\
m &= \frac{M}{M^*} & y &= \frac{x}{L}
\end{aligned}
\tag{3.59}
$$

where L is the liquid film thickness and the basis for nondimensionlization is given as:

$$C_T = R_{LT} + R_{3,LT} + M$$

$$R* = R^-* = R^+* = R_{LT}$$

$$R_3* = R_3^+* = R_{3,LT}$$

$$A* = A_G = P_{A,bulk}H_A$$

$$S* = S_G = P_{S,bulk}H_S$$

$$B* = C* = M* = S^-* = H* = OH^-* = C_T$$

(3.60)

Furthermore, the diffusivities relationships are as follows:

$$D_A = D_S$$

$$D_B = D_C = D_{R_3} = D_{R_3^+} = D_R = D_{R^-} = D_{R^+} = D_{S^-}$$

(3.61)

# 3.6 System of Nondimensional Equations

## 3.6.1 Differential Equations

Equation (3.25a) is rearranged to give the following balance for $CO_2$:

$$\frac{d^2a}{dy^2} = \frac{L^2}{D_A P_{A,bulk} H_A}\left[(k_1 + \frac{k_2 K_{12}}{C_T h} + \frac{k_3 K_9 K_{12} R_{3,LT} r_3{}^+}{C_T h} + \frac{k_4 R_{LT} r}{\frac{1}{\kappa_B}+1})P_{A,bulk}H_A a\right.$$
$$- \frac{k_2 C_T b}{K_2} - \frac{k_3 C_T R_{3,LT} b r_3{}^+}{K3} - \frac{k_1 C_T^2 bh}{K_1}$$
$$\left. - k_4 \frac{R_{LT} r^- \kappa_{B^+}}{\kappa_B + 1}\right]$$

(3.62)

Where:

$$K_{\tilde{B}} = \frac{\sum k_b \tilde{B}}{k_{-4}} \tag{3.63}$$

$$K_{\tilde{B}^+} = \frac{\sum k_{-b} \tilde{B}^+}{k_4} \tag{3.64}$$

$$\kappa_B = \frac{\sum k_b \tilde{b} \tilde{B}^*}{k_{-4}} = \frac{k_5 R_{LT} r}{k_{-4}} + \frac{k_6 R_{3,LT} r_3}{k_{-4}} + \frac{k_7 C_T h_2 o}{k_{-4}} + \frac{k_8 C_T oh^-}{k_{-4}} \tag{3.65}$$

$$\kappa_{B^+} = \frac{\sum k_{-b} \tilde{b}^+ \tilde{B}^*}{k_4} = \frac{k_{-5} R_{LT} r^+}{k_4} + \frac{k_{-6} R_{3,LT} r_3^+}{k_4} + \frac{k_{-7} C_T h}{k_4} + \frac{k_{-8} C_T h_2 o}{k_4} \tag{3.66}$$

Similarly, eq. (3.25d) is nondimensionalized as follows:

$$\frac{d^2 r^-}{dy^2} = -\frac{k_4 L^2}{D_{R^-}} P_{A,bulk} H_A a r - \frac{r^- \kappa_{B^+}}{\kappa_B} \bigg/ \left(\frac{1}{\kappa_B} + 1\right) \tag{3.67}$$

### 3.6.1.1  Linkage Equations

Equations (3.26) to (3.29) are rearranged to give:

$$\frac{D_A P_A H_A}{D_I C_T} \frac{d^2 a}{dy^2} + \frac{d^2 b}{dy^2} + \frac{d^2 c}{dy^2} + \frac{R_{LT}}{C_T} \frac{d^2 r^-}{dy^2} = \lambda_1 \frac{d^2 a}{dy^2} + \frac{d^2 b}{dy^2} + \frac{d^2 c}{dy^2} + \lambda_2 \frac{d^2 r^-}{dy^2} = 0 \tag{3.68}$$

$$\frac{D_A P_S H_S}{D_I C_T} \frac{d^2 s}{dy^2} + \frac{d^2 s^-}{dy^2} = \lambda_3 \frac{d^2 s}{dy^2} + \frac{d^2 s^-}{dy^2} = 0 \tag{3.69}$$

$$\frac{d^2 r}{dy^2} + \frac{d^2 r^+}{dy^2} + \frac{d^2 r^-}{dy^2} = 0 \tag{3.70}$$

$$\frac{d^2 r_3}{dy^2} + \frac{d^2 r_3^+}{dy^2} = 0 \tag{3.71}$$

## 3.6.2 Boundary conditions

The boundary conditions from section 3.4 are rewritten as

$$\frac{da}{dy}\bigg|_{y=0} = -\frac{D_{G,A}LK_{H,A}}{D_AGRT}(a_G - a_0) = -\lambda_4(a_G - a_0) \tag{3.72}$$

$$\frac{db}{dy}\bigg|_{y=0} + \frac{dc}{dy}\bigg|_{y=0} + \frac{dr^-}{dy}\bigg|_{y=0} = 0 \tag{3.73}$$

$$\frac{dr}{dy}\bigg|_{y=0} + \frac{dr^+}{dy}\bigg|_{y=0} = 0 \tag{3.74}$$

$$\frac{ds}{dy}\bigg|_{y=0} = -\frac{D_{G,S}LK_{H,S}}{D_SGRT}(s_G - s_0) = -\lambda_5(s_G - s_0) \tag{3.75}$$

$$\frac{ds^-}{dy}\bigg|_{y=0} = 0 \tag{3.76}$$

$$\frac{dr_3}{dy}\bigg|_{y=0} + \frac{dr_3^+}{dy}\bigg|_{y=0} = 0 \tag{3.77}$$

$$\frac{dr^-}{dy}\bigg|_{y=0} = 0 \tag{3.78}$$

$$a(y_1) = a_L \tag{3.79}$$

$$b(y_1) = b_L \tag{3.80}$$

$$c(y_1) = c_L \tag{3.81}$$

$$r^-(y_1) = r_L^- \tag{3.82}$$

$$r(y_1) = r_L \tag{3.83}$$

$$r^+(y_1) = r_L^+ = 1 \tag{3.84}$$

$$s(y_1) = s_L + \tag{3.85}$$

$$s^-(y_1) = s_L^- \tag{3.86}$$

$$r_3(y_1) = r_{3,L} \tag{3.87}$$

$$r_3^+(y_1) = r_{3,L}^+ = 1 \tag{3.88}$$

### 3.6.3 Integrated Linkage Equations

The dimensionless linkage equations derived in section 3.6.1.1 are integrated using the boundary conditions to give useful relations to connect the different species. Integration of eqs. (3.68) to (3.71) and insertion of the relevant boundary conditions leads to a set of integrated linkage equations.

#### 3.6.3.1 Carbon Linkage Equation

Equation (3.68) is integrated twice to give:

$$\lambda_1 a + b + c + \lambda_2 \mathrm{r}^- = c_1 y + c_2$$

Using the boundary condition at $y = 0$:

$$\lambda_1 \frac{da}{dy}\bigg|_{y=0} = -\lambda_1 \lambda_4 (a_{,G} - a_{,0}) = c_1$$

Similarly, using the boundary condition at $y = 1$:

$$\lambda_1 a_L + b_L + c_L + \lambda_2 \mathrm{r}_L^- - c_1 = c_2$$

Leading to the final form of the linkage equation at any point (y):

$$\lambda_1 a + b + c + \lambda_2 \mathrm{r}^- = [-\lambda_1 \lambda_4 (a_{,G} - a_{,0})]y + \lambda_1 a_L + b_L + c_L + \lambda_2 \mathrm{r}_L^- + \lambda_1 \lambda_4 (a_{,G} - a_{,0})$$

$$(3.89)$$

### 3.6.3.2   Sulphur Linkage Equation

Equation (3.69) is integrated twice to give:

$$\lambda_3 s + s^- = c_1 y + c_2$$

At $y = 0$:

$$\lambda_3 \frac{ds}{dy}\bigg|_{y=0} = -\lambda_3 \lambda_5 (s_{,G} - s_{,0}) = c_1$$

At $y = 1$:

$$\lambda_3 s_L + s_L^- - c_1 = c_2$$

Therefore

$$\lambda_3 s + s^- = [-\lambda_3 \lambda_5 (s_{,G} - s_{,0})]y + \lambda_3 s_L + s_L^- + \lambda_3 \lambda_5 (s_{,G} - s_{,0}) \qquad (3.90)$$

### 3.6.3.3   Secondary Amine Linkage Equation

Similarly, eq. (3.70) is integrated twice to give:

$$r + r^+ + r^- = c_1 y + c_2$$

At $y = 0$:

$$c_1 = 0$$

28

At $y = 1$:

$$r_L + \mathrm{r}_L^+ + \mathrm{r}_L^- - c_1 = c_2$$

Therefore

$$r + \mathrm{r}^+ + \mathrm{r}^- = r_L + \mathrm{r}_L^+ + \mathrm{r}_L^- = 1 \tag{3.91}$$

### 3.6.3.4 Tertiary Amine Linkage Equation

Equation (3.71) is integrated twice to give:

$$r^3 + \mathrm{r_3}^+ = c_1 y + c_2$$

At $y = 0$:

$$c_1 = 0$$

At $y = 1$:

$$r_L^3 + \mathrm{r}_{3L}^+ - c_2 = c_2$$

Therefore

$$r^3 + \mathrm{r_3}^+ = r_L^3 + \mathrm{r}_{3L}^+ = 1 \tag{3.92}$$

## 3.6.4 Electroneutrality

The nondimensionalized electroneutrality equation gives the following relation:

$$\frac{R_{3,LT}}{C_T}\mathrm{r_3}^+ + \frac{R_{LT}}{C_T}\mathrm{r}^+ + m + \mathrm{h} = b + 2c + \frac{R_{LT}}{C_T}\mathrm{r}^- + \mathrm{s}^- - \mathrm{oh}^- \tag{3.93}$$

This is now simplified to:

$$\lambda_6 r_3{}^+ + \lambda_2 r^+ + m + h = b + 2c + \lambda_2 r^- + s^- - oh^- \qquad (3.94)$$

## 3.6.5   Instantaneous Reaction Equilibria

The five equilibrium relationships from section 3.3.5 are written in dimensionless terms as

$$r_3{}^+ = \frac{C_T^2 r_3 h}{K_9 K_{12}} = \lambda_7 r_3 h \qquad\qquad r^+ = \frac{C_T^2 r h}{K_{10} K_{12}} = \lambda_8 r h \qquad (3.95)$$

$$c = \frac{K_{11} K_{12} b}{C_T^2 h} = \frac{\lambda_9 b}{h} \qquad\qquad s^- = \frac{K_{13} P_S H_S s}{C_T^2 h} = \frac{\lambda_{10} s}{h} \qquad (3.96)$$

$$oh^- = \frac{K_{12}}{C_T^2 h} = \lambda_{11} h \qquad\qquad\qquad\qquad\qquad\qquad\qquad (3.97)$$

## 3.6.6   Dimensionless constants

$$\lambda_1 = \frac{D_A P_A H_A}{D_I C_T} \qquad\qquad\qquad \lambda_2 = \frac{R_{LT}}{C_T}$$

$$\lambda_3 = \frac{D_A P_S H_S}{D_I C_T} \qquad\qquad\qquad \lambda_4 = \frac{D_{G,A} L K_{H,A}}{D_A G R T}$$

$$\lambda_5 = \frac{D_{G,S} L K_H, S}{D_S G R T} \qquad\qquad\qquad \lambda_6 = \frac{R_{3,LT}}{C_T}$$

$$\lambda_7 = \frac{C_T^2}{K_9 K_{12}} \qquad\qquad\qquad\qquad \lambda_8 = \frac{C_T^2}{K_{10} K_{12}}$$

$$\lambda_9 = \frac{K_{11} K_{12}}{C_T^2} \qquad\qquad\qquad\qquad \lambda_{10} = \frac{K_{13} P_S H_S}{C_T^2}$$

$$\lambda_{11} = \frac{K_{12}}{C_T^2} \qquad\qquad\qquad\qquad\qquad \lambda_{12} = \frac{C T^2}{K_1 P_A H_A}$$

$$\lambda_{13} = \frac{K_4 K_5 P_A H_A}{\lambda_8}$$

## 3.7    Numerical Solution

The numerical methods were solved using MATLAB's in-built boundary value problem ODE solver, bvp4c (R2016a, The MathWorks, Natick, Massachusetts). Appendix B shows the code used in implementation.

# Chapter 4

# Van Krevelen and Hoftijzer Method

The Van Krevelen and Hoftijzer approximation method linearizes non-linear differential equations. As introduced in Chapter 1, the linearization is done by holding constant -in the differential equations' reaction rate terms - the concentrations of all species other than the one whose mass balance is expressed in the differential equation. The concentrations of those species are held constant at their interfacial ($y = 0$) values. In previous VKH method applications to the reactive absorption problem, there was typically only one volatile reactive species (Brian *et al.*, 1961; Hikita and Asai, 1964; Santiago and Farina, 1970; DeCoursey, 1974).

In the case at hand, there are two volatile species, the acid gases $CO_2$ and $H_2S$. It will, therefore, be necessary, when linearizing the differential equations, to hold constant in reaction rate terms, the concentrations of non-volatile components, $H^+$ and $HS^-$. Since those two non-volatile components are assumed to be in local equilibrium with $H_2S$, the concentration of dissolved $H_2S$ will implicitly also be treated as constant in reaction rate terms.

We will apply two VKH-like linearizations to solve the two coupled differential equations derived in Chapter 3 and reproduced below:

$$\frac{d^2\mathbf{a}}{dy^2} = \frac{L^2}{D_A P_{A,bulk} H_A}\left[(k_1 + \frac{k_2 K_{12}}{C_T h} + \frac{k_3 K_9 K_{12} R_{3,LT} \mathbf{r_3}^+}{C_T h} + \frac{k_4 R_{LT} r}{\frac{1}{\kappa_B} + 1})P_{A,bulk} H_A \mathbf{a}\right.$$
$$- \frac{k_2 C_T b}{K_2} - \frac{k_3 C_T R_{3,LT} b \mathbf{r_3}^+}{K3} - \frac{k_1 C_T^2 bh}{K_1}$$
$$\left. - k_4 \frac{R_{LT}\kappa_{B+}\mathbf{r}^-}{\kappa_B + 1}\right]$$

$$(3.62)$$

$$\frac{d^2\mathbf{r}^-}{dy^2} = -\frac{k_4 L^2}{D_{\mathrm{R}^-}}\frac{P_{A,bulk} H_A \mathbf{a} r - \frac{\mathbf{r}^-\kappa_{B+}}{\kappa_B}}{\frac{1}{\kappa_B} + 1} \qquad (3.67)$$

The colored letters denote the dimensionless concentrations not held constant on the righthand sides of the differential equations, which may be rewritten as follows:

$$\frac{d^2 a}{dy^2} = \phi_1(\phi_2 a + \phi_3 \mathrm{r}^- + \phi_4) \qquad (4.1)$$

following:

$$\frac{d^2 \mathrm{r}^-}{dy^2} = \phi_6(\phi_7 a + \phi_8 \mathrm{r}^-) \qquad (4.2)$$

These two ODEs actually constitute the second VKH-like linearization (which was developed in the PhD thesis of Fiordalis (2017), that we will apply to eqs. (3.62) and (3.67). The first is based on further simplification of eq. (3.62) to treat $\mathrm{r}^-$ as a constant in eq. (4.1);, i.e.:

$$\frac{d^2 a}{dy^2} = \phi_1\phi_2 a + \phi_5 \qquad (4.3)$$

33

The constants in these equations are defined as follows:

$$\phi_1 = \frac{L^2}{D_A P_A H_A} \qquad \phi_2 = (k_1 + \frac{k_2 K_{12}}{C_T h_0} + \frac{k_3 K_9 K_{12} R_{3,LT} \mathrm{r}_{30}^+}{C_T h_0} + \frac{k_4 R_{LT} r_0}{\frac{1}{\kappa_{B,0}} + 1}) P_A H_A$$

$$\phi_3 = -k_4 \frac{R_{LT} \kappa_{B_0^+}}{\kappa_{B,0} + 1} \qquad \phi_4 = -\frac{k_2 C_T b_0}{K_2} - \frac{k_3 C_T R_{3,LT} b_0 \mathrm{r}_{30}^+}{K3} - \frac{k_1 C_T^2 b_0 h_0}{K_1}$$

$$\phi_5 = \phi_1(\phi_3 \mathrm{r}_0^- + \phi_4) \qquad\qquad\qquad\qquad \phi_6 = \frac{-k_4 L^2}{D_{\mathrm{R}^-}}$$

$$\phi_7 = \frac{P_A H_A r_0}{\frac{1}{\kappa_{B,0}} + 1} \qquad\qquad\qquad\qquad \phi_8 = -\frac{\kappa_{B_0^+}}{\kappa_{B,0} + 1}$$

$$(4.4)$$

The following sections outline the two VKH-like solutions.

## 4.1   Determining Interfacial Concentrations

Two interfacial concentrations, $r_0$ and $r_0^+$ are guessed. Then, applying the integrated linkage (eqs. (3.89) to (3.92)), equilibrium (eq. (3.97)) and electroneutrality (eq. (3.94)) equations, all remaining nonvolatile interfacial concentrations (at y=0) are calculated.

$$h_0 = \frac{\mathrm{r}_0^+}{\lambda_8 r_0} \tag{4.5}$$

$$r_{3,0} = \frac{1}{(1 + \lambda_7 h_0)} \tag{4.6}$$

$$s_0 = \frac{\lambda_3 s_L + \mathrm{s}_L^- + \lambda_3 \lambda_5 s_{,G}}{\lambda_3(1 + \frac{\lambda_{10}}{h_0} + \lambda_3 \lambda_5)} \tag{4.7}$$

$$a_0 = \frac{\lambda_1 a_L + b_L + c_L + \lambda_2 \mathrm{r}_L^- + \lambda_1 \lambda_4 a_{,G} - b_0(1 + \frac{\lambda_9}{h_0}) - \lambda_2(1 - r_0 - \mathrm{r}_0^+)}{\lambda_1 + \lambda_1 \lambda_4} \tag{4.8}$$

$$b_0 = \frac{\lambda_6 r_{3,0} \lambda_7 h_0 - \lambda_2(1 - r_0 - 2\mathrm{r}_0^+) - \frac{\lambda_{10} s}{h_0} - \lambda_{11} h_0 + m + h_0}{1 + 2\frac{\lambda_9}{h_0}} \tag{4.9}$$

These are inserted in eq. (4.4) to calculate $\phi_2$, $\phi_5$, $\phi_7$ and $\phi_8$ for linearizing the differential equations.

## 4.2  Integration of linearized ODEs

### 4.2.1  Method 1

Equations (4.2) and (4.3) are rewritten as follows:

$$\frac{d^2a}{dy^2} = \eta_1 a + \eta_2 \tag{4.10}$$

$$\frac{d^2\mathrm{r}^-}{dy^2} = \eta_3 a - \eta_4 \mathrm{r}^- \tag{4.11}$$

$$\text{where:} \quad \eta_1 = \phi_1\phi_2 \quad \eta_2 = \phi_5 \quad \eta_3 = \phi_6\phi_7 \quad \eta_4 = -\phi_6\phi_8 \tag{4.12}$$

In order to find an exact solution to the ODEs, the following relationships can be defined:

$$\alpha = a + \omega_a \qquad \beta = \mathrm{r}^- + \omega_{\mathrm{r}^-} \tag{4.13}$$

$$\frac{d^2\alpha}{dy^2} = \eta_1 \alpha = \eta_1(\alpha - \omega_a) + \eta_2 \tag{4.14}$$

$$\frac{d^2\beta}{dy^2} = \eta_3 \alpha - \eta_4 \beta = \eta_3(\alpha - \omega_a) - \eta_4(\beta - \omega_{\mathrm{r}^-}) \tag{4.15}$$

$$\text{where } \omega_a \text{ and } \omega_{\mathrm{r}^-} \text{ are:} \quad \omega_a = \frac{\eta_2}{\eta_1} \qquad \omega_{\mathrm{r}^-} = \frac{\eta_2\eta_3}{\eta_1\eta_4} \tag{4.16}$$

The ODEs can now be rewritten as follows:

$$\frac{d^2\alpha}{dy^2} = \eta_1 \alpha \tag{4.17}$$

$$\frac{d^2\beta}{dy^2} = \eta_3 \alpha - \eta_4 \beta \tag{4.18}$$

The solution can then be assumed to be of the following form:

$$\alpha = \psi_A e^{\mu y} \qquad \beta = \psi_B e^{\mu y} \tag{4.19}$$

The solution forms can then be differentiated and equated to known terms:

$$\mu^2 \psi_A e^{\mu y} = \eta_1 \psi_A e^{\mu y} \qquad \text{or:} \qquad (\mu^2 - \eta_1)\psi_A = 0 \tag{4.20}$$

$$\mu^2 \psi_B e^{\mu y} = \eta_3 \psi_A e^{\mu y} - \eta_4 \psi_B e^{\mu y} \qquad \text{or:} \qquad \eta_3 \psi_A - (\mu^2 + \eta_4)\psi_B = 0 \tag{4.21}$$

Equations (4.20) and (4.21) can be rewritten in the coefficient matrix:

$$-(\mu^2 - \eta_1)(\mu^2 + \eta_4) - 0 = 0 \tag{4.22}$$

Therefore $\mu^2$ has two values:

$$\mu_1^2 = -\eta_4 \tag{4.23}$$

$$\mu_2^2 = \eta_1 \tag{4.24}$$

Therefore, there are four $\mu$ values, $\pm\mu_1$ and $\pm\mu_2$, such that

$$\alpha = \sum_{j=1}^{4} \psi_{Aj} e^{\mu_j y} \qquad \beta = \sum_{j=1}^{4} \psi_{Bj} e^{\mu_j y} \tag{4.25}$$

where $\psi_A$ can be related to $\psi_B$ from eq. (4.21):

$$\psi_{Aj} = \frac{(\mu_j^2 + \eta_4)\psi_{Bj}}{\eta_3} = \Lambda_j \psi_{Bj} \tag{4.26}$$

The four $\psi_{Bj}$ values are found from the boundary conditions eqs. (3.72), (3.78), (3.79) and (3.82):

$$\alpha_L = a_L + \omega_a = \sum_{j=1}^{4} \Lambda_j \psi_{Bj} e^{\mu_j} \qquad \text{or:} \qquad a_L = \sum_{j=1}^{4} \Lambda_j \psi_{Bj} e^{\mu_j} - \omega_a \qquad (4.27)$$

Although $a_0$ is unknown, it necessary to define the boundary condition represented by the interfacial flux $\frac{da}{dy}\big|_{y=0} = -\lambda_4(a_{,G} - a_{,0})$ (eq. (3.79)). Therefore, $a_0$ in terms of the assumed solution is written as:

$$\alpha_0 = a_0 + \omega_a = \sum_{j=1}^{4} \Lambda_j \psi_{Bj} \qquad \text{or:} \qquad a_0 = \sum_{j=1}^{4} \Lambda_j \psi_{Bj} - \omega_a \qquad (4.28)$$

Therefore, the flux can be written as:

$$\frac{da}{dy}\bigg|_{y=0} = \frac{d\alpha}{dy}\bigg|_{y=0} = \sum_{j=1}^{4} \mu_j \Lambda_j \psi_{Bj} = -\lambda_4(a_G - a_0)$$

$$\text{rearranged to:} \qquad a_G = \frac{\lambda_4(\sum_{j=1}^{4} \Lambda_j \psi_{Bj} - \omega_a) - \sum_{j=1}^{4} \mu_j \Lambda_j \psi_{Bj}}{\lambda_4} \qquad (4.29)$$

The last two equations come from the boundary conditions for $\text{r}^-$, eqs. (3.78) and (3.82):

$$\beta_L = \text{r}^-_L + \omega_{\text{r}^-} = \sum_{j=1}^{4} \psi_{Bj} e^{\mu_j} \qquad \text{or:} \qquad \text{r}^-_L = \sum_{j=1}^{4} \psi_{Bj} e^{\mu_j} - \omega_{\text{r}^-} \qquad (4.30)$$

$$\frac{d\beta}{dy}\bigg|_{y=0} = \frac{d\text{r}^-}{dy}\bigg|_{y=0} = \sum_{j=1}^{4} \mu_j \psi_{Bj} = 0 \qquad (4.31)$$

Using the four equations, eqs. (4.27) and (4.29) to (4.31), the four $\psi_B$ values are found; combined with the four $\mu$ values found from eqs. (4.23) and (4.24), the solution for $\alpha$ and $\beta$ (as a function of y), and consequently,

(using eqs. (4.13) and (4.16)) the solution for $a$ and $r^-$ are found. After producing these profiles, $s$, $r$, $r^+$ and all the other concentration profiles are found from the integrated linkage equations(eqs. (3.89) to (3.92)), equilibrium (eq. (3.97)) and electroneutrality (eq. (3.94)) equations. As mentioned before, these solutions are based on a guess of $r_0$ and $r_0^+$. To find the correct solution, a fixed point iteration, comparing the $r_0$ and $r_0^+$ guesses, with the $r_0$ and $r_0^+$ calculated from their VKH-solution profiles as a function of $y$, by setting $y = 0$. The correct solution is achieved when the guesses are exactly the same as the calculated $r_0$ and $r_0^+$ (with a tolerance of $1e^{-8}$).

## 4.2.2 Method 2

Equations (4.1) and (4.2) are rewritten as follows:

$$\frac{d^2 a}{dy^2} = \eta_1 a + \eta_2 r^- + \eta_3 \qquad (4.32)$$

$$\frac{d^2 r^-}{dy^2} = \eta_4 a + \eta_5 r^- \qquad (4.33)$$

where: $\quad \eta_1 = \phi_1 \phi_2 \qquad \eta_2 = \phi_1 \phi_3 \qquad \eta_3 = \phi_1 \phi_4 \qquad \eta_4 = \phi_5 \phi_6 \qquad \eta_5 = \phi_5 \phi_7$

$$(4.34)$$

In order to find an exact solution to the ODEs, the following relationships can again be defined:

$$\alpha = a + \omega_a \qquad \beta = r^- + \omega_{r^-} \qquad (4.35)$$

$$\frac{d^2 \alpha}{dy^2} = \eta_1 \alpha + \eta_2 \beta = \eta_1(\alpha - \omega_a) + \eta_2(\beta - \omega_{r^-}) + \eta_3$$

$$(4.36)$$

$$\frac{d^2 \beta}{dy^2} = \eta_4 \alpha + \eta_5 \beta = \eta_4(\alpha - \omega_a) + \eta_5(\beta - \omega_{r^-})$$

$$(4.37)$$

38

where $\omega_a$ and $\omega_{r^-}$ are:

$$\omega_{r^-} = -\frac{\eta_4 \omega_a}{\eta_5} \qquad \omega_a = \frac{\eta_3}{\eta_1 - \frac{\eta_2 \eta_4}{\eta_5}} \tag{4.38}$$

The ODEs can now be rewritten as follows:

$$\frac{d^2\alpha}{dy^2} = \eta_1\alpha + \eta_2\beta \tag{4.39}$$

$$\frac{d^2\beta}{dy^2} = \eta_4\alpha + \eta_5\beta \tag{4.40}$$

The solution can then be assumed to be in the following form:

$$\alpha = \psi_A e^{\mu y} \qquad \beta = \psi_B e^{\mu y}$$

$$\tag{4.41}$$

The solution forms can then be differentiated and equated to known terms:

$$\mu^2 \psi_A e^{\mu y} = \eta_1 \psi_A e^{\mu y} + \eta_2 \psi_B e^{\mu y} \qquad \text{or:} \qquad (\eta_1 - \mu^2)\psi_A + \eta_2\psi_B = 0 \tag{4.42}$$

$$\mu^2 \psi_B e^{\mu y} = \eta_4 \psi_A e^{\mu y} + \eta_5 \psi_B e^{\mu y} \qquad \text{or:} \qquad \eta_4\psi_A + (\eta_5 - \mu^2)\psi_B = 0 \tag{4.43}$$

Equations (4.42) and (4.43) can be rewritten in the coefficient matrix:

$$(\eta_1 - \mu^2)(\eta_5 - \mu^2) - \eta_2\eta_4 = 0 \tag{4.44}$$

Therefore $\mu^2$ has two values:

$$\mu_1^2 = \frac{(\eta_1 + \eta_5)}{2}\left[1 + \sqrt{1 + \frac{4(\eta_1\eta_5 - \eta_2\eta_4)}{(\eta_1 + \eta_5)^2}}\right] \qquad (4.45)$$

$$\mu_2^2 = \frac{(\eta_1 + \eta_5)}{2}\left[1 - \sqrt{1 + \frac{4(\eta_1\eta_5 - \eta_2\eta_4)}{(\eta_1 + \eta_5)^2}}\right] \qquad (4.46)$$

Similar to Method 1, using the four $\mu$ values in eqs. (4.45) and (4.46) and the four $\psi_A$ and $\psi_B$ values are found from eqs. (4.26), (4.27) and (4.29) to (4.31), the solution for $\alpha$ and $\beta$ (as a function of y), and consequently, (using eqs. (4.13) and (4.16)) the solution for $a$ and $r^-$ are found. After producing these profiles, $s$, $r$, $r^+$ and all the other concentration profiles are found from the integrated linkage equations(eqs. (3.89) to (3.92)), equilibrium (eq. (3.97)) and electroneutrality (eq. (3.94)) equations. Using the iterative method described before in section 4.2.1, the correct solutions for all the concentration profiles are found.

## 4.3   Enhancement Factor Calculations

The enhancement factor is a common constant used to quantify the advantage reaction gives over merely physical absorption for a given species and set of conditions. It is calculated by finding the ratio of dimensional flux in the presence versus the absence of reaction as follows:

$$E_\varphi = \frac{\text{reactive absorption rate}}{\text{absorption rate without reaction}} = \frac{\Phi_{\varphi,o}}{k_L(C_{\varphi,0,no\ rxn} - C_{\varphi,L})} \qquad (4.47)$$

$C_{\varphi,0,no\ rxn}$ is defined as the hypothetical interfacial concentration for the same bulk conditions but in the absence of reaction effects:

$$k_G(C_{\varphi,G} - C_{\varphi,0,no\ rxn}) = k_L(C_{\varphi,0,no\ rxn} - C_{\varphi,L})$$

(4.48)

This can be rewritten as: $\qquad C_{\varphi,0,no\ rxn} = \dfrac{k_G C_{\varphi,G} + k_L C_{\varphi,L}}{k_G + k_L}$ (4.49)

$k_L$ and $k_G$ are the liquid and gas phase mass transfer coefficients, respectively, where $k_L = \frac{D_L}{L}$ and $k_G = \frac{D_G}{G}$. Using the dimensionless concentration profiles for $a$ and $s$ as a function of y (to find a at $y = 0$ and s at $y = 0$), the flux is found as follows:

$$\Phi_{A,0} = -D_A \left.\frac{dA}{dx}\right|_{x=0} = -\frac{D_A P_A H_A \left.\frac{da}{dy}\right|_{y=0}}{L} = \frac{D_A P_A H_A \lambda_4 (a_G - a_0)}{L}$$

(4.50)

$$\Phi_{S,0} = -D_S \left.\frac{dS}{dx}\right|_{x=0} = -\frac{D_S P_S H_S \left.\frac{ds}{dy}\right|_{y=0}}{L} = \frac{D_S P_S H_S \lambda_4 (s_G - s_0)}{L}$$

(4.51)

$a_G$ is known from eq. (3.60). This is then used to define the enhancement factors for $CO_2$ and $H_2S$ as follows:

$$E_A = \frac{\Phi_{A,0}}{k_L(A_{0,no\ rxn} - A_L)}$$

(4.52)

$$E_S = \frac{\Phi_{S,0}}{k_L(S_{0,no\ rxn} - S_L)}$$

(4.53)

$CO_2$ and $H_2S$ are assumed to have the same $k_L$ and $k_G$ values.

# Chapter 5

# Limiting Cases

This chapter presents analyses of the derivations of two limiting cases. The first is the absence of reaction effects. The second is when all reactions occur instantaneously, so that local equilibrium is attained. This condition is approached when the liquid film is sufficiently thick. The numerical and approximate solutions converge to expected results for large thicknesses.

## 5.1   No Reactions Effects Limit

In this scenario, the acid gas differential mass balances simplify to

$$\frac{d^2a}{dy^2} = 0 \tag{5.1}$$

$$\frac{d^2\mathrm{s}}{dy^2} = 0 \tag{5.2}$$

The boundary conditions remain the same:

$$\left.\frac{da}{dy}\right|_{y=0} = -\lambda_4(a_G - a_0) \tag{3.72}$$

$$\left.\frac{ds}{dy}\right|_{y=0} = -\lambda_5(s_G - s_0) \tag{3.75}$$

$$a(y_1) = a_L \tag{3.79}$$

$$s(y_1) = s_L \tag{3.85}$$

The differential equations are easily solved to yield the following expressions for $a_0$ and $s_0$:

$$a_0 = \frac{\lambda_4 a_G + a_L}{\lambda_4 + 1} = a_{0,no\ rxn} \tag{5.3}$$

$$s_0 = \frac{\lambda_5 s_G + s_L}{\lambda_5 + 1} = s_{0,no\ rxn} \tag{5.4}$$

# 5.2   Local Reaction Equilibrium

In sufficiently thick films the reactions attain equilibria locally throughout the liquid film.

## 5.2.1   Mathematical Development

The linkage differential equations remain:

$$\lambda_1 \frac{d^2 a}{dy^2} + \frac{d^2 b}{dy^2} + \frac{d^2 c}{dy^2} + \lambda_2 \frac{d^2 r^-}{dy^2} = 0 \tag{5.5}$$

$$\frac{d^2 r}{dy^2} + \frac{d^2 r^+}{dy^2} + \frac{d^2 r^-}{dy^2} = 0 \tag{5.6}$$

$$\lambda_3 \frac{d^2 s}{dy^2} + \frac{d^2 s^-}{dy^2} = 0 \tag{5.7}$$

$$\frac{d^2 r_3}{dy^2} + \frac{d^2 r_3^+}{dy^2} = 0 \tag{5.8}$$

The boundary conditions continue to hold:

$$\frac{da}{dy}\bigg|_{y=0} = -\lambda_4(a_G - a_0) \tag{5.9}$$

$$\frac{db}{dy}\bigg|_{y=0} + \frac{dc}{dy}\bigg|_{y=0} + \frac{d\mathrm{r}^-}{dy}\bigg|_{y=0} = 0 \tag{5.10}$$

$$\frac{dr}{dy}\bigg|_{y=0} + \frac{d\mathrm{r}^-}{dy}\bigg|_{y=0} + \frac{d\mathrm{r}^+}{dy}\bigg|_{y=0} = 0 \tag{5.11}$$

$$\frac{ds}{dy}\bigg|_{y=0} = -\lambda_5(s_G - s_0) \tag{5.12}$$

$$\frac{d\mathrm{s}^-}{dy}\bigg|_{y=0} = 0 \tag{5.13}$$

$$\frac{d\mathrm{r}_3}{dy}\bigg|_{y=0} + \frac{d\mathrm{r}_3^+}{dy}\bigg|_{y=0} = 0 \tag{5.14}$$

The generally applicable equilibrium relationships of course still hold, i.e.:

$$\begin{aligned} \mathrm{r}_3^+ &= \frac{C_T^2 \mathrm{r}_3 h}{K_9 K_{12}} = \lambda_7 \mathrm{r}_3 h & \mathrm{r}^+ &= \frac{C_T^2 r h}{K_{10} K_{12}} = \lambda_8 r h \\ c &= \frac{K_{11} K_{12} b}{C_T^2 h} = \frac{\lambda_9 b}{h} & \mathrm{s}^- &= \frac{K_{13} P_S H_S s}{C_T^2 h} = \frac{\lambda_{10} s}{h} \\ \mathrm{oh}^- &= \frac{K_{12}}{C_T^2 h} = \lambda_{11} h \end{aligned} \tag{5.15}$$

In the local equilibrium limit, there are two additional equilibria to enforce, i.e.:

$$a = \frac{bhCT^2}{K_1 P_A H_A} = \lambda_{12} bh \tag{5.16}$$

$$\mathrm{r}^- = \frac{K_4 K_5 P_A H_A a r}{\lambda_8 h} = \lambda_{13} \lambda_{12} br \tag{5.17}$$

Electroneutrality still holds:

$$\lambda_6 \mathrm{r}_3^+ + \lambda_2 \mathrm{r}^+ + m + \mathrm{h} = b + 2c + \lambda_2 \mathrm{r}^- + \mathrm{s}^- - \mathrm{oh}^- \tag{5.18}$$

44

## 5.2.2   Method of Solution

The differential and linkage equations above are integrated as in Section 3.6.3 to give:

$$\lambda_1 a + b + c + \lambda_2 \mathrm{r}^- = [-\lambda_1 \lambda_4 (a_G - a_0)]y + \lambda_1 a_L + b_L + c_L + \lambda_2 \mathrm{r}_L^- + \lambda_1 \lambda_4 (a_G - a_0)$$

(5.19)

$$\lambda_3 s + \mathrm{s}^- = [-\lambda_3 \lambda_5 (s_G - s_0)]y + \lambda_3 s_L + \mathrm{s}_L^- + \lambda_3 \lambda_5 (s_G - s_0) \tag{5.20}$$

$$r + \mathrm{r}^+ + \mathrm{r}^- = r_L + \mathrm{r}_L^+ + \mathrm{r}_L^- = 1 \tag{5.21}$$

$$r^3 + \mathrm{r_3}^+ = r_L^3 + \mathrm{r}_{3L}^+ = 1 \tag{5.22}$$

It follows that at $y = 0$:

$$\lambda_1 \lambda_{12} b_0 h_0 + \lambda_1 \lambda_4 \lambda_{12} b_0 h_0 + b_0 + c_0 + \lambda_2 \lambda_{13} \lambda_{12} b_0 r_0$$
$$= \lambda_1 a_L + b_L + c_L + \lambda_2 \mathrm{r}_L^- + \lambda_1 \lambda_4 a_G$$

(5.23)

$$s_0 \left( \lambda_3 + \frac{\lambda_{10}}{h_0} + \lambda_3 \lambda_5 \right) = \lambda_3 s_L + \mathrm{s}_L^- + \lambda_3 \lambda_5 s_G \tag{5.24}$$

$$r_0 (1 + \lambda_8 h_0 + \lambda_{13} \lambda_{12} b_0) = r_L + \mathrm{r}_L^+ + \mathrm{r}_L^- = 1 \tag{5.25}$$

$$r_{3,0} (1 + \lambda_7 h_0) = r_{3,L} + \mathrm{r}_{3L}^+ = 1 \tag{5.26}$$

$$\lambda_6 \lambda_7 r_{3,0} h_0 + \lambda_2 (\lambda_8 r_0 h_0 - \lambda_{12} b_0 r_0) + m - b_0 - 2c_0 - \frac{\lambda_{10} s_0}{h_0} = 0 \tag{5.27}$$

These can be combined to yield the following two equations:

$$b_0 - \chi_1 + c_0 + \frac{\lambda_1 \lambda_9 \lambda_{12} b_0^2}{c_0} + \frac{\lambda_2 \lambda_{12} \lambda_{13} b_0}{\lambda_{12} \lambda_{13} b_0 + \frac{\lambda_8 \lambda_9 b_0}{c_0} + 1} + \frac{\lambda_1 \lambda_4 \lambda_9 \lambda_{12} b_0^2}{c_0} = 0 \tag{5.28}$$

$$m - 2c_0 - b_0 + \frac{\lambda_6 \lambda_7 \lambda_9 b_0}{c_0 + \lambda_7 \lambda_9 b_0} - \frac{\lambda_2 \lambda_{12} \lambda_{13} b_0}{\lambda_{12} \lambda_{13} b_0 + \frac{\lambda_8 \lambda_9 b_0}{c_0} + 1}$$
$$- \frac{\chi_2 \lambda_{10} c_0}{\lambda_9 b_0 (\lambda_3 + \lambda_3 \lambda_5 + \frac{\lambda_{10} c_0}{\lambda_9 b_0})} + \frac{\lambda_2 \lambda_8 \lambda_9 b_0}{c_0 (\lambda_{12} \lambda_{13} b_0 + \frac{\lambda_8 \lambda_9 b_0}{c_0} + 1)} = 0$$

(5.29)

45

where $\chi_1$ and $\chi_2$ are sums of the bulk liquid conditions defined as follows:

$$\chi_1 = \lambda_1 a_L + b_L + c_L + \lambda_2 \mathrm{r}_L^- + \lambda_1 \lambda_4 a_G \qquad (5.30)$$

$$\chi_2 = \lambda_3 s_L + \mathrm{s}_L^- + \lambda_3 \lambda_5 s_G \qquad (5.31)$$

Using the two equations, eqs. (5.28) and (5.29), $b_0$ and $c_0$ and using a root solver to solve these equations iteratively, $a_0$ is found and consequently, the flux and the enhancement factor is calculated.

# Chapter 6

# Physicochemical Properties and Model Parameter Estimation

## 6.1 Kinetic Parameters

Table 6.1 presents expressions for calculating kinetic and equilibrium parameters for reactions 3.9 - 3.21, and their values at 298.15 K.

In addition, the following kinetics data were taken from (**a**) Danckwerts and Sharma (1966), (**b**) Versteeg and van Swaaij (1988) and (**c**) Littel *et al.* (1992):

$$
\begin{aligned}
&k_1 = 0.026 \ s^{-1} \ ^{\mathbf{a}} & &k_4 = 3.13 \cdot 10^6 \frac{cm^3}{mol \ s}^{\mathbf{c}} \\[2ex]
&\frac{k_5}{k_{-4}} = 231 \frac{cm^3}{mol}^{\mathbf{c}} & &\frac{k_{6,DEMEA}}{k_{-4}} = 3.5 \cdot 10^{-1} \frac{dm^3}{mol}^{\mathbf{c}} \\[2ex]
&\frac{k_{6,\mathrm{MDEA}}}{k_{-4}} = 113 \frac{cm^3}{mol}^{\mathbf{c}} & &\frac{k_{6,\mathrm{TEA}}}{k_{-4}} = 2.22 \cdot 10^{-2} \frac{dm^3}{mol}^{\mathbf{b}} \\[2ex]
&\frac{k_7}{k_{-4}} = 5.37 \cdot 10^{-1} \frac{cm^3}{mol}^{\mathbf{c}} & &\frac{k_8}{k_{-4}} = 22.5 \cdot 10^3 \frac{cm^3}{mol}^{\mathbf{c}}
\end{aligned}
\tag{6.1}
$$

47

| Kinetic Parameter | Correlation | Temp Range(K) | Value at 298.15 K | Reference |
|---|---|---|---|---|
| $k_2$ | $log_{10}(k_2) = 13.635 - \frac{2895}{T}$ | 273-313 | $8.4 \cdot 10^6 \frac{cm^3}{mol\ s}$ | Pinsent *et al.* (1956) |
| $k_3$ | $k_3 = 2.91 \cdot 10^7 exp(\frac{-4579}{T})$ | 293-342 | $6.22 \cdot 10^3 \frac{cm^3}{mol\ s}$ | Rinker *et al.* (1995) |
| $k_4$ | $k_4 = 1.24 \cdot 10^6 exp(\frac{-1701}{T})$ | 293-343 | $4.1 \cdot 10^6 \frac{cm^3}{mol\ s}$ | Rinker *et al.* (1996) |
| $\frac{k_4 k_5}{k_{-4}}$ | $\frac{k_4 k_5}{k_{-4}} = 3.18 \cdot 10^7 exp(\frac{-3040}{T})$ | 293-343 | $1.1 \cdot 10^9 \frac{cm^6}{mol^2\ s}$ | Rinker *et al.* (1996) |
| $K_1$ | $log_{10}(K_1) = 179.648 + 0.019244T - 67.341 log_{10}(T) - \frac{7495.441}{T}$ | 273 -523 | $4.156 \cdot 10^{-10} \frac{mol}{cm^3}$ | Read (1975) |
| $K_{12}$ | $log_{10}(K_{12}) = 8909.483 - \frac{142613.6}{T} - 4229.195\ log_{10}(T) + 9.7384T - 0.0129638T^2 + (1.15068 \cdot 10^{-5})T^3 - (4.602 \cdot 10^{-9})T^4$ | 293 -573 | $10^{-20} \frac{mol^2}{cm^6}$ | Oloffson and Hepler (1975) |
| $K_9$ | $log_{10}(K_9 K_{12}) = -14.01 + 0.018T$ | 298 -333 | $2.274 \cdot 10^8 \frac{cm^3}{mol}$ | Barth *et al.* (1981) |
| $K_{10}$ | $log_{10}(K_{10} K_{12}) = -4.0302 - \frac{1830.15}{T} + 0.0043T$ | 298 -333 | $1.299 \cdot 10^8 \frac{cm^3}{mol}$ | Barth *et al.* (1981) |
| $K_{11}$ | $log_{10}(K_{11} K_{12}) = 6.498 - 0.0238T - \frac{2902.4}{T}$ | 273 -323 | $4.6 \cdot 10^6 \frac{cm^3}{mol}$ | Danckwerts and Sharma (1966) |
| $K_4 K_5 K_{10} K_{12}$ | $log_{10}(K_4 K_5 K_{10} K_{12}) = -10.5492 + \frac{1526.27}{T}$ | 298 -333 | $3.7148 \cdot 10^{-6}$ | Barth *et al.* (1981) |
| $K_{13}$ | $ln K_{13} = 218.599 - 33.5471\ ln T - \frac{12995.4}{T}$ | 273 -423 | $9.925 \cdot 10^{-11} \frac{mol}{cm^3}$ | Edwards *et al.* (1978) |

Table 6.1: Reaction kinetic and equilibrium parameter values at 298.15 K.

| Parameter | Value | | | |
|---|---|---|---|---|
| | **DIPA** | **MEA** | **DEMEA** | **TEA** |
| $pK_a$ | $8.89^{\mathbf{d}}$ | $9.51^{\mathbf{d}}$ | $9.61^{\mathbf{c}}$ | $7.88^{\ \mathbf{c}}$ |
| $k_3\ \left(\frac{dm^3}{mol\ s}\right)$ | - | - | $43.8^{\mathbf{c}}$ | $3.74^{\mathbf{c}}$ |
| $K_4 K_5$ | $1.73 \cdot 10^{-6\ \mathbf{a}}$ | $8.61 \cdot 10^{-6\ \mathbf{e}}$ | - | - |
| $k_4\ \left(\frac{dm^3}{mol\ s}\right)$ | $2.78 \cdot 10^{3\ \mathbf{d}}$ | $4.45 \cdot 10^{3\ \mathbf{d}}$ | - | - |
| $\frac{k_5}{k_{-4}}\ \left(\frac{dm^3}{mol}\right)$ | $7.19 \cdot 10^{-2\ \mathbf{d}}$ | $2.22^{\ \mathbf{f}}$ | - | - |
| $\frac{k_{6,\mathrm{DEMEA}}}{k_{-4}}\ \left(\frac{dm^3}{mol}\right)$ | $1.64 \cdot 10^{-1\ \mathbf{b}}$ | - | - | - |
| $\frac{k_{6,\mathrm{MDEA}}}{k_{-4}}\ \left(\frac{dm^3}{mol}\right)$ | $5.99 \cdot 10^{-2\ \mathbf{b}}$ | $6.8 \cdot 10^{-2\ \mathbf{f}}$ | - | - |
| $\frac{k_{6,\mathrm{TEA}}}{k_{-4}}\ \left(\frac{dm^3}{mol}\right)$ | $1.03 \cdot 10^{-2\ \mathbf{b}}$ | $1.08^{\ \mathbf{g}}$ | - | - |
| $\frac{k_7}{k_{-4}}\ \left(\frac{dm^3}{mol}\right)$ | $1.83 \cdot 10^{-4\ \mathbf{b}}$ | $1.5 \cdot 10^{-3\ \mathbf{f}}$ | - | - |

**a** Blauwhoff *et al.* (1985), **b** Versteeg and van Swaaij (1988), **c** Littel *et al.* (1990), **d** Littel *et al.* (1992),**e** Aroua *et al.* (1999), **f** Horng and Li (2002), **g**Liao and Li (2002)

Table 6.2: Kinetic parameters for DIPA, MEA, DEMEA and TEA.

All other equilibrium constants are related as follows to those listed:

$$K_2 = \frac{K_1}{K_{12}} \qquad K_3 = \frac{K_1}{K_9 K_{12}} \qquad K_6 = \frac{K_5 K_{10}}{K_9} \qquad K_7 = K_5 K_{10} K_{12} \qquad K_8 = K_5 K_{10}$$

$$(6.2)$$

Kinetic data used for the other amines used to compare with DEA and MDEA, i.e., di-isopropanolamine (DIPA), monoethanolamine (MEA), diethyl monoethanolamine (DEMEA) and triethylamine (TEA), are summarized in Table 6.2.

## 6.2 Physical Parameters

Liquid-phase diffusivities are estimated at a temperature of 298.15 K from experimental interpolations ((**a**)Cents *et al.* (2005) and (**b**) Sema *et al.* (2012).

$$^{\mathbf{a}}D_A = D_S = 2 \cdot 10^{-5}\ \frac{cm^2}{s}$$

$$^{\mathbf{b}}D_B = D_C = D_R = D_{R^-} = D_{R^+} = D_{R_3} = D_{R_3^+} = D_{S^-} = 2 \cdot 10^{-5}\ \frac{cm^2}{s} \qquad (6.3)$$

Gas-phase diffusion coefficients for $CO_2$ and $H_2S$ are both estimated at

$2 \cdot 10^{-1} \frac{cm^2}{s}$ (Bergman *et al.*, 2011). The industrially relevant film thickness ranges are as follows ((**a**)Hoffmann *et al.* (2007) and (**b**) Rejl *et al.* (2009)):

$$L^{\mathbf{a}} = 1 \cdot 10^{-4} - 1 \cdot 10^{-2} \ cm = 1 - 100 \ \mu m$$
$$G^{\mathbf{b}} = 1 \cdot 10^{-2} - 1 \cdot 10^{-1} \ cm = 100 - 1000 \ \mu m \tag{6.4}$$

However, for enhancement factor calculation purposes, in analyses, the film thicknesses were varied over wider ranges. The baseline thicknesses were set at $1 \cdot 10^{-3}$ cm (10 $\mu$m) and $1 \cdot 10^{-2}$ cm (100 $\mu$m) for the liquid and gas films, respectively.

Bulk gas partial pressures were fixed at 1 atm for $CO_2$ and 0.1 atm for $H_2S$. The baseline bulk liquid acid gas loadings were set at zero. The bulk liquid pH was fixed at 10 by adjusting the concentration of strong acid (or, if necessary, base), M in $\frac{mol}{L}$, in the electroneutrality equation (eq. (3.52)). The baseline amine blend was 2.5 M MDEA plus 1.5 M DEA; they were varied in the theoretical calculations over the industrially relevant ranges of 10 to 30 wt% DEA and 30-50 wt % MDEA (Kohl and Nielsen, 1997).

# Chapter 7

# Results

This chapter presents calculated enhancement factors (defined in eq. (4.47)) for $CO_2$ and $H_2S$ absorption. Base case conditions were as follows: T=298K, bulk liquid: 13.9 wt% (1.5 M) DEA, 26.5 wt% (2.5 M) MDEA; acid gas loadings = 0; pH fixed at 10 by the inclusion of strong acid, (or, if necessary, base, ) - to satisfy the electroneutrality equation (eq. (3.52)). Unless indicated otherwise, bulk gas phase $CO_2$ and $H_2S$ partial pressures were 1 atm and 0.1 atm, respectively, and the gas and liquid film thicknesses were 100 and 10 $\mu$m, respectively.

The absorption rates of the two acid gases are expressed in terms of two dimensionless ratios;

(1) the aforementioned enhancement factors (E) defined as follows:

$$\text{E} = \frac{\text{reactive absorption rate}}{\text{absorption rate without reaction}} = \frac{\Phi_{\varphi,0}}{k_L(C_{\varphi,0,no\ rxn} - C_{\varphi,L})} \qquad (4.47)$$

where $\Phi_{\varphi,0}$ is the absorption (or desportion) flux of species $\varphi$ at the interface (where $x = 0$) and $C_{\varphi,0,no\ rxn}$ denotes its hypothetical interfacial concentration of $\varphi$ in a system with the same bulk gas and equilibrium bulk liquid partial pressures, but without reaction effects (i.e., with zero gradients in the

concentrations of nonvolatile solutes).

(2), selectivity for $H_2S$ [the maximization of which is frequently the operational goal see, for example, Xu *et al.* (2002)], defined here as the ratio of $H_2S$ and $CO_2$ fluxes, divided by the ratio of their absorption driving forces (i.e., the differences between their partial pressures in bulk gas and in equilibrium with bulk liquid):

$$\text{Selectivity, S} = \frac{(P_{A,G} - C_{A,L} \times K_{H,A})\Phi_S}{(P_{S,G} - C_{S,L} \times K_{H,S})\Phi_A} \tag{7.1}$$

where $K_{H,A}$ and $K_{H,S}$ are $CO_2$ and $H_2S$ volatility constants.

In the figures that immediately follow, enhancement factors and $H_2S$ selectivity are plotted vs. gas film thicknesses, G, or the Hatta number, i.e.,:

$$Ha_1 = L\sqrt{\frac{k_1}{D_A}} \tag{7.2}$$

Since the $CO_2$ hydration rate constant, $k_1$, and diffusivity, $D_A$, are fixed at constant values, $Ha_1$ is a dimensionless surrogate for L.

As was noted in section 6.2, typical operating gas and liquid film thickness ranges are, respectively, 100-1000 $\mu$m and 1-100 $\mu$m ($Ha_1$=0.03-0.3). When the plotted range is wider, gray shading delimits the typical range.

Average absolute deviation (AAD), defined below, is used to quantify the mismatch between results based on one of the VKH ("A" for "approximate") solutions and the numerical ("N") solutions for each set of n data points:

$$AAD = \frac{\sum_{k=1}^{n} |A_k - N_k|}{\sum_{k=1}^{n} |N_k|} \times 100 \tag{7.3}$$

## 7.1 Dependence upon Gas and Liquid Film Thicknesses

Figures 7-1a and 7-1b present the two VKH-based estimates of the respective enhancement factors for $CO_2$ and $H_2S$ absorption ($E_A$ and $E_S$) vs. gas film thickness, G, in the range 0.1-1100 $\mu$m. Included for comparison are E values based on essentially exact numerical analysis. The two VKH methods were discussed in depth in Chapter 4: VKH Method 1 (Section 4.2.1) solves the two ODEs sequentially, and VKH Method 2 (Section 4.2.2) is a modified method introduced by Fiordalis (2017), which solves the OD$E_S$ simultaneously.

An interesting observation based on the plots is that the absorption rate of $H_2S$ significantly decreases (by 50%) over the typical range of operating G values. Hamour *et al.* (1987) were among the early pioneers to identify the dependence of $H_2S$ absorption on the gas-phase mass transfer coefficient, $k_G$, which they vaired by adjusting the speed of a gas phase impeller. Based on their stirred-cell experiments and film theory model predictions, they deduced that the $H_2S$ concentration at the gas-liquid interface could approach zero, in which limiting case $H_2S$ absorption became entirely gas-phase mass transfer-controlled. Larger gas mass transfer coefficients increased selectivity for $H_2S$ absorption. The gas mass transfer coefficient in our simulations was determined by the gas-film thickness, G (where $G = \frac{D_{G,\varphi}}{k_{G,\varphi}}$ for species $\varphi$). Figure 7-2 shows the dependence of $H_2S$ selectivity (based on the calculated enhancement factors plotted in figs. 7-1a and 7-1b) upon gas film thickness changes, which is consistent with the observation of Hamour *et al.*.
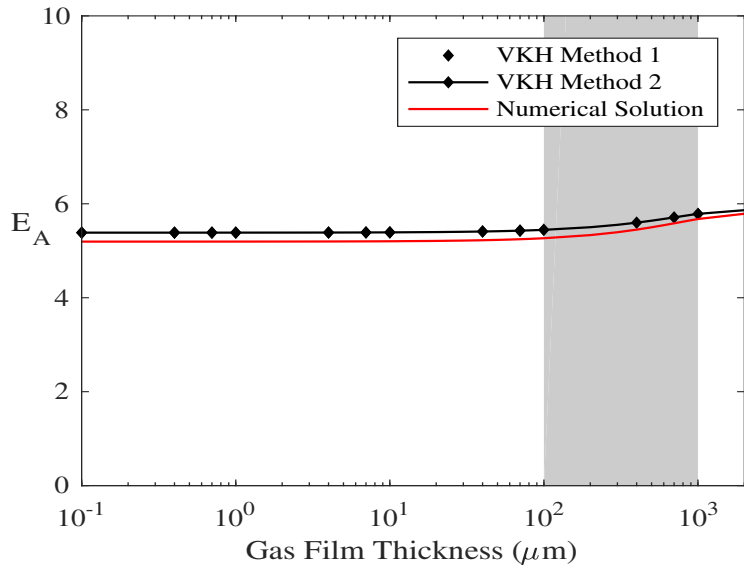
(a)
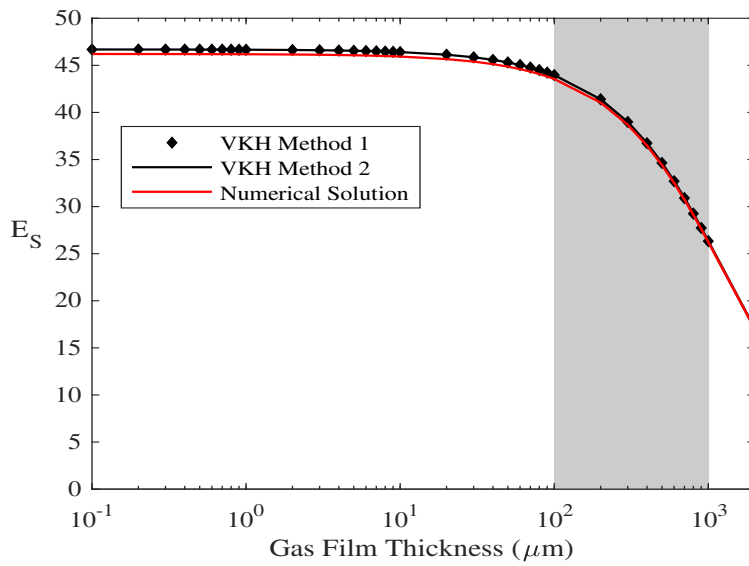


(b)

Figure 7-1: $CO_2$ (a) and $H_2S$ (b) enhancement factor vs. gas film thickness under baseline conditions.
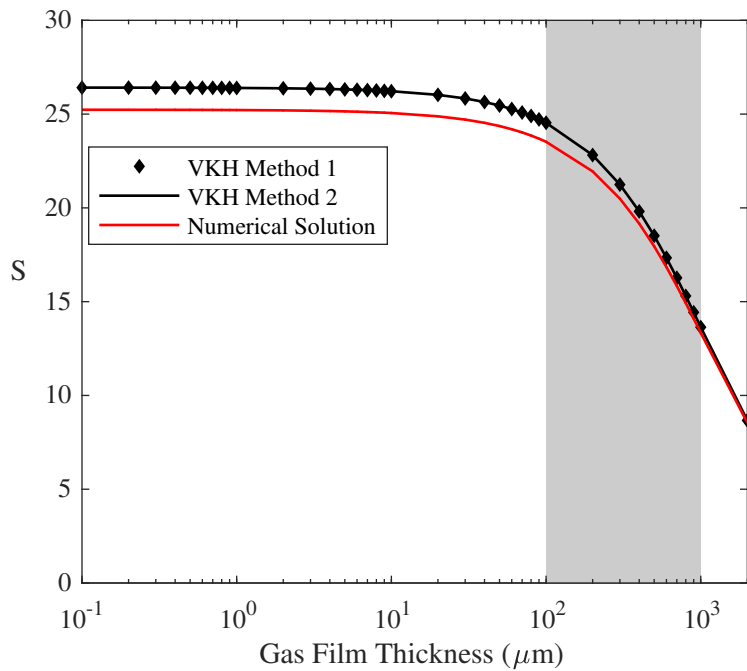
54

Figure 7-2: H$_2$S Selectivity vs. gas film thickness under baseline conditions.
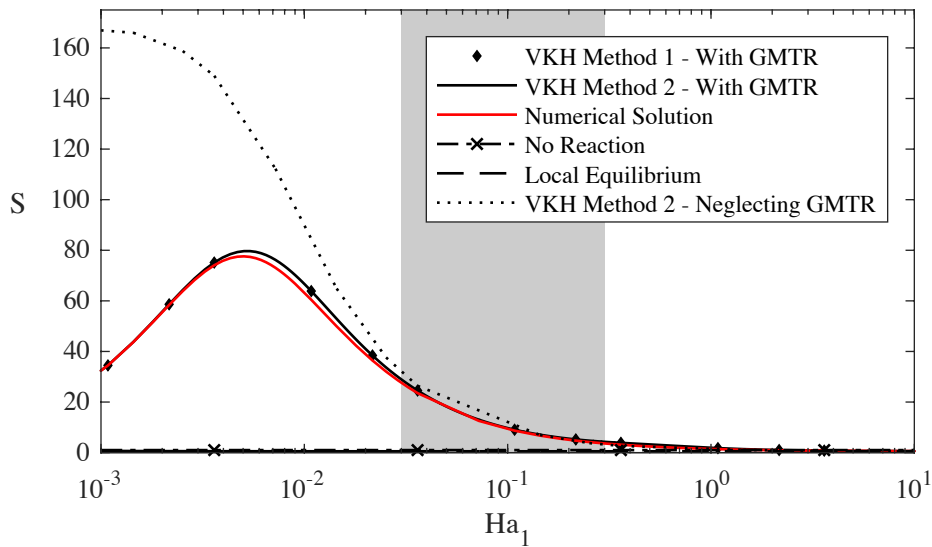


Figure 7-3: H$_2$S Selectivity vs. Hatta number under baseline conditions.

Figure 7-3 depicts the corresponding dependence of S on $Ha_1$(note that in industrial-scale packed columns, typical operating Hatta numbers $(Ha_1)$ are in the range 0.03-0.3). Included for comparison are selectivity values calculated

via exact numerical analysis, and via VKH approximate method 2 assuming no gas-phase mass transfer resistance. The significant errors introduced by the latter assumption are apparent, including in the typical $Ha_1$ range, and especially at lower Hatta numbers, corresponding to the thinner liquid films which prevail under turbulent conditions. The reason for deviation is due to the neglected $H_2S$ gas-phase mass transfer resistance. As may be seen in Table 7.1, the selectivities based on VKH methods 1 and 2, and accounting for gas mass transfer resistance, are in close agreement with results based on numerical analysis (AAD=3.69% and 2.5%, respectively). This may be compared with the 20 % error reported by Glasscock and Rochelle (1993) in their results for a similar system, as discussed in Chapter 2.

The next two figures, Figures 7-4a and 7-4b, depict the dependence of $E_A$ and $E_S$ on the Hatta number for the same conditions as indicated in Figure 7-3. The limiting behavior described in Chapter 5 - (1) the limit of no enhancement of $CO_2$ absorption, or $E_A = 1$, (where bulk equilibrium is retained but no reaction-enhanced CO2 absorption occurs), and (2) the local equilibrium limit (where all reactions are assumed to attain local equilibrium) - are included for comparison. When the Hatta number is less than 0.003, $E_A$ is barely above one, because $CO_2$ reaction times far exceed diffusion times. As the liquid film thickness increases, $H_2S$ absorption is no longer gas-phase controlled and liquid-phase resistance becomes significant. Initially, $H_2S$ absorption is enhanced much more than that of $CO_2$ because $CO_2$'s reactions are still too slow. When $Ha_1$ increases beyond 0.01, $CO_2$ absorption is noticeably enhanced, leading to changes in pH which decrease both $E_S$ and $H_2S$ selectivity. When $Ha_1$ exceeds 6, $E_A$ and $E_S$ approach their local equilibrium limits.

Al Hashimi (2000) found $H_2S$ to perform similarly when simulating absorp-

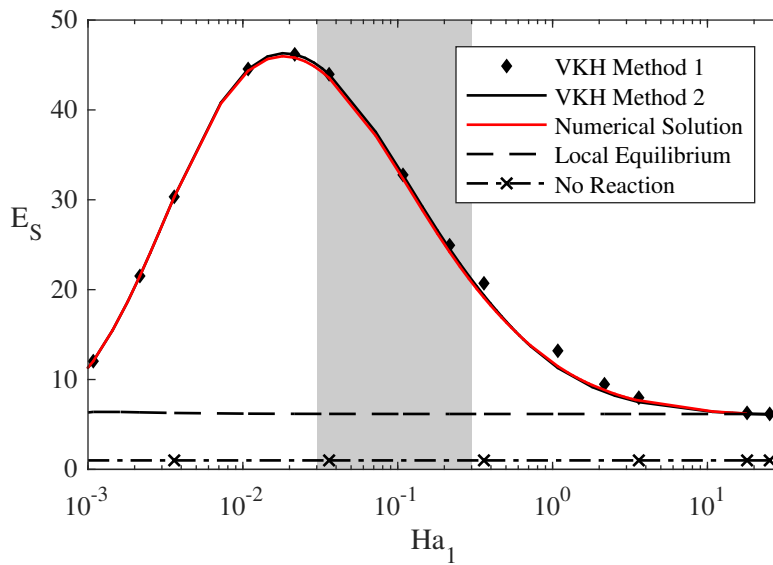| Condition | AAD % | | | | | |
|---|---|---|---|---|---|---|
| | $E_A$ | | $E_S$ | | Selectivity | |
| | VKH Method | | VKH Method | | VKH Method | |
| | 1 | 2 | 1 | 2 | 1 | 2 |
| Varying Gas Film Thickness | 3.15 | 3.09 | 0.94 | 0.94 | 4.37 | 4.30 |
| Varying Liquid Film Thickness | 11.3 | 2.09 | 3.35 | 0.89 | 3.69 | 2.51 |

Table 7.1: AAD values for simulations with varying gas and liquid film thicknesses.

tion of the same two acid gases in a simple aqueous alkali carbonate solutions.

Table 7.1 summarizes the accuracies (expressed as AAD percentages) of the $E_A$ and $E_S$ values calculated based on the two VKH-based approximate solutions, as functions of gas and liquid film thicknesses. Both linearization methods exhibit AAD values of 1-4% as the gas film thickness is varied. The difference between the two VKH methods is most noticeable in fig. 7-4a in the Hatta number range of 0.1-10, where a 15% maximum deviation between the two approximate methods is observed, leading VKH Method 2 to outperform the VKH Method 1 in matching the numerical solution over the wide range of Hatta numbers.
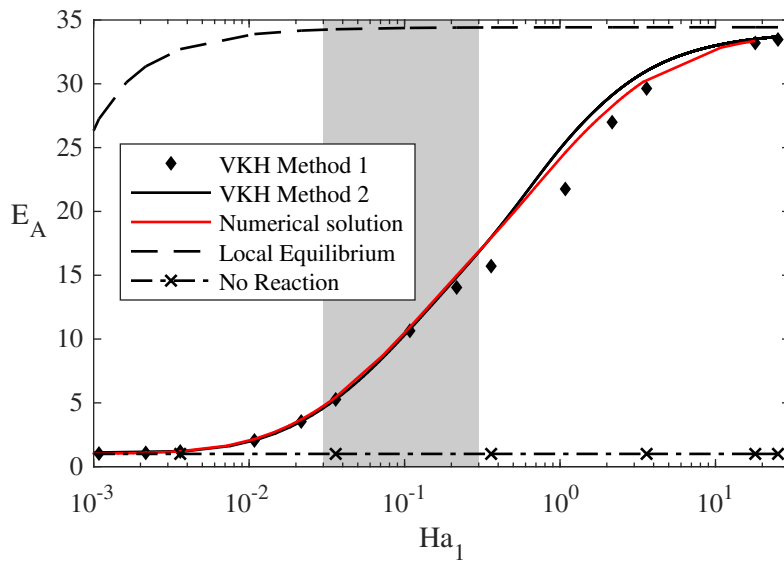
Figure 7-4: $CO_2$ (a) and $H_2S$ (b) enhancement factors vs. Hatta number under baseline conditions.

## 7.2 Reaction Parameter Sensitivity Analysis

For effective simulation studies, it is important to evaluate the sensitivity to changes in each reaction parameter. Such an analysis identifies parameters which need to be accurately known. Figures 7-5 to 7-7 depict the relative changes in calculated $E_A$ and $E_S$ values when the reaction rate and equilibrium constants ($k_i^0$, $K_i^0$) are multiplied by factors ($\epsilon$) at baseline conditions (1.5 M DEA/2.5 M MDEA, zero bulk liquid loadings, $pH = 10$, $CO_2$ and $H_2S$ bulk gas partial pressures are, respectively, 1 and 0.1 atm, at T=298K). Figure 7-7 shows that the two enhancement factors are most sensitive to changes in the primary/secondary amine's $K_a$ ($K_{10}$).

CO$_2$ absorption's critical dependence on reaction rates is underscored by $E_A$'s 50% change as compared to $E_S$'s 20% change when the kinetic rate constants (excluding $k_4$) increase or decrease by two orders of magnitude. The value of the zwitterion formation rate constant, $k_4$, is most critical in determining the CO$_2$ enhancement factor, which increases 200 % when $k_4$ is increased by two orders of magnitude. In the case of H$_2$S, its enhancement factor is, as one might imagine, most sensitive to change in its acid dissociation constant, $K_{13}$, but it is also sensitive to changes in $k_4$ - via its impact on $E_A$, and therefore on pH, and indirectly in turn, on H$_2$S dissociation.
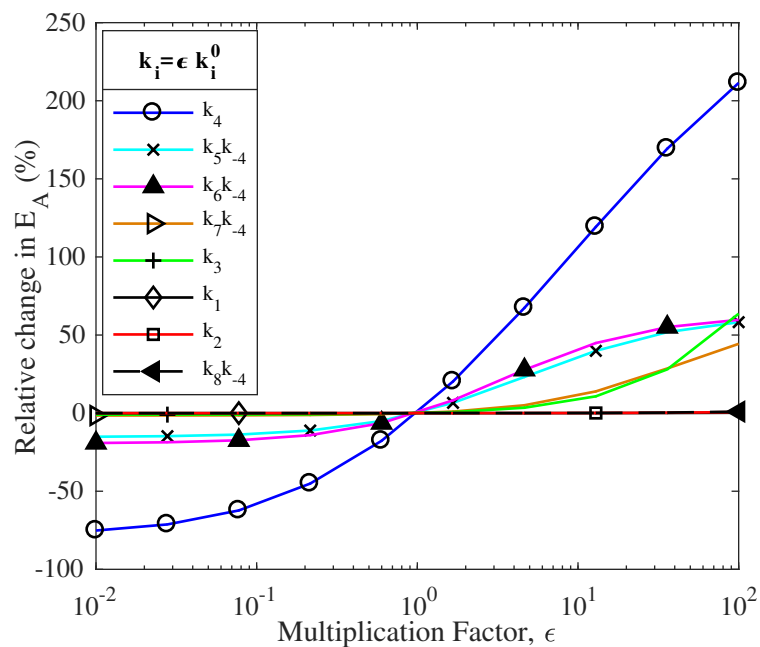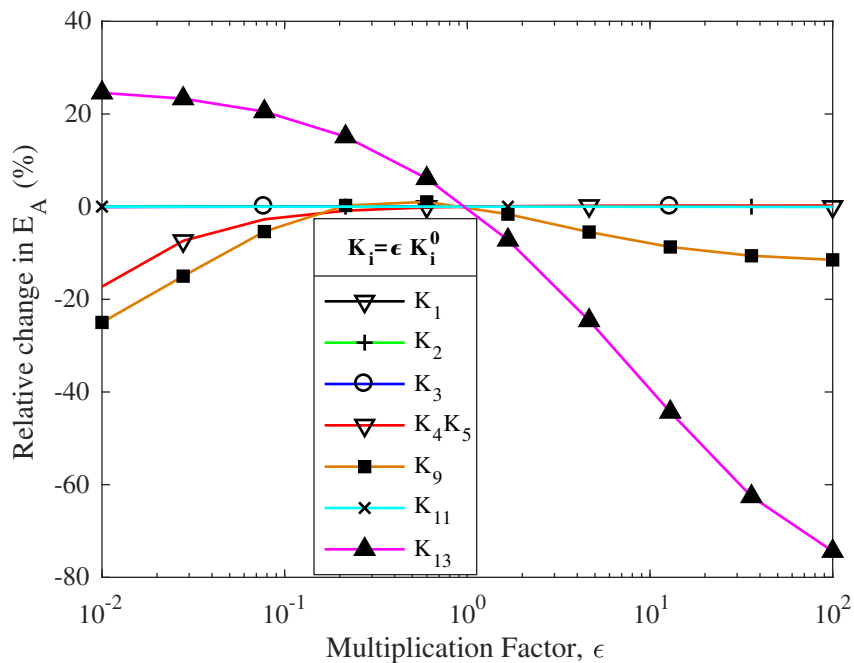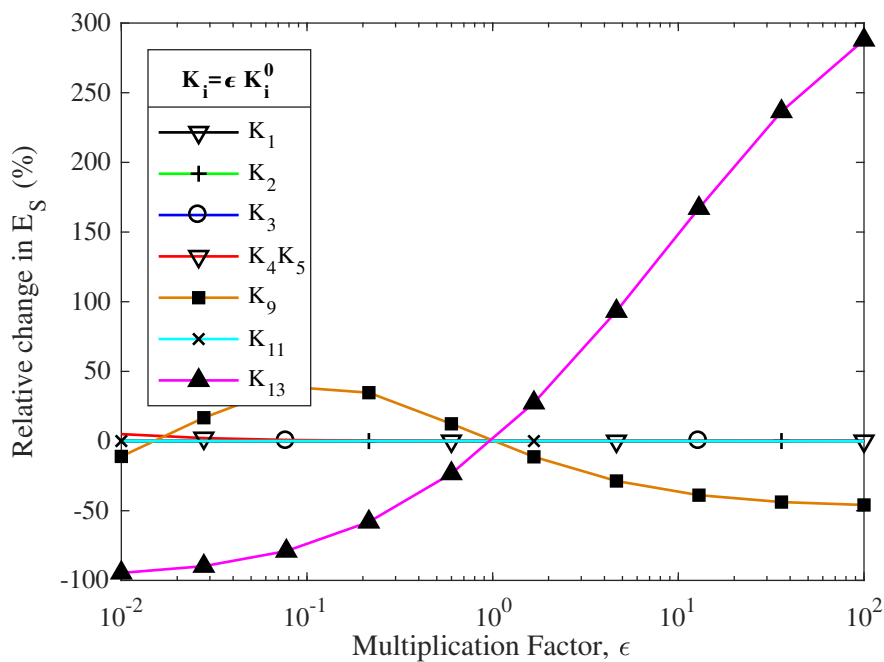
(a)
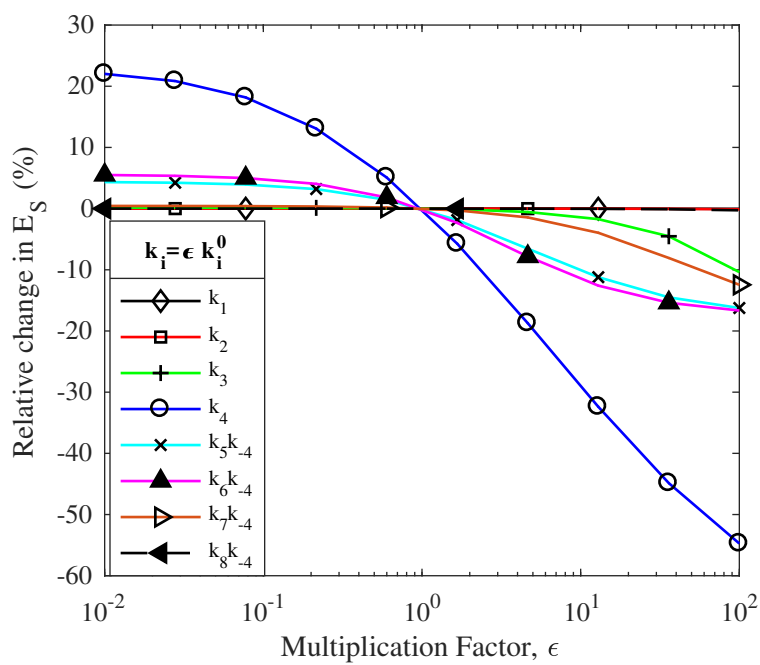


(b)

Figure 7-5: Sensitivity of calculated enhancement factors to changes in reaction rate constants. Curves: results of VKH approximate method 2; Symbols: results of numerical analysis.

(a)



(b)

Figure 7-6: Sensitivity of calculated enhancement factors to changes in reaction equilibrium constants other than $K_{10}$. Curves: results of VKH approximate method 2; Symbols: results of numerical analysis.
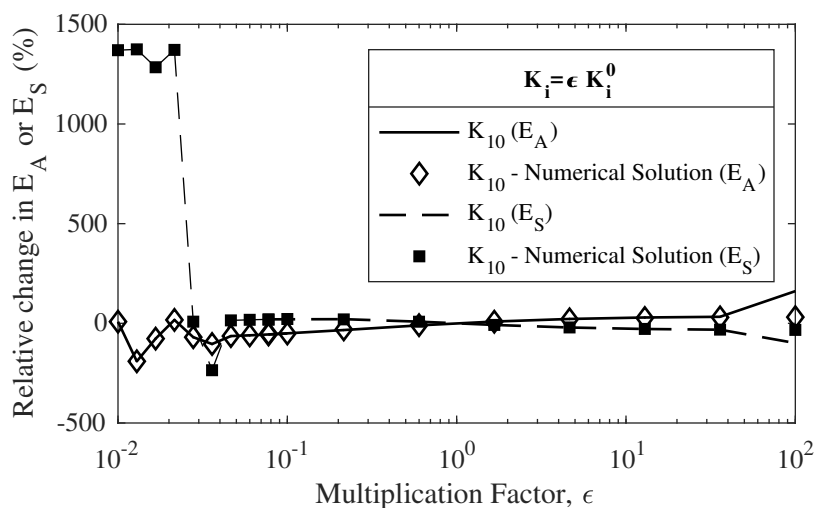
Figure 7-7: Sensitivity of calculated enhancement factors to changes in $K_{10}$. Curves: results of VKH approximate method 2; Symbols: results of numerical analysis.

## 7.3 Bulk Composition Effects

The figures in this section show the calculated dependence on $Ha_1$ of $E_A$, $E_S$ and $H_2S$ selectivity, for several of the industrially relevant amine scrubbing solutions discussed by Kohl and Nielsen (1997), and compare results based on VKH method 2 and numerical analysis. Numerous prior authors have explored the dependence of absorption rates on amine concentrations using both experimental and theoretical methods (for example, Hagewiesche *et al.* (1995); Rinker *et al.* (2000); Liao and Li (2002); Lin *et al.* (2009)). Although the examined papers did not define or seek to find an optimum blend, they all concluded that by mixing a primary or secondary amine with a tertiary amine, $CO_2$'s absorption rate and enhancement factor are both significantly increased. In most experimental investigations, there was no control experiment to provide a basis for comparing the performance of blends. In our simulations, the results of which follow, controls are explicitly defined.

Figures 7-8 to 7-11 explore the performance of DEA and MDEA in single-amine solutions. Figures 7-8b and 7-10b, in particular, show that $E_S$ is more sensitive to changes in MDEA than in DEA concentration, showing a greater increase as MDEA concentration increases. Since DEA and MDEA both act as bases for $H_2S$ deprotonation, it might have been expected that 10 wt% changes in the concentration of either amine, would lead to similar changes in $E_S$. However, $CO_2$ reacts much faster with DEA than with MDEA, and, as result, $CO_2$ absorption in a DEA solution causes a greater drop in pH (which impairs $H_2S$ absorption) than does its absorption in an MDEA solution. The much faster reaction of $CO_2$ with DEA than with MDEA (with reaction constants for DEA and MDEA: $k_3$ and $k_4$, at $T = 298$K as 6.0 and 3100 $\frac{m^3}{kmol\ s}$ respectively) is also responsible for the striking contrast between the behavior of $E_A$ with DEA versus with MDEA seen in figs. 7-8a and 7-10a, respectively. It is also consistent with the data of Rinker *et al.* (1996, 2000), who reported the $CO_2$-amine forward reaction rate constants for MDEA and DEA.

Figures 7-12 and 7-13 depict the calculated dependence of $E_A$, $E_S$ and $H_2S$ selectivity on $Ha_1$ and the proportions of DEA and MDEA in 50 wt% amine blends. As expected, $CO_2$ absorption rates increase and $H_2S$ absorption rates decrease with increase in the proportion of DEA. Thus, $H_2S$ selectivity is promoted by higher MDEA contents.

Chakravarty *et al.* (1985) similarly noted that MDEA favors $H_2S$ absorption. They simulated $CO_2$ absorption in 30 wt% blends of monoethanolamine (MEA, a primary amine) and MDEA in order to identify the optimal proportions. They found 30 wt% MEA optimal at 40 °C, and a blend favorable at higher temperature, but provided no explanation. Lin *et al.* (2009) performed wetted-wall column absorption experiments at similarly temperatures with 20 wt% blends of DEA and MDEA and reported marked increases in the $CO_2$

absorption rate with increasing proportion of DEA.
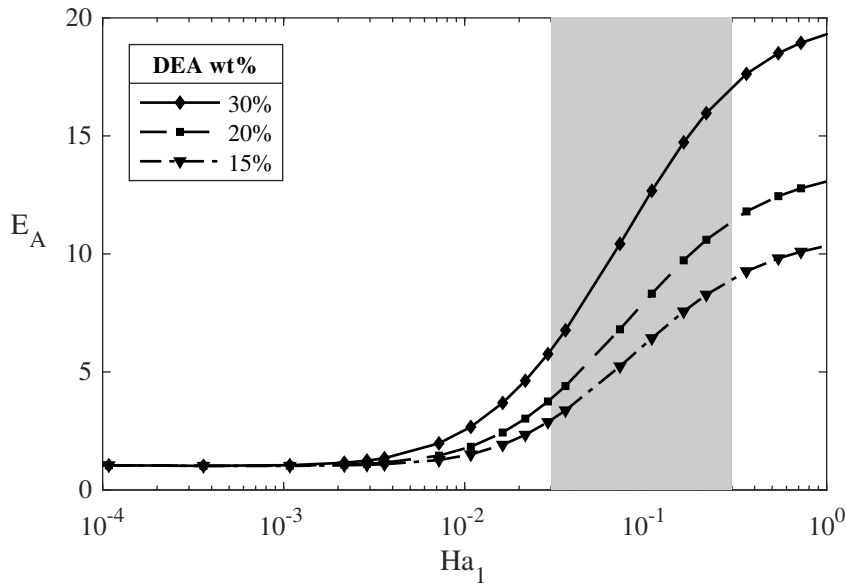


(a)
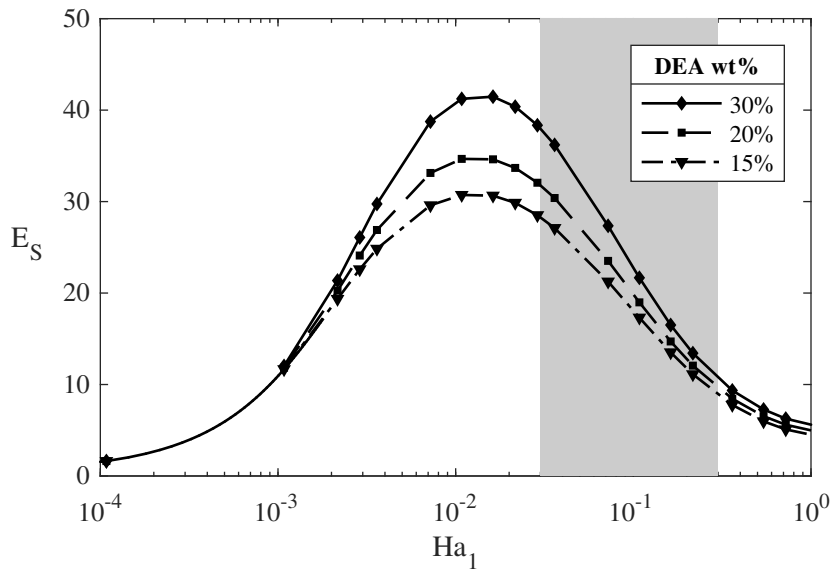


(b)

Figure 7-8: $CO_2$ (a) and $H_2S$ (b) enhancement factors vs. Hatta number and DEA wt%. Curves: results of VKH approximate method 2; Symbols: results of numerical analysis.

Figure 7-9: $H_2S$ selectivity vs. Hatta number and DEA wt%. Curves: results of VKH approximate method 2; Symbols: results of numerical analysis.

(a)



(b)

Figure 7-10: $CO_2$ (a) and $H_2S$ (b) enhancement factors vs. Hatta number and MDEA wt%. Curves: results of VKH approximate method 2; Symbols: results of numerical analysis.
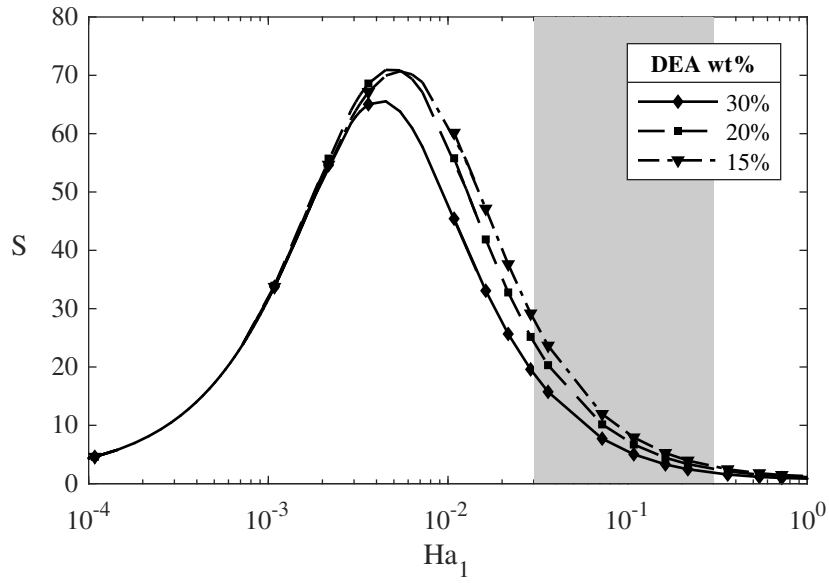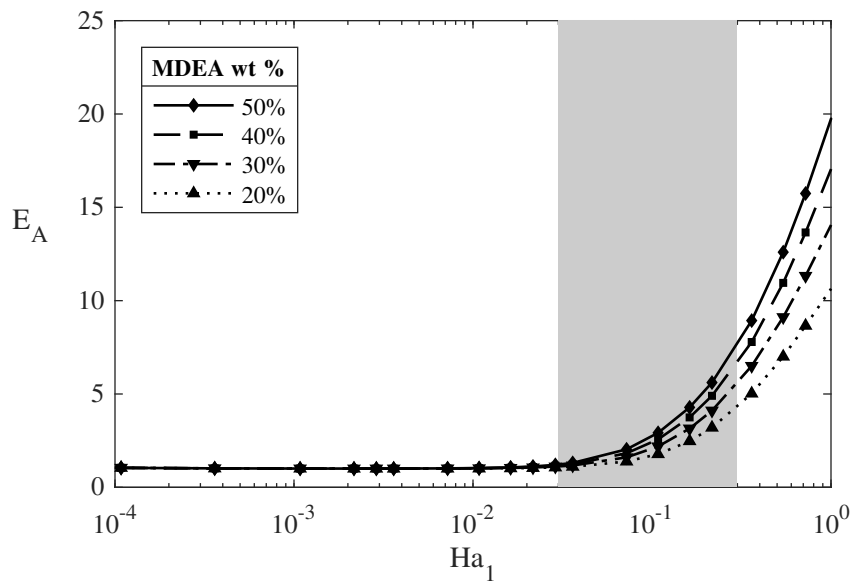
Figure 7-11: H$_2$S selectivity vs. Hatta number and MDEA wt%. Curves: results of VKH approximate method 2; Symbols: results of numerical analysis.

(a)



(b)

Figure 7-12: $CO_2$ (a) and $H_2S$ (b) enhancement factors vs. Hatta number and DEA/MDEA wt%. Curves: results of VKH approximate method 2; Symbols: results of numerical analysis.
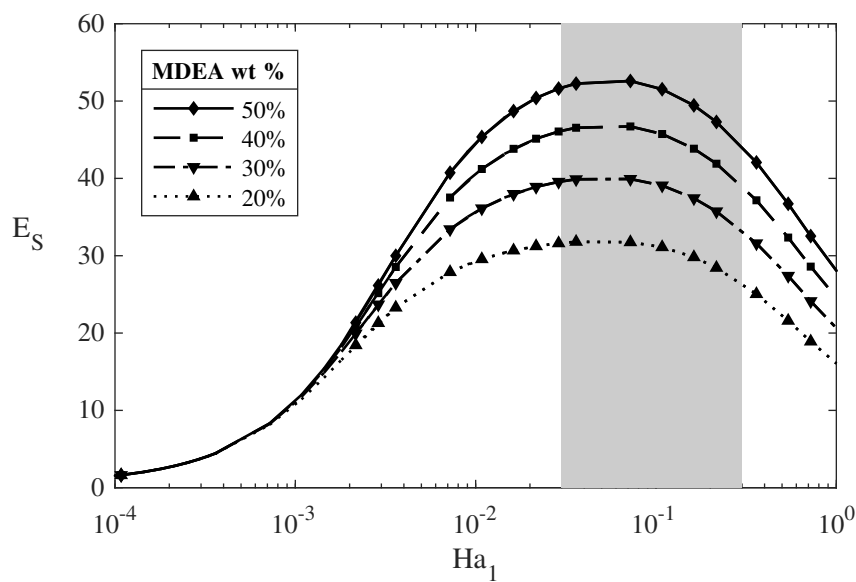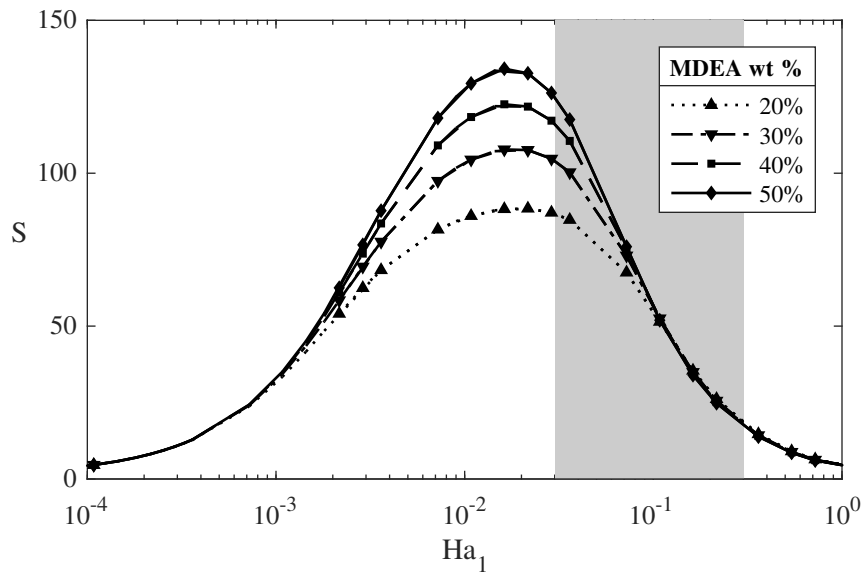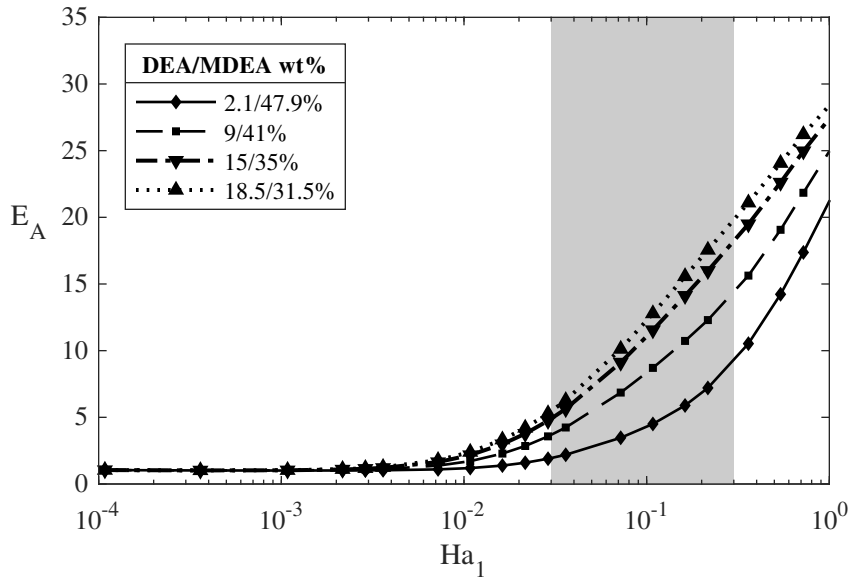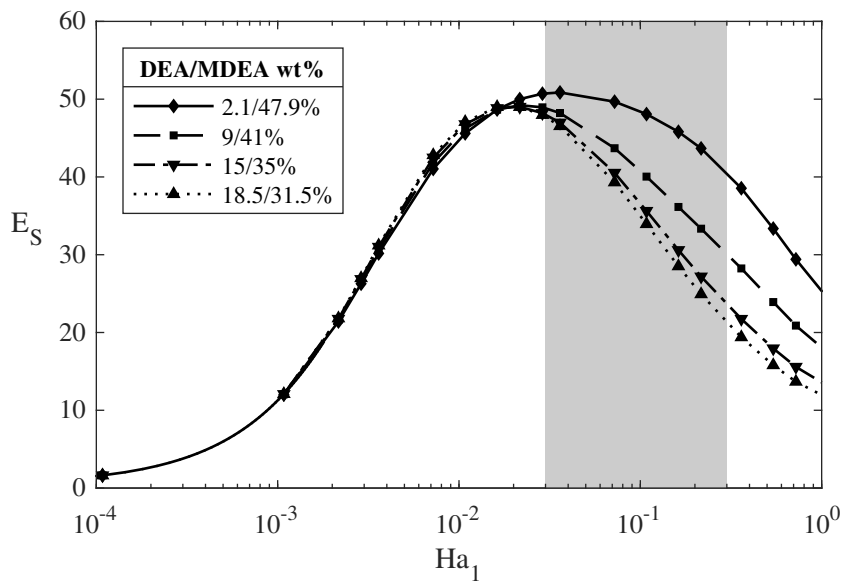
Figure 7-13: $H_2S$ selectivity vs. Hatta number and DEA/MDEA wt%. Curves: results of VKH approximate method 2; Symbols: results of numerical analysis.

## 7.4    VKH Method's Utility In Process Design

Having confirmed the accuracy and speed of the VKH method, it is next used to identify optimal compositions for either selective $H_2S$ absorption or simultaneous absorption of the two acid gases with DEA, MDEA or blends thereof.

### 7.4.1    Amine concentrations

Figures 7-14 and 7-15 show $E_A$, $E_S$ and $H_2S$ selectivity values calculated for some better-performing amine solutions in the industrially relevant $Ha_1$ range (based on the results in Section 7.3 for solutions containing up to 50 wt% amine). Over much of that range, the $E_A$ profiles for DEA-alone and 1:2 weight ratio DEA:MDEA blend are strikingly similar. Notably, the amine concentrations examined in the prior literature had not exceeded 30 wt % (Hagewiesche *et al.*, 1995; Liao and Li, 2002; Lin *et al.*, 2009). As a rule, DEA

concentrations above 30 wt% are uneconomical because of the higher heats of reaction of DEA with $CO_2$ and $H_2S$ and, therefore, greater stripping heat duties (Kohl and Nielsen, 1997). However, adding MDEA, with lower heats of reaction with $CO_2$ and $H_2S$, allows for further increase of the overall wt % beyond the 30 wt% limit and can lead to higher $CO_2$ absorption rates and with still manageable operating costs, since unlike DEA, MDEA does not require significant heat duties to strip $CO_2$ and $H_2S$ from solution (Chakravarty $et$ $al.$, 1985).

It is clear that $Ha_1$ (controlled by the effective liquid film thickness, L) determines the appropriate amine concentration for maximized $E_A$. Simultaneous acid gas absorption (e.g., in natural gas purification to avoid dry ice formation in cryogenic liquefaction equipment), where maximized an $E_A$ value is ideal, is therefore, controlled by the operational liquid mass transfer coefficient, $k_L$ which provides an estimate of L (when L is equated with $\frac{k_L}{D_A}$), which determines appropriate amine concentrations (Mandal and Bandyopadhyay, 2006; Yildirim $et$ $al.$, 2012). For a process running on the lower end of the Hatta number spectrum (or larger $k_L$ values), a 30 wt% DEA solution offers maximum $CO_2$ enhancement, with minimal selectivity for $H_2S$. However, with higher $Ha_1$ values, the 18.5/31.5 DEA/MDEA wt% blend maximizes $E_A$ values, with reasonably low values of $E_S$ and, therefore, $H_2S$ selectivity.

For $H_2S$-selective absorption, an MDEA-alone solution will clearly function most effectively. Refinery operations tend to favor this mode of operation because the requirements for $CO_2$ removal are less stringent and $H_2S$ must be removed because of its toxicity, corrosiveness and poisoning of catalysts (Yildirim $et$ $al.$, 2012).
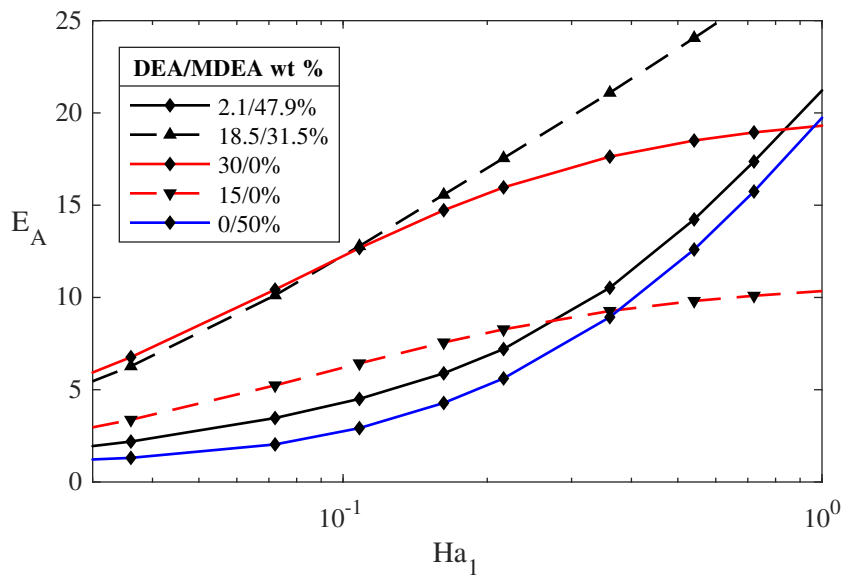
(a)



(b)

Figure 7-14: $CO_2$ (a) and $H_2S$ (b) enhancement factor vs. Hatta number and DEA/MDEA wt%. Curves: results of VKH approximate method 2; Symbols: results of numerical analysis.
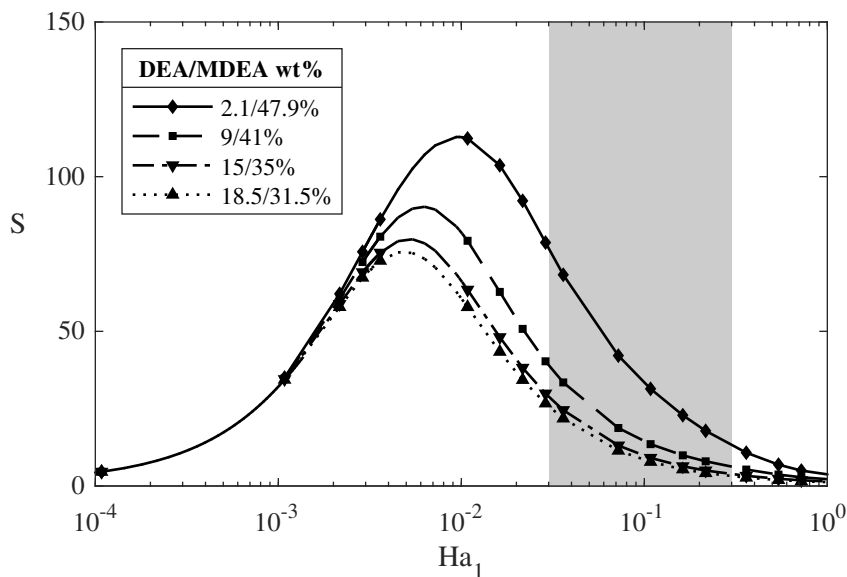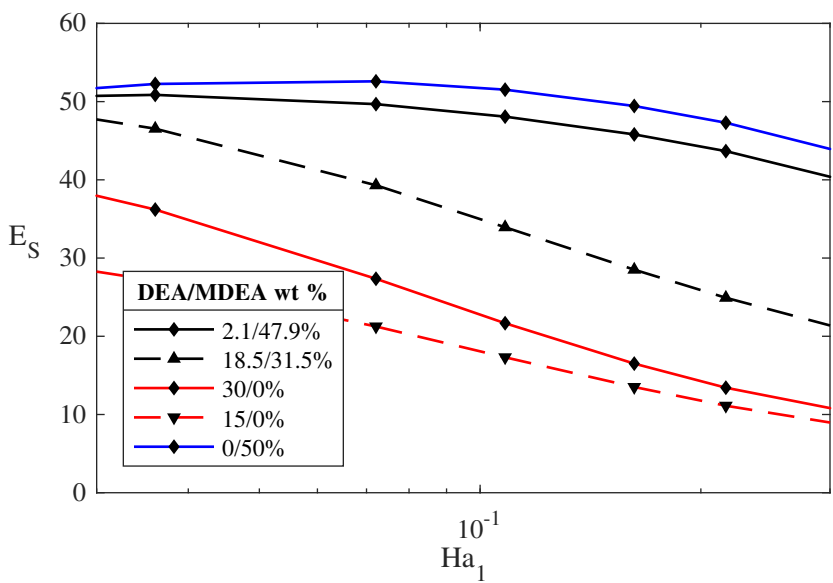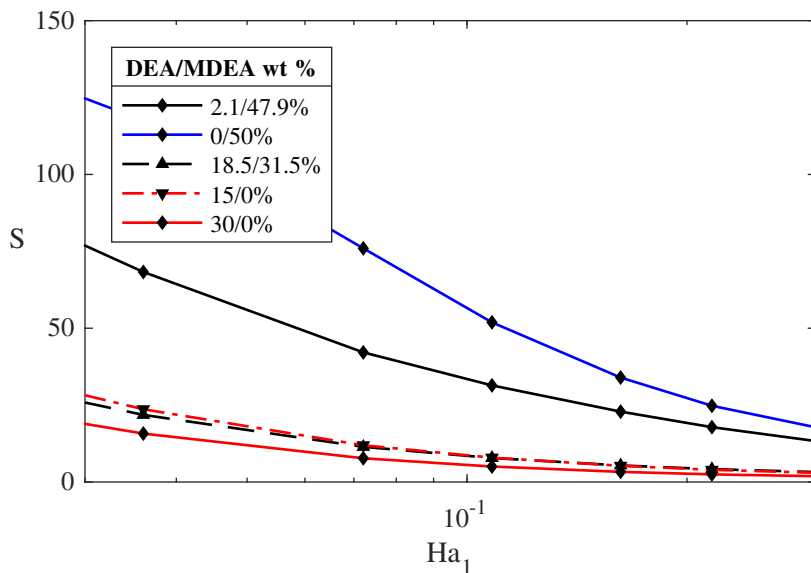
Figure 7-15: $H_2S$ selectivity vs. Hatta number and DEA/MDEA wt%. Curves: results of VKH approximate method 2; Symbols: results of numerical analysis.

## 7.4.2 Amine Selection

The results presented in the previous section established that a blend of the secondary amine, DEA, and the tertiary amine, MDEA, enhances $CO_2$ absorption rates to greater extents than DEA or MDEA alone. In this section, the same VKH-based analysis is applied to identify the best blend for simultaneous acid gas absorption.

Figures 7-16 and 7-17 present $E_A$, $E_S$ and $H_2S$ selectivity profiles for nine different blends consisting of 1.5 M of a primary or secondary amine plus 2.5 M of a tertiary amine (as before with zero bulk liquid loadings, bulk liquid $pH = 10$, bulk gas $CO_2$ and $H_2S$ partial pressures of respectively 1 and 0.1 atm, T=298 K), liquid and gas film thicknesses 10 and 100 $\mu m$, respectively. Again included for comparison are enhancement factors obtained via numerical methods. Three tertiary amines were selected, distinguished by their $pK_a$ values on the x-axis: triethylamine (TEA): 7.88, MDEA: 8.52 and

72

diethyl monoethanolamine (DEMEA): 9.61. Two secondary amines, DEA and di-isopropanolamine (DIPA), along with the primary amine, MEA, were hypothetically blended with each tertiary amines. Results for each carbamate-forming primary and secondary amine are plotted vs. the tertiary amine's pKA.

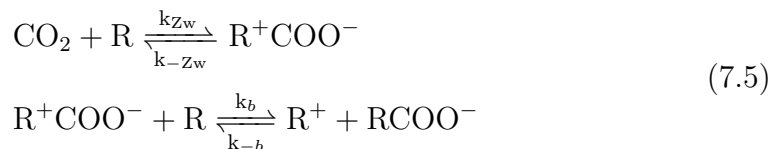$CO_2$-MEA was simulated using two different mechanisms (in light of the absence of agreement and, as result, considerable discrepancies between reported rate constants.):

(1) One-step carbamate form:

$$CO_2 + R \underset{k_{-Ca}}{\overset{k_{Ca}}{\rightleftharpoons}} H^+ + RCOO^- \tag{7.4}$$

(2) Two-step zwitterion-mediated:

$$CO_2 + R \underset{k_{-Zw}}{\overset{k_{Zw}}{\rightleftharpoons}} R^+COO^-$$
$$R^+COO^- + R \underset{k_{-b}}{\overset{k_b}{\rightleftharpoons}} R^+ + RCOO^- \tag{7.5}$$

A number of earlier publications presented experimental data consistent with zwitterion formation being the rate-determining step for MEA. Accordingly, their authors concluded that eq. (7.4) suffices to characterize MEA-carbamate formation, obviating the need to invoke a two-step zwitterion-mediated mechanism (see Hikita *et al.* (1977); Donaldson and Nguyen (1980b); Laddha and Danckwerts (1981); Blauwhoff *et al.* (1984)).

More recent investigators, however, have provided evidence in support of the two-step zwitterion mechanism for MEA (eq. (7.5)) derived from molecular orbital reaction pathway simulation, and classical Molecular Dynamics software, and $C^{13}$ nuclear magnetic resonance data analysis (Xie *et al.*, 2010; Lv *et al.*, 2015; Hwang *et al.*, 2015; Ma *et al.*, 2015). Experimental studies

73

have deduced kinetic constants for the MEA two-step zwitterion mechanism that have successfully reconciled model predictions and experimental results (Horng and Li, 2002; Liao and Li, 2002; Ali, 2005; Ramachandran *et al.*, 2006). It is difficult to properly assess the mechanisms because the more recent authors fit their kinetic expressions to different sets of experimental data. In fig. 7-16, the MEA enhancement factor results show sensitivity to the different mechanisms, with the non-zwitterion mechanism tending to inflate $E_A$ and conversely, deflate $E_S$ and $H_2S$ selectivity. This ambiguity of MEA's absorption performance is a potential source of uncertainty in process design; this suggests a need for additional kinetics studies. For the remainder of this chapter, all results are based on the kinetic constants for the two-step zwitterion mechanism.

For the secondary amines, DEA and DIPA, however, there is general agreement in literature that they form the carbamate ion via a zwitterion-intermediate (eq. (7.5)), with deprotonation of the zwitterion as the rate-determining step (Donaldson and Nguyen, 1980b; Blauwhoff *et al.*, 1984; Vaidya and Kenig, 2007; Sutar *et al.*, 2012).

The substantial differences between the $E_A$ values in fig. 7-16 for DEA,DIPA and MEA reflect differences among the kinetic constants. The primary amine, MEA, has the highest reaction rate constants and, therefore, the highest $E_A$ values. Notably, as well, DIPA's $pK_a$ exceeds that of DEA. However, DEA's reaction rate constants, and therefore, its enhancement factors, exceed those for DIPA.

The fact that both $E_A$ and $E_S$ increase as a tertiary amine $pK_a$ approaches the (fixed) bulk liquid pH of 10, indicates that buffering capacity (which maximizes when the pH equals the buffer's $pK_a$ value) is responsible for the more enhanced absorption rates. Of the trio of tertiary amines, DEMEA's $pK_a$ is

the closest to 10, while TEA's is the furthest. Not surprisingly, then, fig. 7-18 shows that the gradient in liquid film pH is smallest in the DEMEA-containing blends.

Reactions undergone by both of the dissolved "acid" gases, $CO_2$ and $H_2S$, produce hydrogen ions. Buffers, by definition, combine with hydrogen ions, thereby enhancing the extents of those reactions and, in turn, the rates of absorption of $CO_2$ and $H_2S$ This is consistent with the experimental data of Li *et al.* (2007) showing that DEMEA promotes $CO_2$ absorption to a greater extent than MDEA.

It is also interesting to note in fig. 7-18 that the primary and secondary amines do not play significant roles as buffers - which is apparently attributable to the loss of buffering capacity when the amino group is converted to carbamate.

Further insight into the performance of the various blends may be gained by revisiting the linkage equations (3.26 to 3.29), on the basis of which the dimensionless $CO_2$ and $H_2S$ absorption rates ($\Phi_A$ and $\Phi_S$) may be resolved into contributions from differences across the liquid film, in the dimensionless concentrations of carbon-containing and sulfur-containing species:

$$\Phi_A = a_0 - a_L + \frac{b_0 - b_L}{\lambda_1} + \frac{c_0 - c_L}{\lambda_1} + \frac{\lambda_2(\mathrm{r}_0^- - \mathrm{r}_L^-)}{\lambda_1} \tag{7.6}$$

$$\Phi_S = s_0 - s_L + \frac{b_0 - b_L}{\lambda_3} \tag{7.7}$$

where $\lambda_1 = \frac{D_A P_A H_A}{D_I C_T}$, $\lambda_2 = \frac{R_{LT}}{C_T}$ and $\lambda_3 = \frac{D_A P_S H_S}{D_I C_T}$.

Figures 7-19 and 7-20 present dimensionless of carbamate, $\mathrm{R}^-$, bicarbonate, $\mathrm{HCO_3}^-$, and bisulfide, $\mathrm{HS}^-$ profiles for blends of 2.5 M DEMEA plus 1.5 M DEA, DIPA and MEA at the usual baseline conditions. The carbonate ion

profile is not shown because it is at least two orders of magnitude smaller than the listed profiles, thus, it is insignificant in maximizing $CO_2$ flux. The large MEA carbamate ion gradient is primarily responsible for the highest $CO_2$ flux ($\lambda_2 = 0.375$).

Notably, the DIPA-containing blend promotes the largest bisulfide ion gradient among the three blends with DEMEA, and is, therefore, the most selective for $H_2S$. This is apparently because DIPA's relatively slow carbamate formation rate - compared to MEA and DEA - makes more DIPA available, as a buffer, to promote $H_2S$ dissociation at the gas-liquid interface. Thus, DIPA best promotes $H_2S$-selective absorption.
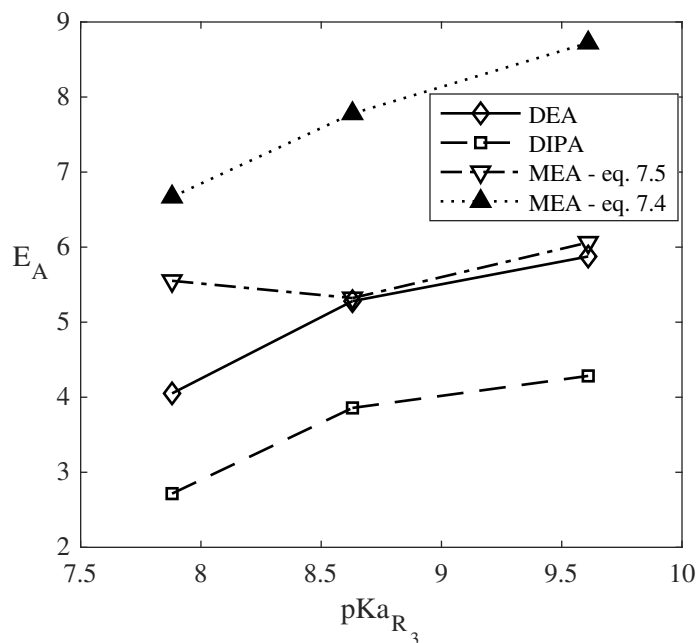
(a)
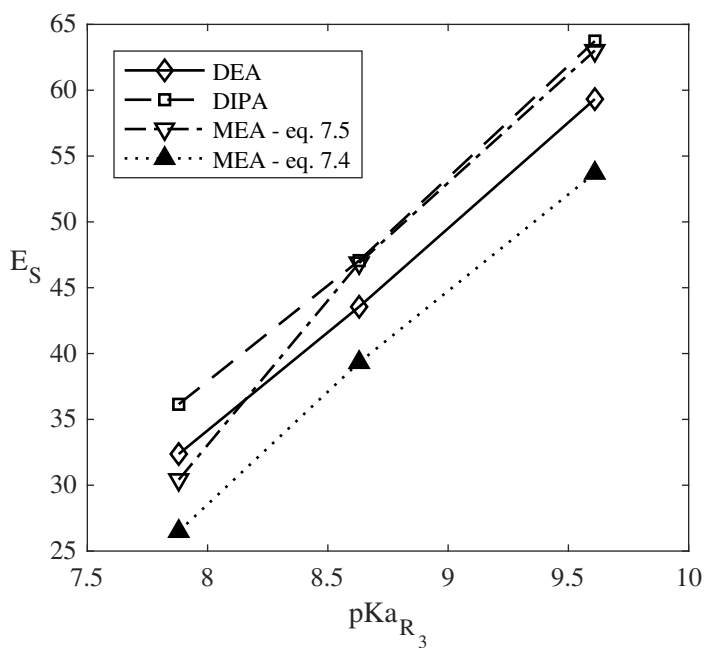


(b)

Figure 7-16: $E_A$ (a) and $E_S$ (b) vs. tertiary amine $pKa_{R3}$ for 9 different amine blend combinations. The tertiary amines pKa's are as follows: TEA= 7.88, MDEA= 8.52 and DEMEA= 9.61. Curves: results of VKH approximate method 2; Symbols: results of numerical analysis.
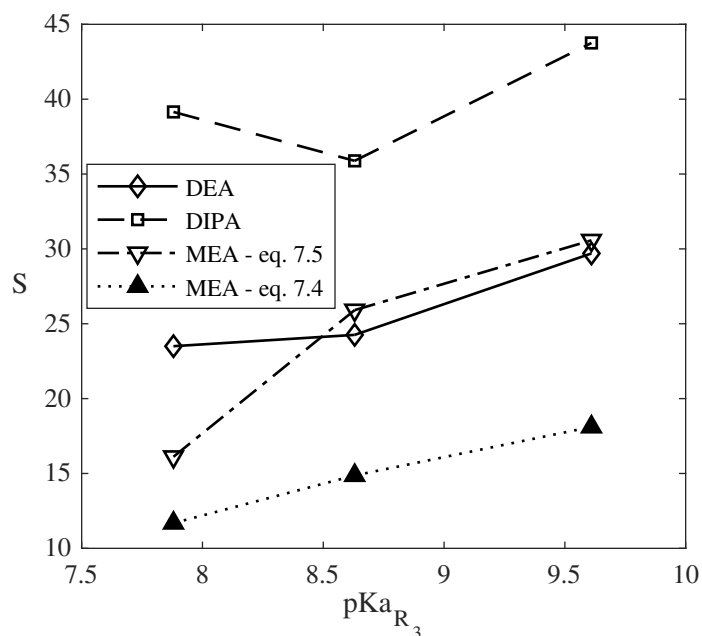
Figure 7-17: $H_2S$ selectivity vs. tertiary amine $pKa_{R3}$ for 9 different amine blend combinations. The tertiary amines pKa's are as follows: TEA= 7.88, MDEA= 8.52 and DEMEA= 9.61. Curves: results of VKH approximate method 2; Symbols: results of numerical analysis.
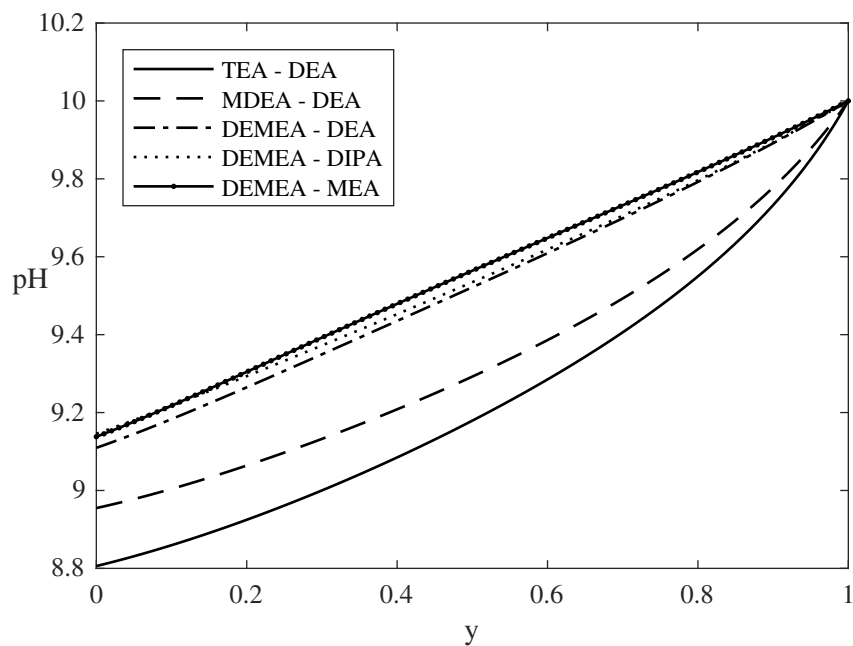


Figure 7-18: pH profile in liquid film.
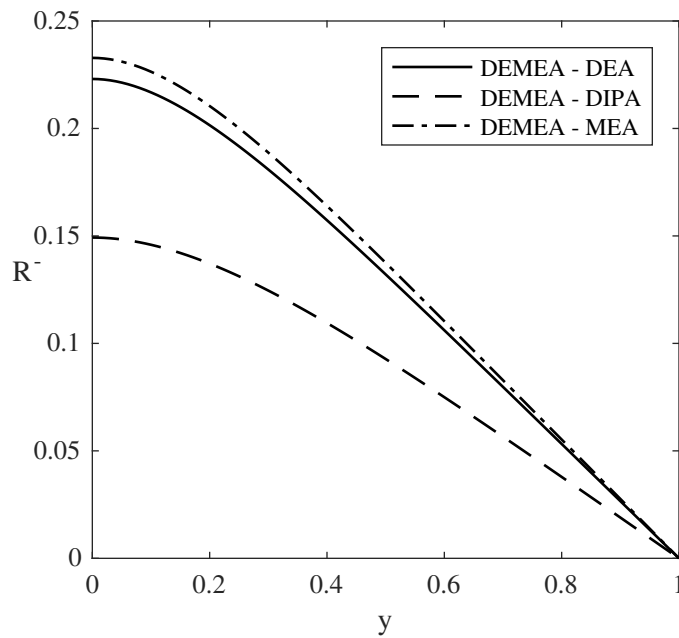
(a)
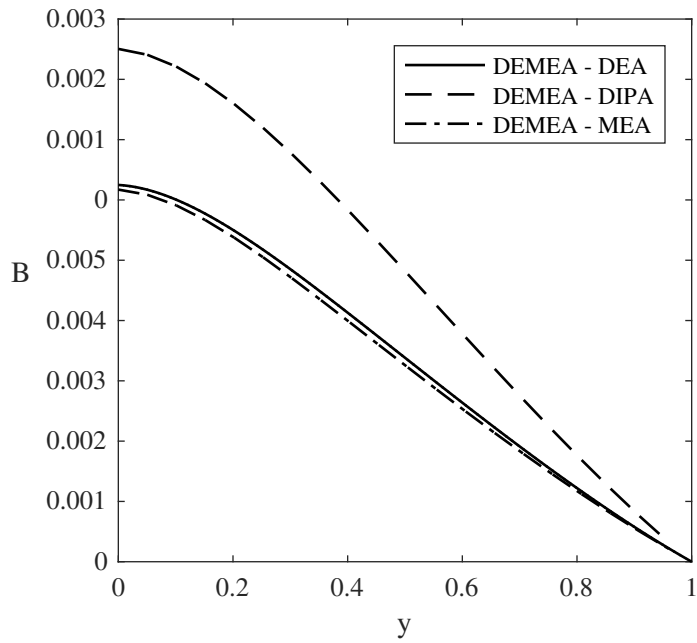


(b)

Figure 7-19: $R^-$ (a) and B ($HCO_3{}^-$) (b) dimensionless concentration profiles in liquid film for different blends.
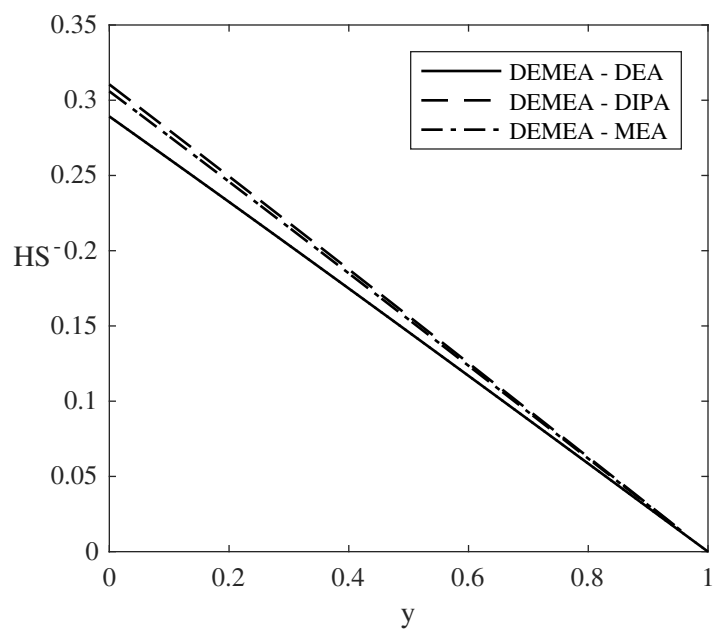
Figure 7-20: HS$^-$, dimensionless concentration profile in liquid film for different blends.

# Chapter 8

# Conclusions

The linearization scheme originally developed by Van Krevelen and Hoftjzer (1948) has been successfully applied to simulate acid gas absorption in aqueous amine blends. Calculated $CO_2$ and $H_2S$ enhancement factors, and $H_2S$ selectivities were favorably compared to exact values obtained via MATLAB numerical analysis software. The modified VKH method developed by Fiordalis (2017) proved more accurate over large ranges of the gas film thickness and liquid-phase Hatta number. The approximate methods accurately modeled the industrially relevant gas film thickness range in which gas mass transfer limitations on $H_2S$ absorption rates were most apparent. Optimal scrubbing solutions for both simultaneous acid gas and $H_2S$-selective absorption were identified based on calculated rates of absorption in blends pairing three different tertiary with three different primary or secondary amines.

# Appendix A

# Amine Concentration

# Calculations

The different DEA and MDEA concentrations used are calculated from weight percentage sand density in this appendix. Densities of the different weight percentages were found in Al-Ghawas *et al.* (1989); Rinker *et al.* (1994) as shown in table A.1.

| mass % DEA | mass % MDEA | Density $\left(\frac{g}{cm^3}\right)$ |
|---|---|---|
| 0 | 20 | 1.0152 |
| 0 | 30 | 1.0250 |
| 0 | 40 | 1.0346 |
| 0 | 50 | 1.0427 |
| 10 | 0 | 1.0101 |
| 20 | 0 | 1.0220 |
| 30 | 0 | 1.0342 |
| 2.1 | 47.9 | 1.0465 |
| 9.0 | 41 | 1.0489 |
| 15 | 35 | 1.0509 |
| 18.5 | 31.5 | 1.0517 |

Table A.1: Densities of DEA and/or MDEA solutions at 298.15 K

The concentrations, $C_\varphi$ are then found from the weight fractions, $X_\varphi$ as

follows:

$$C_\varphi = \frac{\text{density of solution} \times X_\varphi}{\text{Molecular weight of species, } \varphi} \qquad \text{(A.1)}$$

The molecular weights of DEA, MDEA and water are taken as 105.14, 119.163 and 18 $\frac{g}{mol}$.

# Appendix B

# MATLAB Listings

## B.1  Numerical Solution

```matlab
1  global R_LT R_3LT CT Wa Da Di lambda K k A_bulkg M aL bL cL
      sL smL rmL...
2        ag sg
3  %Acid gas partial pressures
4  Pa=1;
5  Ps=0.1;
6  %Volatility constants in atm/M
7  Kha=29.411;
8  Khs=10;
9  %Henry constants in M/atm
10 Ha=1/Kha;
11 Hs=1/Khs;
12 %Acid gas partial pressures conversion into concentrations
13 A_bulkg=Ha*Pa; %Pa,bulk*Ha
14 S_bulkg=Hs*Ps;
15 Loading=[0  0]; %Liquid Loading factor
16 %The bulk liquid total amine and water concentrations (M)
17 R_LT=1.5;
18 R_3LT=2.5;
19 Wat=37.34;
20 %Liquid and Gas diffusivities
21 Da=2e-7; %dm2/s %For carbon dioxide
22 Di=1e-7; %dm2/s %For all volatile species
23 Dga=2e-3; %dm2/s
24 Dgs=2e-3; %dm2/s
25
```

```matlab
26
27
28  %This line links to an m.file that solves for the bulk
        liquid conditions
29  %for all species given the total amine concentrations
30  [aL,sL,smL,bL,cL,rmL,M,Wa]=findingbulkcon(K,R_LT,R_3LT,Wat,
        pH,Loading);
31
32
33  %Bulk Gas dimensionless concencentrations:
34  ag=1; %A_bulkg/A_bulkg
35  sg=1; %S_bulkg/S_bulkg
36
37  [lambda]=lambdacalcs(L,G,Da,Di,Dga,Dgs,K,A_bulkg,S_bulkg,
        R_3LT,R_LT);
38
39
40  %The non-reactive absorption interfacial concentrations  eq
         4.35
41  Ao_norxn=(ag*A_bulkg*(Dga/G)+AL*(Da/L))/((Dga/G)+(Da/L));
42  So_norxn=(sg*S_bulkg*(Dgs/G)+SL*(Da/L))/((Dgs/G)+(Da/L));
43
44
45  %The solver used in numerical solution is called the
        Boundary value problem
46  %solver (bvp4c). It requires input  of an initial guess for
        each species
47  %that has a 1st order differential equation defined for it.
        In our case,
48  %because all the species have second order differential
        equations, the
49  %system will require a guess for both the species and its
        differentiated
50  %form. (See odefcn1a for how the 2nd order differential
        equations were
51  %turned into 1st order).
52  %The species of interest are a, rm, b+c and lambda(3)*s+sm
        in that order
53
54  %Defining the initial guess
55  %The guess for the numerical solver is very sensitive.
        Therefore the
56  %solution to VKH at 50 points between 0 and 1 is used as the
         initial guess
57  %@bvpg is the function that computes the profiles for a, rm,
         b+c and
```

```
58  %lambda(3)*s+sm in that order and their gradients at 50
        points
59  fun2=@bvpiniguess;
60  numericaliniguess=@(x) fun2(x,rgee,L);
61  solinit=bvpinit(linspace(0, 1,50),numericaliniguess);
62
63
64  %The boundary conditions for the 8 profiles are in @bcfun1a;
65  fun3=@bcfun;
66  boundaryconditions=@(ya,yb) fun3(ya,yb);
67
68
69  %The differential equations for the 8 profiles are in @
        odefcn1a;
70  fun4=@odefcn;
71  DiffEqns=@(x,y) fun4(x,y,L);
72  %The following line is the call to start the numerical
        solution solver. It
73  %outputs profiles of the species and their gradients as a
        function of the
74  %distance from interface.
75  sol=bvp4c(DiffEqns,boundaryconditions,solinit);
76  x=linspace(0,1);
77  y=deval(sol,x);
78
79
80  %Flux and enhancement calculations, eq. 4.36-39
81  Fluxa=-Da*A_bulkg*y(2,1)/(L);
82  Fluxs=-Da*S_bulkg*y(8,1)/(lambda(3)*L);
83
84  %Enhancement Factor Calculations
85  Ea=Fluxa/(kL*(Ao_norxn-aL*A_bulkg));
86  Es=Fluxs/(kL*(So_norxn-sL*S_bulkg));
87
88  %Selectivity is shown in results. It is the ratio of fluxes
        to the ratio of
89  %partial pressures gradients.
90  Pa0=A_bulkg*y(1,1);
91  Ps0=S_bulkg*y(7,1);
92  Selectivity=(Pa-Pa0)*Fluxs/((Ps-Ps0)*Fluxa);
93      end
```

```
1  function V=bvpiniguess(x,rgee,L)
2  %Solution to VKH method used to calculate the initial guess
        for bvp
3  %This function is called at each position vector x, which is
        a
4  %dimensionless distance from the interface
```

```matlab
 5  global R_LT R_3LT CT Wa Da Di lambda K k...
 6      A_bulkg M aL bL cL sL smL rmL ag sg
 7
 8  %%%%%%%%%%%%%%%%%%%%%%%%%%%%%%%%%%%%%%%%%%%%%%%%%%%%%%%%%%%%%
 9
10
11  drdy=0;
12  %Section 5.1
13  r0=rgee(1);
14  rp0=rgee(2);
15  rm0=1-r0-rp0;
16
17  %From the guesses all other components are calculated using
        eq 4.5-4.9 and
18  %eq 3.9-11
19  h0=rp0/(lambda(8)*r0);
20  Oh0=K(12)/(h0*CT^2);
21  r3p0=1/(1+lambda(8)*r0/(lambda(7)*rp0));
22  s0=(lambda(3)*sL+smL+lambda(3)*lambda(5)*sg)/(lambda(3)+
        lambda(3)...
23      *lambda(5)+lambda(10)/h0);
24  sm0=lambda(10)*s0/h0;
25  b0=(lambda(6)*r3p0+lambda(2)*rp0+M+h0-Oh0-lambda(2)*rm0-sm0)
        /(1+2*...
26      lambda(9)/h0);
27  c0=lambda(9)*b0/h0;
28  a0=(lambda(1)*aL+bL+cL+lambda(2)*rmL+lambda(1)*lambda(4)*ag-
        b0-c0-...
29      lambda(2)*rm0)/(lambda(1)+lambda(1)*lambda(4));
30  r30=r3p0/(lambda(7)*h0);
31
32  %Section 4.2
33  kb0=k(5)*r0*R_LT+k(6)*r30*R_3LT+k(7)*Wa*CT+k(8)*Oh0*CT;
34  kbp0=k(9)*rp0*R_LT+k(10)*r3p0*R_3LT+k(11)*h0*CT+k(12)*Wa*CT;
35
36  %Linearizing differential equations 3.64 and 3.69
37  %The constants are defined in eq 4.4
38  phi1=(L^2)/(Da*A_bulkg);
39  phi2=(k(1)+k(2)*K(12)/(CT*h0)+k(3)*r30*R_3LT+k(4)*r0*R_LT
        /(1+1/kb0))...
40      *A_bulkg;
41  phi3=-k(4)*R_LT*kbp0/(1+kb0);
42  phi4=-k(2)*CT*b0/K(2)-k(3)*CT*R_3LT*b0*r3p0/K(3)-k(1)*CT*CT*
        b0*h0/K(1);
43  phi5=-k(4)*L*L/Di;
44  phi6=A_bulkg*r0/(1+1/kb0);
45  phi7=-kbp0/(1+kb0);
```

```matlab
46  phi8=phi1*(phi3*rm0+phi4);
47
48  %Eqn 4.10-4.12
49  eta1=phi1*phi2;
50  eta2=phi8;
51  eta3=phi5*phi6;
52  eta4=-phi5*phi7;
53  %Eqn 4.16
54  omega_a=eta2/eta1;
55  omega_r=eta2*eta3/(eta1*eta4);
56  %mu1^2=m1sq, and is defined in eq 4.25 and 4.26
57  mu_1sq=-eta4;
58  mu_2sq=eta1;
59  mu_1=mu_1sq^(1/2);
60  mu_2=-mu_1sq^(1/2);
61  mu_3=mu_2sq^(1/2);
62  mu_4=-mu_2sq^(1/2);
63  %Lambdas are defined in eq 4.28
64  Lambda1=(mu_1sq+eta4)/eta3;
65  Lambda2=(mu_1sq+eta4)/eta3;
66  Lambda3=(mu_2sq+eta4)/eta3;
67  Lambda4=(mu_2sq+eta4)/eta3;
68
69  %To find the psib's in eq4.27 eqns 4.29-4.33 are organized
        into a matrix A
70  %and b, and the unknown are solved for by A\b.
71  A=[Lambda1*exp(mu_1) Lambda2*exp(mu_2) Lambda3*exp(mu_3)...
72      Lambda4*exp(mu_4); (Lambda1-mu_1*Lambda1/lambda(4))...
73      (Lambda2-mu_2*Lambda2/lambda(4)) (Lambda3-mu_3*Lambda3/
            lambda(4))...
74      (Lambda4-mu_4*Lambda4/lambda(4)); exp(mu_1) exp(mu_2)
            exp(mu_3)...
75      exp(mu_4); mu_1 mu_2 mu_3 mu_4];
76  b=[aL+omega_a; ag+omega_a; rmL+omega_r; drdy];
77  Psi_B=A\b;
78  %The profiles are found from 4.27, 4.13, and 3.9-11
79  ax=Lambda1*Psi_B(1)*exp(mu_1*x)+Lambda2*Psi_B(2)*exp(mu_2*x)
        +Lambda3...
80      *Psi_B(3)*exp(mu_3*x)+Lambda4*Psi_B(4)*exp(mu_4*x)-
            omega_a;
81  rmx=Psi_B(1)*exp(mu_1*x)+Psi_B(2)*exp(mu_2*x)+Psi_B(3)*exp(
        mu_3*x)...
82      +Psi_B(4)*exp(mu_4*x)-omega_r;
83  axF=Lambda1*Psi_B(1)*mu_1*exp(mu_1*x)+Lambda2*Psi_B(2)*mu_2*
        exp(mu_2*x)...
84      +Lambda3*mu_3*Psi_B(3)*exp(mu_3*x)+Lambda4*Psi_B(4)*mu_4
            *exp(mu_4*x);
```

```matlab
85  rmxF=Psi_B(1)*mu_1*exp(mu_1*x)+Psi_B(2)*mu_2*exp(mu_2*x)+
        Psi_B(3)...
86          *mu_3*exp(mu_3*x)+Psi_B(4)*mu_4*exp(mu_4*x);
87  bcx=(-lambda(1)*lambda(4)*(ag-a0)*x)+lambda(1)*aL+bL+cL+
        lambda(2)*rmL+...
88          lambda(1)*lambda(4)*(ag-a0)-lambda(1)*ax-lambda(2)*rmx;
89  bcxF=-lambda(1)*lambda(4)*(ag-a0)-lambda(1)*axF-lambda(2)*
        rmxF;
90  spsmx=(-lambda(3)*lambda(5)*(sg-s0)*x)+lambda(3)*sL+smL+
        lambda(3)...
91          *lambda(5)*(sg-s0);
92  spsmxF=-lambda(3)*lambda(5)*(sg-s0);
93  %They are reported as a vector at specified position x
94  V=[ax axF rmx rmxF bcx bcxF spsmx spsmxF];
95  end
```

```matlab
1   function dydx=odefcn(x,y,L)
2   %System of differential equations for numerical solution
3   %Because only 4 "species" are defined, a,rm, b+c and lambda
        (3)*s+sm,
4   %corresponding to y1,y3,y5 and y7 in the differential
        equations below,
5   %odefcn1a codes for 8 differential equations: the 1st and
        second order
6   %differentials in y1,y3,y5 and y7.
7
8   global R_LT R_3LT CT Wa Da Di lambda K k A_bulkg M
9
10  %%%%%%%%%%%%%%%%%%%%%%%%%%%%%%%%%%%%%%%%%%%%%%%%%%%%%%%%%%%%%%%
11
12  %In writing out the differential equations, eq4.5 and 4.60,
        other
13  %components, such as r3, r3p, r, rp, Oh, h etc need to be
        explicitly
14  %defined. To do so,the species r is selected because it can
        be defined in
15  %a polynomial to solve all other components.
16  coeffsv=polyf1(y);
17  r=roots(coeffsv);
18  N=length(r);
19  for j=1:N
20              if isreal(r(j))==1
21          Aa(j)=r(j);
22              else
23                  Aa(j)=1000; %in order to avoid selecting an
                        imaginary root
24              end
25  end
```

```matlab
26
27  for i=1:N
28      if Aa(i)<0
29      Aa(i)=1000;%in order to avoid selecting a negative root
30      end
31  end
32  R=min(Aa);
33
34  %From finding R all the other species are found
35  rp=1-R-y(3); %eq 3.88
36  h=rp/(lambda(9)*R); %eq 3.92
37  Oh=lambda(12)/h; %eq 3.94
38  r3=1/(1+lambda(8)*h); %eq 3.89
39  r3p=lambda(8)*r3*h; %eq 3.92
40  b=y(5)/(1+lambda(10)/h); %eq 3.93
41
42  dydx(1)=y(2); %a (eq.3.64)
43  dydx(2)=(L^2/(A_bulkg*Da))*((k(1)+((R*R_LT)*k(4))/(1/(((Oh*
        CT)*k(8)) + ...
44      ((R*R_LT)*k(5)) + ((r3*R_3LT)*k(6)) + ((Wa*CT)*k(7))) +
            1)...
45      + (K(12)*k(2))/(h*CT) + k(3)*(r3*R_3LT))*(y(1)*A_bulkg)
            - ((b*CT)*...
46      k(2))/K(2)...
47      - ((b*CT)*(r3p*R_3LT)*k(3))/K(3) - ((b*CT)*(h*CT)*k(1))/
            K(1) - ...
48      ((y(3)*R_LT)*k(4)*(((h*CT)*k(11)...
49      + (r3p*R_3LT)*k(10) + (rp*R_LT)*k(9)...
50      + (Wa*CT)*k(12))/(((Oh*CT)*k(8) + ...
51      (R*R_LT)*k(5) + (r3*R_3LT)*k(6) + (Wa*CT)*k(7)) + 1 ))))
            ;
52
53  dydx(3)=y(4); %Rm (eq3.69)
54  dydx(4)=-(L^2/(Di))*k(4)*(((y(1)*A_bulkg)*(R) - (y(3))*(((h*
        CT)*k(11) +...
55      (r3p*R_3LT)*k(10) + (rp*R_LT)*k(9) +...
56      (Wa*CT)*k(12))/((Oh*CT)*k(8) +...
57      (R*R_LT)*k(5) + (r3*R_3LT)*k(6) + (Wa*CT)*k(7))))/(1/((
            Oh*CT)*k(8) +...
58      (R*R_LT)*k(5) + (r3*R_3LT)*k(6) + (Wa*CT)*k(7)) + 1));
59
60  dydx(5)=y(6);%b+c=b(1+lambda(9)/h)
61  %From considering the reactions b and c are involved in, eq3
        .9-11 and 3.19
62
63  dydx(6)=(L^2/(Di*CT))*(-k(1)*(y(1)*A_bulkg)+(k(1)/K(1))*(b*
        CT)*(h*CT)...
```

```matlab
64          -k(2)*(y(1)*A_bulkg)*Oh*CT)+(k(2)/K(2))*(b*CT)-k(3)*(y
                (1)*A_bulkg)...
65        *(r3*R_3LT)+(k(3)/K(3))*(r3p*R_3LT)*(b*CT);
66
67  dydx(7)=y(8);%=lambda(3)*s+sm (eq3.73)
68  dydx(8)=0;
69
70  end
```

```matlab
1   function res=bcfun(ya,yb)
2   %Boundary conditions for numerical solution from section
        3.7.2
3   %There is a long derivation becase on of the boundary
        conditions for
4   %lambda(3)*s+sm, is defined in terms of s0 and NOT sm0, so
        there needs to
5   %be a way to solve for s0, given a0, rm0, b0+c0 and lambda
        (3)*s0+sm0 which
6   %are represented by ya1,ya3,ya5 and ya7 respectively
7
8   %bvc4c attempts to find the numerical profile that satisfies
         the
9   %differential equations and the boundary conditions
10
11  global lambda M aL bL cL sL smL rmL ag sg
12  %%%%%%%%%%%%%%%%%%%%%%%%%%%%%%%%%%%%%%%%%%%%%%%%%%%%%%%
13
14  %To solve for s0, using the 4 values shown above, one more
        species is
15  %needed. The species, r0, is selected.
16  coeffsv0=polyf1(ya,lambda,M);
17  r0=roots(coeffsv0);
18  N=length(r0);
19  for j=1:N
20              if isreal(r0(j))==1
21          Aa(j)=r0(j);
22              else
23                  Aa(j)=1000; %in order to avoid selecting an
                        imaginary root
24              end
25  end
26  for i=1:N
27      if Aa(i)<0
28      Aa(i)=1000; %in order to avoid selecting a negative root
29      end
30  end
31  R0=min(Aa);
32
```

```
33  %R0 is found so s0 can now be found and the boundary
        conditions are all
34  %found.
35  h0=(1−R0−ya(3))/(lambda(8)*R0);
36  s0=ya(7)/(lambda(3)+lambda(10)/h0);

38  res=[ya(2)+lambda(4)*(ag−ya(1)); ya(4); ya(6); ya(8)+lambda
        (5)*lambda(3)...
39      *(sg−s0); yb(1)−aL; yb(3)−rmL; yb(5)−bL−cL; yb(7)−lambda
            (3)*sL−smL];
40  end
```

```
1  function [aL,sL,smL,bL,cL,rmL,M,Wa]=findingbulkcon(K,R_LT,
        R_3LT,Wat,pH,...
2      Loading)
3
4  CT=R_LT+R_3LT; %Total Amine Concetration
5  A_bulkL=CT*Loading(1); %CO2 Bulk liquid loading
6  S_bulkL=CT*Loading(2); %H2S Bulk liquid loading
7  HL=10^−(pH);
8
9  %The derivation is shown in section 3.4.1
10 %AaL represents AL, which is to be solved according to the
        quadratic
11 %function defined in eq. 3.54−3.59
12 syms AaL
13 theta1=K(1)*K(4)*K(10)*K(12)/(HL^2)+K(4)*K(10)*K(12)/HL+K(1)
        *K(4)*K(10)...
14     *K(11)*K(12)*K(12)/(HL^3);
15 theta2=1+HL/(K(10)*K(12))+K(1)/HL+K(1)/(K(10)*K(12))+K(1)*K
        (11)*K(12)/...
16     (HL^2)+K(1)*K(11)/(K(10)*HL)+K(4)*K(10)*K(12)*Rin/HL−K
            (4)*K(10)*...
17     K(12)*A_bulkL/HL;
18 theta3=−A_bulkL*(1+HL/(K(10)*K(12)));
19
20 x=vpasolve((theta1*(AaL*1e−9)^2+theta2*AaL*1e−9+theta3)*1e10
        ,AaL1);
21 if x(1)>=0
22 AL=double(x(1))*1e−9;
23 else
24 AL=double(x(2))*1e−9;
25 end
26 %once AL is found, eq 3.48 is used to achieve
        electroneutrality by finding
27 %the optimum M to maintain pH=10 in the bulk.
28 myfunction=@findingbulkconfunc;
29 funct=@(conc) myfunction(conc,R_3LT,R_LT,HL,AL,Loading);
```

```matlab
30  options = optimoptions('fsolve','MaxFunEvals', 10000000, '
        MaxIter',...
31      10000000,'TolFun',1e-30,'TolX',1e-30);
32  [x]=fsolve(funct,1,options);
33  Em=x;
34
35  %From finding M, the rest of the boundary conditions can be
        found.
36  RL=Rin/(1+K(4)*K(10)*K(12)*AL/HL+HL/(K(10)*K(12)));%eq3.46
37  RpL=RL*HL/(K(10)*K(12)); %eq3.43
38  RmL=R_LT-RL-RpL; %eq3.46
39  BL=K(1)*AL/HL; %eq3.43
40  CL=K(11)*K(12)*BL/HL; %eq3.43
41  SL=S_bulkL/(1+K(13)/HL); %eq3.45
42  SmL=K(13)*SL/HL; %eq3.43
43  R3L=R_3LT/(1+HL/(K(9)*K(12))); %eq3.47
44
45  %The non dimensionalizing of the bulk conditions
46  %Bulk Liquid:
47  M=Em/CT;
48  Wa= Wat/CT;
49  aL=AL/A_bulkg;
50  bL=BL/CT;
51  cL=CL/CT;
52  rmL=RmL/R_LT;
53  sL=SL/S_bulkg;
54  smL=SmL/CT;
55
56  end
```

```matlab
1   function F=findingbulkconfunc(conc,R_3LT,R_LT,HL,AL,Loading)
2
3   CT=R_LT+R_3LT; %Total Amine Concetration
4   A_bulkL=CT*Loading(1); %CO2 Bulk liquid loading
5   S_bulkL=CT*Loading(2); %H2S Bulk liquid loading
6   M=conc;
7   %AL found in the function above and HL (from pH) is used to
        calculated
8   %all the species
9   BL=K(1)*AL/HL; %eq3.43
10  RL=R_LT/(1+K(4)*K(10)*K(12)*AL/HL+HL/(K(10)*K(12))); %eq346
11  RpL=RL*HL/(K(10)*K(12)); %eq3.43
12  RmL=R_LT-RL-RpL; %eq3.46
13  CL=K(11)*K(12)*BL/HL; %eq3.43
14  SL=S_bulkL/(1+K(13)/HL); %eq3.45
15  SmL=K(13)*SL/HL; %eq3.43
16  R3L=R_3LT/(1+HL/(K(9)*K(12)));%eq3.47
17  R3pL=R3L*HL/(K(9)*K(12));%eq3.43
```

```
18  OHL=K(12)/HL;%eq3.43
19
20  %The RmL found above is compared to one found using the
        electroneutrality
21  %eqn  3.48
22  RmL2=−(OHL+BL+2*CL+SmL−R3pL−RpL−M−HL);
23  %F is minimized by finding the optimum M (named conc)
24  F=((RmL−RmL2)*1000).^2;
25  end
```

```
1   function  lambda=lambdacalcs(L,G,Da,Di,Dga,Dgs,K,A_bulkg,
        S_bulkg,R_3LT,R_LT)
2   CT=R_LT+R_3LT;
3
4   %Dimensionless  parameters − section  3.7.6
5   lambda(1)=Da*A_bulkg/(Di*CT);
6   lambda(2)=R_LT/CT;
7   lambda(3)=Da*S_bulkg/(Di*CT);
8   lambda(6)=R_3LT/CT;
9   lambda(8)=CT/(K(10)*K(12));
10  lambda(7)=CT/(K(9)*K(12));
11  lambda(9)=K(11)*K(12)/CT;
12  lambda(10)=K(13)*S_bulkg/(CT^2);
13  lambda(12)=(CT^2)/(K(1)*A_bulkg);
14  lambda(13)=K(4)*A_bulkg/lambda(8);
15  lambda(4)=Dga*L*Kha/(Da*G*R*T);
16  lambda(5)=Dgs*L*Khs/(Da*G*R*T);
17
18  end
```

## B.2   VKH Approximation

```
1   global  R_LT R_3LT CT Wa Da Di lambda K A_bulkg M aL bL cL sL
        smL rmL ag sg
2   L=1e−4;%dm
3   G=1e−3;%dm
4   %Acid gas partial pressures
5   Pa=1;
6   Ps=0.1;
7   %Volatility constants in atm/M
8   Kha=29.411;
9   Khs=10;
10  %Henry constants in M/atm
11  Ha=1/Kha;
12  Hs=1/Khs;
13  %Acid gas partial pressures conversion into concentrations
```

```matlab
14  A_bulkg=Ha*Pa; %Pa,bulk*Ha
15  S_bulkg=Hs*Ps;
16  Loading=[0 0]; %Liquid Loading factor
17  %The bulk liquid total amine and water concentrations (M)
18  R_LT=1.5;
19  R_3LT=2.5;
20  Wat=37.34;
21  pH=10;
22  %Liquid and Gas diffusivities
23  Da=2e-7; %dm2/s %For carbon dioxide
24  Di=1e-7; %dm2/s %For all volatile species
25  Dga=2e-3; %dm2/s
26  Dgs=2e-3; %dm2/s
27
28
29
30  %This line solves for the dimensionless bulk liquid
         concentrations
31  %according to Section 3.4.1
32  [aL,sL,smL,bL,cL,rmL,M,Wa]=findingbulkcon(K,R_LT,R_3LT,Wat,
         pH,Loading);
33
34
35  %Bulk Gas dimensionless concencentrations:
36  ag=1; %A_bulkg/A_bulkg
37  sg=1; %S_bulkg/S_bulkg
38
39  [lambda]=lambdacalcs(L,G,Da,Di,Dga,Dgs,K,A_bulkg,S_bulkg,
         R_3LT,R_LT);
40
41  %VKH Solution - Chapter 4
42
43  %This is solved first to get specific enough guesses for
         Numerical solution
44  %for convergence
45
46  %Initial guess for VKH root solver
47  rguess(1,:)=[0.1,0.1];
48
49
50  %The non-reactive absorption interfacial concentrations eq
         4.35
51  Ao_norxn=(ag*A_bulkg*(Dga/G)+AL*(Da/L))/((Dga/G)+(Da/L));
52  So_norxn=(sg*S_bulkg*(Dgs/G)+SL*(Da/L))/((Dgs/G)+(Da/L));
53
54  %This is the line that calls the root solver based on
         section 5.1 and 5.2
```

```matlab
55   fun1=@VKHSolver;
56   VKHsolver=@(r) fun1(r,L);
57   r=fsolve(VKHsolver,rguess(1,:));
58   r0=r(1);
59   rp0=r(2);
60
61   %This is the seed for calculating the numerical (bvp4c
        guesses at each
62   %thickness, L)
63   rg(1,:)=[r0 rp0];
64
65   %r0 and rp0 allow all other solutions to be found using eq
66   %5.5-5.9 and 4.77-4.81
67   rm0=1-r0-rp0;
68   h0=rp0/(lambda(8)*r0);
69   Oh0=K(12)/(h0*CT^2);
70   r3p0=1/(1+lambda(8)*r0/(lambda(7)*rp0));
71   s0=(lambda(3)*sL+smL+lambda(3)*lambda(5)*sg)/(lambda(3)+
        lambda(3)*...
72       lambda(5)+lambda(10)/h0);
73   sm0=lambda(10)*s0/h0;
74   b0=(lambda(6)*r3p0+lambda(2)*rp0+CountL+h0-Oh0-lambda(2)*rm0
        -sm0)/...
75       (1+2*lambda(9)/h0);
76   c0=lambda(9)*b0/h0;
77   a0=(lambda(1)*aL+bL+cL+lambda(2)*rmL+lambda(1)*lambda(4)*ag-
        b0-c0-...
78       lambda(2)*rm0)/(lambda(1)+lambda(1)*lambda(4));
79   Pa0=A_bulkg*a0;
80   Ps0=S_bulkg*s0;
81
82   %Flux and enhancement calculations, eq. 5.35-5.38
83   kL=Da/L;
84   Fluxa=Da*lambda(4)*A_bulkg*(ag-a0)/L;
85   Fluxs=Da*lambda(5)*S_bulkg*(sg-s0)/L;
86   Ea=Fluxa/(kL*(Ao_norxn-aL*A_bulkg));
87   Es=Fluxs/(kL*(So_norxn-sL*S_bulkg));
88   %Selectivity is shown in results. It is the ratio of fluxes
        to the ratio of
89   %partial pressures.
90   Selectivity=(Pa-Pa0)*Fluxs/((Ps-Ps0)*Fluxa);
91       end
```

```matlab
1   function F= VKHSolver(r,L)
2   % Root solver for VKH method
3   global R_LT R_3LT CT Wa Da Di lambda K k...
4       A_bulkg M aL bL cL sL smL rmL ag sg
5
```

```matlab
 6  drdy=0;
 7
 8  %Section 4.1
 9  r0=r(1);
10  rp0=r(2);
11  %From the guesses all other components are calculated using
        eq 4.5-4.9 and
12  %eq 3.9-11
13  rm0=1-r0-rp0;
14  h0=rp0/(lambda(8)*r0);
15  Oh0=K(12)/(h0*CT^2);
16  r3p0=1/(1+lambda(8)*r0/(lambda(7)*rp0));
17  s0=(lambda(3)*sL+smL+lambda(3)*lambda(5)*sg)/(lambda(3)+
        lambda(3)*...
18      lambda(5)+lambda(10)/h0);
19  sm0=lambda(10)*s0/h0;
20  b0=(lambda(6)*r3p0+lambda(2)*rp0+M+h0-Oh0-lambda(2)*rm0-sm0)
        /(1+2*...
21      lambda(9)/h0);
22  c0=lambda(9)*b0/h0;
23  a0=(lambda(1)*aL+bL+cL+lambda(2)*rmL+lambda(1)*lambda(4)*ag-
        b0-c0-...
24      lambda(2)*rm0)/(lambda(1)+lambda(1)*lambda(4));
25  r30=r3p0/(lambda(7)*h0);
26
27  Flux1=-lambda(4)*(ag-a0);%|F| eq3.74
28
29  %Section 4.2
30
31  %Linearizing differential equations 3.64 and 3.69
32
33  %The constants are defined in eq 4.4
34  kb0=k(5)*r0*R_LT+k(6)*r30*R_3LT+k(7)*Wa*CT+k(8)*Oh0*CT;
35  kbp0=k(9)*rp0*R_LT+k(10)*r3p0*R_3LT+k(11)*h0*CT+k(12)*Wa*CT;
36  phi1=(L^2)/(Da*A_bulkg);
37  phi2=(k(1)+k(2)*K(12)/(CT*h0)+k(3)*r30*R_3LT+k(4)*r0*R_LT
        /(1+1/kb0))*...
38      A_bulkg;
39  phi3=-k(4)*R_LT*kbp0/(1+kb0);
40  phi4=-k(2)*CT*b0/K(2)-k(3)*CT*R_3LT*b0*r3p0/K(3)-k(1)*CT*CT*
        b0*h0/K(1);
41  phi5=-k(4)*L*L/Di;
42  phi6=A_bulkg*r0/(1+1/kb0);
43  phi7=-kbp0/(1+kb0);
44  phi8=phi1*(phi3*rm0+phi4); %For VKH Method 1
45
46  %Eqn 4.10-4.12
```

```matlab
47  eta1=phi1*phi2;
48  eta2=phi8;
49  eta3=phi5*phi6;
50  eta4=-phi5*phi7;
51
52  %Eqn 4.16
53  omega_a=eta2/eta1;
54  omega_r=eta2*eta3/(eta1*eta4);
55
56  %mu_i's are defined in eq 4.25 and 4.26
57  mu_1sq=-eta4;
58  mu_2sq=eta1;
59  mu_1=mu_1sq^(1/2);
60  mu_2=-mu_1sq^(1/2);
61  mu_3=mu_2sq^(1/2);
62  mu_4=-mu_2sq^(1/2);
63
64  %Lambdas are defined in eq 4.28
65  Lambda1=(mu_1sq+eta4)/eta3;
66  Lambda2=(mu_1sq+eta4)/eta3;
67  Lambda3=(mu_2sq+eta4)/eta3;
68  Lambda4=(mu_2sq+eta4)/eta3;
69
70  %The eqns 4.29-4.33 are organized into a matrix A and b, and
        the unknown
71  %psib's are solved for by A\b.
72  A=[Lambda1*exp(mu_1) Lambda2*exp(mu_2) Lambda3*exp(mu_3)
        Lambda4*...
73      exp(mu_4);(Lambda1-mu_1*Lambda1/lambda(4)) (Lambda2-mu_2
            *Lambda2/...
74      lambda(4)) (Lambda3-mu_3*Lambda3/lambda(4)) (Lambda4-
            mu_4*Lambda4/...
75      lambda(4)); exp(mu_1) exp(mu_2) exp(mu_3) exp(mu_4);
            mu_1 mu_2 mu_3...
76      mu_4];
77  b=[aL+omega_a; ag+omega_a; rmL+omega_r; drdy];
78  Psi_B=A\b;
79
80  %The can then be resubstitued into eq 4.19 to find a0 and
        rm0
81  a0_2=(Lambda1*Psi_B(1)+Lambda2*Psi_B(2)+Lambda3*Psi_B(3)+
        Lambda4*...
82      Psi_B(4))-omega_a;
83  rm0_2=Psi_B(1)+Psi_B(2)+Psi_B(3)+Psi_B(4)-omega_r;
84
85  Flux2=-lambda(4)*(ag-a0_2);%|F| eq 3.74 This is computed
        again to
```

```matlab
86  %compare the value found by the guesses r0 and rp0 values
        and the other
87  %value found using the linearization.
88
89  %This compares fluxes and rm0 values, this function
        minimizes this value to
90  %as close to zero as possible.
91  F(1)=((Flux1-Flux2)^2)*1e8;
92  F(2)=((rm0-rm0_2)^2)*1e8;
93  end
```

## B.3  Local Equilibrium Limit

```matlab
1   function []=localeq()
2   %Localeq solution
3   global R_LT R_3LT CT Wa Da Di lambda K A_bulkg M aL bL cL sL
        smL rmL ag sg
4   %Acid gas partial pressures
5   Pa=1;
6   Ps=0.1;
7   %Volatility constants in atm/M
8   Kha=29.411;
9   Khs=10;
10  %Henry constants in M/atm
11  Ha=1/Kha;
12  Hs=1/Khs;
13  %Acid gas partial pressures conversion into concentrations
14  A_bulkg=Ha*Pa; %Pa,bulk*Ha
15  S_bulkg=Hs*Ps;
16  Loading=[0 0]; %Liquid Loading factor
17  %The bulk liquid total amine and water concentrations (M)
18  R_LT=1.5;
19  R_3LT=2.5;
20  Wat=37.34;
21  %Liquid and Gas diffusivities
22  Da=2e-7; %dm2/s %For carbon dioxide
23  Di=1e-7; %dm2/s %For all volatile species
24  Dga=2e-3; %dm2/s
25  Dgs=2e-3; %dm2/s
26
27
28
29  %This line links to an m.file that solves for the bulk
        liquid conditions
30  %for all species given the total amine concentrations
```

```matlab
31  [aL,sL,smL,bL,cL,rmL,M,Wa]=findingbulkcon(K,R_LT,R_3LT,Wat,
        pH,Loading);
32
33
34  %Bulk Gas dimensionless concencentrations:
35  ag=1; %A_bulkg/A_bulkg
36  sg=1; %S_bulkg/S_bulkg
37
38  [lambda]=lambdacalcs(L,G,Da,Di,Dga,Dgs,K,A_bulkg,S_bulkg,
        R_3LT,R_LT);
39
40
41  rguesslc(1,:)=[0.3,0.001];
42  %The non-reactive absorption interfacial concentrations  eq
        4.35
43  Ao_norxn=(ag*A_bulkg*(Dga/G)+AL*(Da/L))/((Dga/G)+(Da/L));
44  So_norxn=(sg*S_bulkg*(Dgs/G)+SL*(Da/L))/((Dgs/G)+(Da/L));
45
46  chi_2=lambda(3)*sL+smL+lambda(3)*lambda(5)*sg; %chi_2 is
        defined in eq5.24
47
48  fun5=@localequilsolve;
49  Localequilsolve=@(r) fun5(r,L);
50  %This is the line that calls the root solver@findingbc to
        calculate b0 and
51  %c0 according to eq 5.28 and 5.29
52  rr=fsolve(Localequilsolve,rguesslc(p-1,:));
53  rguesslc(p,:)=rr;
54  b=rr(1);
55  c=rr(2);
56  h=lambda(9)*b/c;%eq 5.15
57  s=chi_2/(lambda(3)+lambda(3)*lambda(5)+lambda(10)/h);%eq
        5.25
58  a=lambda(12)*h*b;%eq5.16
59
60
61  %Flux and enhancement calculations, eq. 4.36-39
62  Fluxa=Da*lambda(4)*A_bulkg*(ag-a)/L;
63  Fluxs=Da*lambda(5)*S_bulkg*(sg-s)/L;
64  Ea=Fluxa/(kL*(Ao_norxn-aL*A_bulkg));
65  Es=Fluxs/(kL*(So_norxn-sL*S_bulkg));
66  %Selectivity is shown in results. It is the ratio of fluxes
        to the ratio of
67  %partial pressures.
68  Pa0=A_bulkg*a;
69  Ps0=S_bulkg*s;
70  Selectivity=(Pa-Pa0)*Fluxs/((Ps-Ps0)*Fluxa);
```

```matlab
71  end
```

```matlab
1   function F= localequilsolve(r,L)
2   % Local Equilibrium root solver - Section 5.2
3   global lambda M aL bL cL sL smL rmL ag sg
4
5   %chi1 and chi2 are from eq 5.24 and 5.25
6   chi_1=lambda(1)*aL+bL+cL+lambda(2)*rmL+lambda(1)*lambda(4)*
        ag;
7   chi_2=lambda(3)*sL+smL+lambda(3)*lambda(5)*sg;
8   b=r(1);
9   c=r(2);
10  %Eqns 5.28 and 5.29 (F1 and F2 below) are minimized and the
        values of b
11  %and c that make F1 and F2 zero.
12  F1=b-chi_1+c+lambda(1)*lambda(9)*lambda(12)*(b^2)/c+lambda
        (2)*...
13      lambda(12)*lambda(13)*b/(1+lambda(12)*lambda(13)*b+
            lambda(8)*...
14      lambda(9)*b/c)+lambda(1)*lambda(4)*lambda(9)*lambda(12)
            *(b^2)/c;
15  F2=M-2*c-b+lambda(6)*lambda(7)*lambda(9)*b/(c+lambda(7)*
        lambda(9)*b)...
16      -lambda(2)*lambda(12)*lambda(13)*b/(1+lambda(12)*lambda
            (13)*b+...
17      lambda(8)*lambda(9)*b/c)-chi_2*lambda(10)*c/(lambda(9)*b
            *(lambda(3)...
18      +lambda(3)*lambda(5)+lambda(10)*c/(lambda(9)*b)))+lambda
            (2)*...
19      lambda(8)*lambda(9)*b/(c*(1+lambda(12)*lambda(13)*b+
            lambda(8)*...
20      lambda(9)*b/c));
21  F(1)=F1;
22  F(2)=F2;
23
24  end
```

# References

Al-Ghawas, H. A., Hagewiesche, D. P., Ruiz-Ibanez, G., and Sandall, O. C. (1989). Physicochemical properties important for carbon dioxide absorption in aqueous methyldiethanolamine. *Journal of Chemical & Engineering Data*, *34*(4), 385–391.
URL http://dx.doi.org/10.1021/je00058a004

Al Hashimi, S. (2000). *Use of accurate asymptotic analyses of local transport rates in the design of alkaline scrubber/stripper systems for acid gas separation.*. Master's thesis, Tufts University.

Ali, S. H. (2005). Kinetics of the reaction of carbon dioxide with blends of amines in aqueous media using the stopped-flow technique. *International Journal of Chemical Kinetics*, *37*(7), 391–405.
URL http://dx.doi.org/10.1002/kin.20059

Aroua, M. K., Benamor, A., and Haji-Sulaiman, M. Z. (1999). Equilibrium constant for carbamate formation from monoethanolamine and its relationship with temperature. *Journal of Chemical & Engineering Data*, *44*(5), 887–891.

Barchas, R., and Davis, R. (1992). The kerr-mcgee/abb lummus crest technology for the recovery of {CO2} from stack gases. *Energy Conversion and Management*, *33*(5–8), 333 – 340. Proceedings of the First International

Conference on Carbon Doxide Removal.

URL http://www.sciencedirect.com/science/article/pii/019689049290028U

Barth, C., D.; Tondre, Lappai, G., and Delpuech, J. (1981). Kinetic study of carbon dioxide reaction with tertiary amines in aqueous solutions. *J. Phys. Chem.*, *85*, 3660–3667.

Bergman, T., Lavine, A. S., Incropera, F. P., and DeWitt, D. P. (2011). *Fundamentals of Heat and Mass Transfer*. Wiley Subscription Services, Inc., A Wiley Company.

Blauwhoff, P., Kamphuis, B., van Swaaij, W., and Westerterp, K. (1985). Absorber design in sour natural gas treatment plants: Impact of process variables on operation and economics = absorberentwurf für anlagen zur behandlung von sauren erdgasen: Einfluss prozessparameter auf betriebsführung und prozesswirtschaftlichkeit. *Chemical Engineering and Processing*, *19*(1), 1–25.

URL http://doc.utwente.nl/69393/

Blauwhoff, P., Versteeg, G., and Swaaij, W. V. (1984). A study on the reaction between co2 and alkanolamines in aqueous solutions. *Chemical Engineering Science*, *39*(2), 207 – 225.

URL http://www.sciencedirect.com/science/article/pii/0009250984800214

Bolhàr-Nordenkampf, M., Friedl, A., Koss, U., and Tork, T. (2004). Modelling selective {H2S} absorption and desorption in an aqueous mdea-solution using a rate-based non-equilibrium approach. *Chemical Engineering and Processing: Process Intensification*, *43*(6), 701 – 715.

Borhani, T. N. G., Afkhamipour, M., Azarpour, A., Akbari, V., Emadi, S. H., and Manan, Z. A. (2016). Modeling study on {CO2} and {H2S}

simultaneous removal using {MDEA} solution. *Journal of Industrial & Engineering Chemistry*, *34*, 344 – 355.

URL http://www.sciencedirect.com/science/article/pii/S1226086X15005511

Brian, P. L. T., Hurley, J. F., and Hasseltine, E. H. (1961). Penetration theory for gas absorption accompanied by a second order chemical reaction. *A. I. Ch. E. J*, *7*, 226.

Caplow, M. (1968). Kinetics of carbamate formation and breakdown. *J. Am. Chem. Soc.*, *90*, 6795–6803.

Cents, A., Brilman, D., and Versteeg, G. (2005). absorption in carbonate/bicarbonate solutions: The danckwerts-criterion revisited. *Chemical Engineering Science*, *60*(21), 5830 – 5835.

URL http://www.sciencedirect.com/science/article/pii/S0009250905004306

Chakravarty, T., Phukan, U. K., and Weiland, R. H. (1985). Reaction of acid gases with mixtures of amines. *Chem. Eng. Prog.*, *81*(4), 32–36.

Chang, C. S., and Rochelle, G. T. (1982). Mass transfer enhanced by equilibrium reactions. *Industrial & Engineering Chemistry Fundamentals*, *21*, 379.

Danckwerts, P. V. (1951). Significance of liquid-film coefficients in gas absorption. *Industrial & Engineering Chemistry*, *43*(6), 1460–1467.

Danckwerts, P. V. (1970). *Gas-liquid reactions*. McGraw-Hill Book Co.

URL http://dx.doi.org/10.1002/aic.690170204

Danckwerts, P. V., and Sharma, M. (1966). The absorption of carbon dioxide into solutions of akalis and amines (with some notes on hydrogen sulphide and carbonyl sulphide). *Chem. Eng.*, *44*, CE244–CE280.

DeCoursey, W. (1974). Absorption with chemical reaction: development of a new relation for the danckwerts model. *Chemical Engineering Science*, *29*(9), 1867 – 1872.

URL http://www.sciencedirect.com/science/article/pii/0009250974850037

Donaldson, T. L., and Nguyen, Y. N. (1980a). Carbon dioxide reaction kinetics and transport in aqueous amine membranes. *Industrial & Engineering Chemistry Fundamentals*, *19*(3), 260–266.

URL http://dx.doi.org/10.1021/i160075a005

Donaldson, T. L., and Nguyen, Y. N. (1980b). Carbon dioxide reaction kinetics and transport in aqueous amine membranes. *Industrial & Engineering Chemistry Fundamentals*, *19*(3), 260–266.

Edwards, T. J., Maurer, G., Newman, J., and Prausnitz, J. M. (1978). Vapor-liquid equilibria in multicomponent aqueous solutions of volatile weak electrolytes. *AIChE Journal*, *24*(6), 966–976.

URL http://dx.doi.org/10.1002/aic.690240605

ExxonMobil (2012). The outlook for energy: A view to 2040. Tech. rep., ExxonMobil.

Falahat, R., Montazer-Rahmati, M. M., and Bolouri, O. (2011). Rate-based modelling of reactive absorption of acid gases in an aqueous methyldiethanolamine (mdea) solution. *The Canadian Journal of Chemical Engineering*, *89*(1), 132–138.

URL http://dx.doi.org/10.1002/cjce.20374

Fiordalis, A. (2017). *Development of Accurate and Computation-Ecient Linearization Techniques for Modeling Absorption with Complex Chemical Reaction*. Ph.D. thesis, Tufts University.

Fox, M. S., Greenberg, J. W., and Trookman, J. M. (2015). An algebraic derivation of buffer capacity. *World Journal of Chemical Education*, *3*(5), 124–126.

Glasscock, D. A., Critchfield, J. E., and Rochelle, G. T. (1991). Co2 absorption/desorption in mixtures of methyldiethanolamine with monoethanolamine or diethanolamine. *Chemical Engineering Science*, *46*(11), 2829 – 2845.

    URL `http://www.sciencedirect.com/science/article/pii/000925099185152N`

Glasscock, D. A., and Rochelle, G. T. (1989). Numerical simulation of theories for gas absorption with chemical reaction. *AIChE Journal*, *35*(8), 1271–1281.

    URL `http://dx.doi.org/10.1002/aic.690350806`

Glasscock, D. A., and Rochelle, G. T. (1993). Approximate simulation of co2 and h2s absorption into aqueous alkanolamines. *AIChE Journal*, *39*(8), 1389–1397.

    URL `http://dx.doi.org/10.1002/aic.690390816`

Godini, H. R., and Mowla, D. (2008). Selectivity study of {H2S} and {CO2} absorption from gaseous mixtures by {MEA} in packed beds. *Chemical Engineering Research and Design*, *86*(4), 401 – 409. Particle Technology.

    URL `http://www.sciencedirect.com/science/article/pii/S0263876207000317`

Hagewiesche, D. P., Ashour, S. S., Al-Ghawas, H. A., and Sandall, O. C. (1995). Absorption of carbon dioxide into aqueous blends of monoethanolamine and n-methyldiethanolamine. *Chemical Engineering Science*, *50*(7), 1071–1079.

    URL `http://www.sciencedirect.com/science/article/pii/000925099400489E`

Hamour, N., Bidarian, A., and Sandall, O. C. (1987). Simultaneous absorption of h2s and co2 into aqueous methyldiethanolamine. *Separation Science and Technology*, *22*(2-3), 921–947.

URL `http://dx.doi.org/10.1080/01496398708068990`

Higbie, R. (1935). The rate of absorption of a pure gas into a still liquid during short periods of exposure. *Transactions of the AIChE*, *31*(365-389).

Hikita, H., and Asai, S. (1964). Gas absorption with (m,n)-th order irreversible chemical reaction. *Int. Chem. Eng*, *2*, 332–340.

Hikita, H., Asai, S., Ishikawa, H., and Honda, M. (1977). The kinetics of reactions of carbon dioxide with monoethanolamine, diethanolamine and triethanolamine by a rapid mixing method. *the chemical Engineering Journal*, *13*(1), 7–12.

Hoffmann, A., Maćkowiak, J., Górak, A., Haas, M., Löning, J.-M., Runowski, T., and Hallenberger, K. (2007). Standardization of mass transfer measurements: A basis for the description of absorption processes. *Chemical Engineering Research and Design*, *85*(1), 40 – 49.

URL `http://www.sciencedirect.com/science/article/pii/S0263876207730186`

Hogendoorn, J., Bhat, R. V., Kuipers, J., van Swaaij, W., and Versteeg, G. (1997). Approximation for the enhancement factor applicable to reversible reactions of finite rate in chemically loaded solutions. *Chemical Engineering Science*, *52*(24), 4547 – 4559.

URL `http://www.sciencedirect.com/science/article/pii/S0009250997002984`

Horng, S.-Y., and Li, M.-H. (2002). Kinetics of absorption of carbon dioxide into aqueous solutions of monoethanolamine + triethanolamine. *Industrial*

& *Engineering Chemistry Research*, *41*(2), 257–266.

URL http://dx.doi.org/10.1021/ie010671l

Hwang, G. S., Stowe, H. M., Paek, E., and Manogaran, D. (2015). Reaction mechanisms of aqueous monoethanolamine with carbon dioxide: a combined quantum chemical and molecular dynamics study. *Phys. Chem. Chem. Phys.*, *17*, 831–839.

URL http://dx.doi.org/10.1039/C4CP04518A

King, C. J. (1966). Turbulent liquid phase mass transfer at free gas-liquid interface. *Industrial & Engineering Chemistry Fundamentals*, *5*(1), 1–8.

Kohl, A. L., and Nielsen, R. B. (1997). Chapter 2 - alkanolamines for hydrogen sulfide and carbon dioxide removal. In *Gas Purification (Fifth Edition)*, (pp. 40 – 186). Houston: Gulf Professional Publishing, fifth edition ed.

URL http://www.sciencedirect.com/science/article/pii/B9780884152200500021

Kumar, S., Cho, J. H., Moon, I., Kumar, S., Cho, J., and Moon, I. (2014). Ionic liquid-amine blends and co2bols: Prospective solvents for natural gas sweetening and co2 capture technology—a review. *International Journal of Greenhouse Gas Control*, *20*(Complete), 87–116.

Laddha, S., and Danckwerts, P. (1981). Reaction of co2 with ethanolamines: kinetics from gas-absorption. *Chemical engineering science*, *36*(3), 479–482.

Le Chatelier, H. (1891). Sur les transformations moléculaires des métaux et leurs conductibilités électriques. *J. Phys. Theor. Appl.*, *10*(1), 369–374.

URL https://doi.org/10.1051/jphystap:0189100100036901

Lewis, W. K., and Whitman, W. G. (1924). The two-film theory of gas absorption. *Industrial & Engineering Chemistry*, *12*, 1215–1220.

Li, J., Henni, A., and Tontiwachwuthikul, P. (2007). Reaction kinetics of co2 in aqueous ethylenediamine, ethyl ethanolamine, and diethyl monoethanolamine solutions using the stopped-flow technique. *Industrial & Engineering Chemistry Research*, *46*(13), 4426–4434.
URL `http://dx.doi.org/10.1021/ie0614982`

Liao, C.-H., and Li, M.-H. (2002). Kinetics of absorption of carbon dioxide into aqueous solutions of monoethanolamine+n-methyldiethanolamine. *Chemical Engineering Science*, *57*(21), 4569 – 4582.
URL `http://www.sciencedirect.com/science/article/pii/S0009250902003950`

Lin, C.-Y., Soriano, A. N., and Li, M.-H. (2009). Kinetics study of carbon dioxide absorption into aqueous solutions containing n-methyldiethanolamine + diethanolamine. *Journal of the Taiwan Institute of Chemical Engineers*, *40*(4), 403 – 412.
URL `http://www.sciencedirect.com/science/article/pii/S1876107008001776`

Littel, R., Van Swaaij, W., and Versteeg, G. (1990). Kinetics of carbon dioxide with tertiary amines in aqueous solution. *AIChE Journal*, *36*(11), 1633–1640. Cited By 124.

Littel, R., Versteeg, G., and Swaaij, W. V. (1992). Kinetics of co2 with primary and secondary amines in aqueous solutions—i. zwitterion deprotonation kinetics for dea and dipa in aqueous blends of alkanolamines. *Chemical Engineering Science*, *47*(8), 2027 – 2035.
URL `http://www.sciencedirect.com/science/article/pii/0009250992803198`

Lv, B., Guo, B., Zhou, Z., and Jing, G. (2015). Mechanisms of co2 capture into monoethanolamine solution with different co2 loading during the absorption/desorption processes. *Environmental Science & Technology*, *49*(17),

10728–10735. PMID: 26236921.

URL http://dx.doi.org/10.1021/acs.est.5b02356

Ma, C., Pietrucci, F., and Andreoni, W. (2015). Capture and release of co2 in monoethanolamine aqueous solutions: New insights from first-principles reaction dynamics. *Journal of Chemical Theory and Computation*, *11*(7), 3189–3198. PMID: 26575756.

URL http://dx.doi.org/10.1021/acs.jctc.5b00379

MacDowell, N., Florin, N., Buchard, A., Hallett, J., Galindo, A., Jackson, G., Adjiman, C. S., Williams, C. K., Shah, N., and Fennell, P. (2010). An overview of co2 capture technologies. *Energy Environ. Sci.*, *3*, 1645–1669.

URL http://dx.doi.org/10.1039/C004106H

Magné-Drisch, Julia, Gazarian, Jérémy, Gonnard, Sébastien, Schweitzer, Jean-Marc, Chiche, David, Laborie, Géraldine, and Perdu, Gauthier (2016). Cosweettm: A new process to reach very high cos specification on natural gas treatment combined with selective h2s removal. *Oil Gas Sci. Technol. – Rev. IFP Energies nouvelles*, *71*(3), 40.

URL http://dx.doi.org/10.2516/ogst/2015038

Mandal, B., and Bandyopadhyay, S. S. (2006). Simultaneous absorption of co2 and h2s into aqueous blends of n-methyldiethanolamine and diethanolamine. *Environmental Science & Technology*, *40*(19), 6076–6084. PMID: 17051803.

URL http://dx.doi.org/10.1021/es0606475

Oloffson, G., and Hepler, L. G. (1975). Thermodynamics of ionization of water over wide ranges of temperature and pressure. *J. Solution Chem.*, *4*, 127.

Pinsent, B. R. W., Pearson, L., and Roughton, F. J. W. (1956). The kinetics

of combination of carbon dioxide with hydroxide ions. *Trans. Faraday Soc.*, *52*, 1512–1520.

Prasher, B. D., and Fricke, A. L. (1974). Mass transfer at a free gas-liquid interface in turbulent thin films. *Industrial & Engineering Chemistry Process Design and Development*, *13*(4), 336–340.

Prithipal, R., Lokhat, D., Govender, N., Starzak, M., and Ramjugernath, D. (2016). A kinetic study of the selective production of difluoromethoxymethane from chlorodifluoromethane. *Journal of the Taiwan Institute of Chemical Engineers*, *66*, 70 – 79.
URL http://www.sciencedirect.com/science/article/pii/S1876107016302164

Ramachandran, N., Aboudheir, A., Idem, R., and Tontiwachwuthikul, P. (2006). Kinetics of the absorption of co2 into mixed aqueous loaded solutions of monoethanolamine and methyldiethanolamine. *Industrial & Engineering Chemistry Research*, *45*(8), 2608–2616.
URL http://dx.doi.org/10.1021/ie0505716

Read, A. J. (1975). The first ionization constant of carbonic acid from 25 to 250° and to 2000 bar. *J. Solution Chem.*, *4*, 53–70.

Rejl, J., Linek, V., Moucha, T., and Valenz, L. (2009). Methods standardization in the measurement of mass-transfer characteristics in packed absorption columns. *Chemical Engineering Research and Design*, *87*(5), 695 – 704.
URL http://www.sciencedirect.com/science/article/pii/S0263876208002943

Rinker, E. B., Ashour, S. S., and Sandall, O. C. (1996). Kinetics and modelling of carbon dioxide absorption into aqueous solutions of diethanolamine. *nd. Eng. Chem. Res.*, *35*, 1107–1114.

Rinker, E. B., Ashour, S. S., and Sandall, O. C. (2000). Absorption of carbon dioxide into aqueous blends of diethanolamine and methyldiethanolamine. *Industrial & Engineering Chemistry Research*, *39*(11), 4346–4356.

Rinker, E. B., Oelschlager, D. W., Colussi, A. T., Henry, K. R., and Sandall, O. C. (1994). Viscosity, density, and surface tension of binary mixtures of water and n-methyldiethanolamine and water and diethanolamine and tertiary mixtures of these amines with water over the temperature range 20-100.degree.c. *Journal of Chemical & Engineering Data*, *39*(2), 392–395.
URL `http://dx.doi.org/10.1021/je00014a046`

Rinker, E. B., Sami, S., and Sandall, O. C. (1995). Kinetics and modelling of carbon dioxide absorption into aqueous solutions of n-methyldiethanolamine. *Chemical Engineering Science*, *50*(5), 755 – 768.
URL `http://www.sciencedirect.com/science/article/pii/000925099400444V`

Santiago, M., and Farina, I. (1970). Mass transfer with second order reaction. numerical solution. *Chemical Engineering Science*, *25*(4), 744 – 747.
URL `http://www.sciencedirect.com/science/article/pii/0009250970851065`

Sema, T., Naami, A., Fu, K., Edali, M., Liu, H., Shi, H., Liang, Z., Idem, R., and Tontiwachwuthikul, P. (2012). Comprehensive mass transfer and reaction kinetics studies of {CO2} absorption into aqueous solutions of blended mdea–mea. *Chemical Engineering Journal*, *209*, 501 – 512.
URL `http://www.sciencedirect.com/science/article/pii/S1385894712010613`

Stewart, W. E. (1995). Multicomponent mass transfer. by ross taylor and r. krishna, wiley, new york, 1993, 579 pp. *AIChE Journal*, *41*(1), 202–203.
URL `http://dx.doi.org/10.1002/aic.690410124`

Sutar, P. N., Jha, A., Vaidya, P. D., and Kenig, E. Y. (2012). Secondary amines

for {CO2} capture: A kinetic investigation using n-ethylmonoethanolamine. *Chemical Engineering Journal*, *207–208*, 718 – 724. 22nd International Symposium on Chemical Reaction Engineering (ISCRE 22).

URL `http://www.sciencedirect.com/science/article/pii/S1385894712009333`

Torres-Ortega, C. E., Segovia-Hernandez, J. G., Gomez-Castro, F. I., and Hernandez., S. (2014). Optimization of alternative distillation sequences for natural gas sweetening. In *24th European Symposium on Computer Aided Process Engineering*. 24th European Symposium on Computer Aided Process Engineering.

Vaidya, P. D., and Kenig, E. Y. (2007). Co2-alkanolamine reaction kinetics: A review of recent studies. *Chemical Engineering & Technology*, *30*(11), 1467–1474.

URL `http://dx.doi.org/10.1002/ceat.200700268`

van Krevelen, D. W., and Hoftijzer, P. J. (1948). Kinetics of gas-liquid reactions part i. general theory. *Recueil des Travaux Chimiques des Pays-Bas*, *67*(7), 563–586.

URL `http://dx.doi.org/10.1002/recl.19480670708`

Versteeg, G., Kuipers, J., Beckum, F. V., and Swaaij, W. V. (1990). Mass transfer with complex reversible chemical reactions—ii. parallel reversible chemical reactions. *Chemical Engineering Science*, *45*(1), 183 – 197.

URL `http://www.sciencedirect.com/science/article/pii/0009250990870916`

Versteeg, G., and van Swaaij, W. (1988). On the kinetics between co2 and alkanolamines both in aqueous and non-aqueous solutions—i. primary and secondary amines. *Chemical Engineering Science*, *43*(3), 573 – 585.

URL `http://www.sciencedirect.com/science/article/pii/0009250988870179`

Worley, C. (2016). *Linearized Analysis of Gas Sweetening with Tertiary Amines*. Master's thesis, Tufts University.

Xie, H.-B., Zhou, Y., Zhang, Y., and Johnson, J. K. (2010). Reaction mechanism of monoethanolamine with co2 in aqueous solution from molecular modeling. *The Journal of Physical Chemistry A*, *114*(43), 11844–11852. PMID: 20939618.
URL `http://dx.doi.org/10.1021/jp107516k`

Xu, H.-J., Zhang, C.-F., and Zheng, Z.-S. (2002). Selective h2s removal by nonaqueous methyldiethanolamine solutions in an experimental apparatus. *Industrial & Engineering Chemistry Research*, *41*(12), 2953–2956.
URL `http://dx.doi.org/10.1021/ie0109253`

Yildirim, Ö., Kiss, A. A., Hüser, N., Leßmann, K., and Kenig, E. Y. (2012). Reactive absorption in chemical process industry: A review on current activities. *Chemical Engineering Journal*, *213*, 371 – 391.
URL `http://www.sciencedirect.com/science/article/pii/S1385894712013307`

Zhao, W., Han, B., Jakobsson, K., Louhi-Kultanen, M., and Alopaeus, V. (2016). Mathematical model of precipitation of magnesium carbonate with carbon dioxide from the magnesium hydroxide slurry. *Computers & Chemical Engineering*, *87*, 180 – 189.
URL `http://www.sciencedirect.com/science/article/pii/S0098135416300047`

Zhu, N. (2016). *Analysis of Carbon Dioxide Absorption in Tertiary Amine Solution*. Master's thesis, Tufts University.